العنوان:	INTERFACIAL AREA CONCENTRATION AND VOID FRACTION OF TWO PHASE FLOW IN 12.7 mmID PIPE-
المؤلف الرئيسي:	Al Dorwish, Yousef M.
مؤلفين آخرين:	Ishi, Mamoru(Super.)
التاريخ الميلادي:	2000
موقع:	لافاييت
الصفحات:	1 - 120
رقم MD:	614708
نوع المحتوى:	رسائل جامعية
اللغة:	English
الدرجة العلمية:	رسالة ماجستير
الجامعة:	Purdue University
الكلية:	The Graduate School
الدولة:	الولايات المتحدة الأمريكية
قواعد المعلومات:	Dissertations
مواضيع:	الطاقة النووية، الإشعاع النووي، الهندسة النووية
رابط:	https://search.mandumah.com/Record/614708

INTERFACIAL AREA CONCENTRATION AND VOID FRACTION

OF TWO-PHASE FLOW IN 12.7 mm ID PIPE

A Thesis

Submitted to the Faculty

of

Purdue University

by

Yousef M. Aldorwish

In Partial Fulfillment of the

Requirements for the Degree

of

Master of Science in Nuclear Engineering

May 2000

INTERFACIAL AREA CONCENTRATION AND VOID FRACTION OF TWO-PHASE FLOW IN 12.7 mmID PIPE	العنوان:
Al Dorwish, Yousef M.	المؤلف الرئيسي:
Ishi, Mamoru(Super.)	مؤلفين آخرين:
2000	التاريخ الميلادي:
لافاييت	موقع:
1 - 120	الصفحات:
614708	رقم MD:
رسائل جامعية	نوع المحتوى:
English	اللغة:
رسالة ماجستير	الدرجة العلمية:
Purdue University	الجامعة:
The Graduate School	الكلية:
الولايات المتحدة الأمريكية	الدولة:
Dissertations	قواعد المعلومات:
الطاقة النووية، الإشعاع النووي، الهندسة النووية	مواضيع:
https://search.mandumah.com/Record/614708	رابط:

www.manaraa.com

Exerimental Condition: Run 1 at Port1 (L/D=17)

Experimental Conditions:		$j_{g,inlet}[m/s] =$	0.07	loc. press. [psi]=	5.487	Probe Configuration [mm]					
$Q_g[ml/min]=$	75.00	$j_{g,local}$ [m/s] =	0.05	N_{sample}:	8000	$S_{01} =$	2.04	$S_{02} =$	1.94	$S_{03} =$	1.96
$P_{back}[psi]=$	8.50	$j_{f,inlet}$ [m/s] =	0.41	f_{sample}:	8000	$S_{12} =$	0.48	$S_{13} =$	0.19	$S_{23} =$	0.43

$<<v_g>>=$	0.574	m/s	$<\alpha><<v_g>>=$	0.046	m/s	Percent difference between $<j_g>_z$ and $<\alpha>_z<<v_g>>_z =$	13.32	%

Probe Position		No. Loops	Δt_{total}	Bubble Number		α		a_i [1/m]		Total		v_{g1}	v_{g2}	$v_{g,avg}$	D_{sm1}	$\alpha_1 v_1 + \alpha_2 v_2$
r [mm]	r/R	N_{total}	[sec]	N_1	N_2	α_1	α_2	a_{i1}	$a_{i\,2}$	α_{Tot}	a_{iTot}	[m/s]	[m/s]	[m/s]	[cm]	[m/s]
0.00	0.00	50	50.000	1392	0	0.078	0.000	182.70	0.00	0.078	182.70	0.622	0.000	0.622	0.256	0.049
											224.50				0.267	
1.27	0.20	50	50.000	1644	0	0.100	0.000	224.50	0.00	0.100		0.600	0.000	-0.600		0.060
2.54	0.40	50	50.000	1675	0	0.120	0.000	251.40	0.00	0.120	251.40	0.550	0.000	0.550	0.286	0.066
3.18	0.50	50	50.000	1618	0	0.110	0.000	258.80	0.00	0.110	258.80	0.510	0.000	0.510	0.255	0.056
3.81	0.60	50	50.000	1350	0	0.080	0.000	251.60	0.00	0.080	251.60	0.440	0.000	0.440	0.191	0.035
4.45	0.70	50	50.000	1011	0	0.050	0.000	153.50	0.00	0.050	153.50	0.600	0.000	0.600	0.195	0.030
5.09	0.80	50	50.000	1031	0	0.045	0.000	155.70	0.00	0.045	155.70	0.550	0.000	0.700	0.173	0.025
5.72	0.90	50	50.000	1206	0	0.066	0.000	198.50	0.00	0.066	198.50	0.510	0.000	0.510	0.199	0.034
Area Averaged Values		=				0.08	0.00	191.41	0.00	0.08	191.41	0.50	0.00	0.00	0.22	0.05

Experimental Conditions:		$j_{g,inlet}[m/s] =$	8.05	loc. press. [psi]=	14.564	Probe Configuration [mm]	
$Q_g[ml/min]=$	100.00	$j_{g,local}[m/s] =$	8.13	N_{sample}:	8000	$S_{01} =$	0.84
$P_{back}[psi]=$	5.00	$j_{f,inlet}[m/s] =$	0.20	f_{sample}:	55000		

$<<v_g>>=$ 9.064 m/s $<\alpha><<v_g>>=$ 7.376 m/s Percent difference between $<j_g>_z$ and $<\alpha>_z<<v_g>>_z =$ 9.23 %

Probe Position		No. Loops	Δt_{total}	Bubble Number		α		Void fraction	v_{g1}	v_{g2}	$v_{g.avg}$	$\alpha_1 v_1 + \alpha_2 v_2$
r [mm]	r/R	N_{total}	[sec]	N_1	N_2	α_1	α_2	α total	[m/s]	[m/s]	[m/s]	[m/s]
0.00	0.00	87	12.655	1562	420	0.010	0.960	0.970	12.5	9.350	11.2	9.101
										9.500		
1.27	0.20	87	12.655	1444	412	0.033	0.897	0.930	10.5		10.02	8.868
2.54	0.40	87	12.655	1402	404	0.029	0.913	0.942	9.5	9.000	9.26	8.489
3.18	0.50	87	12.655	1203	391	0.027	0.924	0.950	9.6	8.350	8.67	7.969
3.81	0.60	87	12.655	1158	281	0.035	0.906	0.940	8.6	8.060	8.31	7.597
4.45	0.70	87	12.655	1146	281	0.049	0.844	0.892	7.65	7.230	7.42	6.472
5.09	0.80	87	12.655	949	128	0.084	0.699	0.783	8.4	8.230	8.3	6.454
5.72	0.90	87	12.655	666	89	0.078	0.421	0.499	7.800	7.100	7.520	3.598
Area Averaged Values	=											
						0.03	0.78	0.81	8.95	7.93	8.47	7.38

Exerimental Condition for churn flow: Run 5 at Port3 (L/D=217)

Experimental Conditions:		$j_{g,inlet}[m/s] =$	7.09	loc. press. [psi]=	14.23	Probe Configuration [mm]	
$Q_g[ml/min]=$	88.00	$j_{g,local}[m/s] =$	7.32	N_{sample}:	8000	$S_{01} =$	0.84
$P_{back}[psi]=$	5.00	$j_{f,inlet}[m/s] =$	0.15	f_{sample}:	55000		

$<<v_g>>=$ 7.681 m/s $<\alpha><<v_g>>=$ 6.056 m/s   Percent difference between $<j_g>_z$ and $<\alpha>_z<<v_{g2}>>_z =$ 17.25 %

Probe Position		No. Loops	Δt_{total}	Bubble Number		α		Void fraction	v_{g1}	v_{g2}	$v_{g,avg}$	$\alpha_1 v_1 + \alpha_2 v_2$
r [mm]	r/R	N_{total}	[sec]	N_1	N_2	α_1	α_2	α total	[m/s]	[m/s]	[m/s]	[m/s]
0.00	0.00	75	10.909	1620	512	0.012	0.945	0.957	8.9	7.840	8.54	7.516
										8.010		
1.27	0.20	75	10.909	1825	439	0.020	0.928	0.948	8.36		8.15	7.599
2.54	0.40	75	10.909	1462	415	0.023	0.910	0.933	7.46	7.220	7.35	6.740
3.18	0.50	75	10.909	1254	390	0.027	0.845	0.872	8.1	7.640	7.85	6.674
3.81	0.60	75	10.909	1876	342	0.038	0.810	0.848	7.63	7.230	7.44	6.145
4.45	0.70	75	10.909	1032	354	0.042	0.780	0.822	6.85	5.980	6.42	4.951
5.09	0.80	75	10.909	895	180	0.081	0.425	0.506	7.42	6.660	7.02	3.430
5.72	0.90	75	10.909	760	78	0.062	0.350	0.412	5.680	5.600	5.600	2.312
Area Averaged Values		=				0.02	0.77	0.79	7.14	6.70	6.92	6.06

93

Exerimental Condition for churn flow: Run 4 at Port3 (L/D=217)

Experimental Conditions:		$j_{g,inlet}[m/s] =$	8.05	loc. press. [psi]=	13.563	Probe Configuration [mm]	
$Q_g[ml/min]=$	100.00	$j_{g,local}\ [m/s] =$	8.73	$N_{sample;}$	8000	S_{01} =	0.84
$P_{back}[psi]=$	5.00	$j_{f,inlet}\ [m/s] =$	0.10	$f_{sample;}$	55000		

$<<v_g>>=$	9.444	m/s	$<\alpha><<v_g>>=$	7.388	m/s	Percent difference between $<j_g>_z$ and $<\alpha>_z<<v_g>>_z =$	15.33	%

Probe Position		No. Loops	Δt_{total}	Bubble Number		α		Void fraction	v_{g1}	v_{g2}	$v_{g.avg}$	$\alpha_1 v_1 + \alpha_2 v_2$
r [mm]	r/R	N_{total}	[sec]	N_1	N_2	α_1	α_2	α total	[m/s]	[m/s]	[m/s]	[m/s]
0.00	0.00	87	12.655	2150	426	0.025	0.873	0.898	10.5	9.900	10.2	8.900
										9.690		
1.27	0.20	87	12.655	2015	369	0.023	0.900	0.923	9.58		9.52	8.939
2.54	0.40	87	12.655	1826	362	0.031	0.854	0.884	9.26	8.910	9.06	7.891
3.18	0.50	87	12.655	1720	312	0.021	0.941	0.961	9.36	8.650	9.03	8.329
3.81	0.60	87	12.655	1800	294	0.036	0.886	0.921	9.58	9.050	9.24	8.354
4.45	0.70	87	12.655	1256	184	0.034	0.829	0.864	8.98	8.510	8.72	7.364
5.09	0.80	87	12.655	1123	112	0.079	0.502	0.581	8.8	8.900	8.85	5.167
5.72	0.90	87	12.655	658	82	0.080	0.310	0.390	8.690	7.210	8.130	2.930
Area Averaged Values			=									
						0.03	0.76	0.78	8.44	8.28	8.30	7.39

94

Exerimental Condition for churn flow: Run 3 at Port3 (L/D=217)

Experimental Conditions:		$j_{g,inlet}[m/s] =$	7.09	loc. press. [psi]=	13.547	Probe Configuration [mm]	
$Q_g[ml/min]=$	88.00	$j_{g,local}[m/s] =$	7.69	$N_{sample}:$	8000	$S_{01} =$	0.84
$P_{back}[psi]=$	5.00	$j_{f,inlet}[m/s] =$	0.10	$f_{sample}:$	55000		

$<<v_g>>=$	8.328	m/s	$<\alpha><<v_g>>=$	6.450	m/s	Percent difference between $<j_g>_z$ and $<\alpha>_z<<v_g>>_z=$	16.11	%

Probe Position		No. Loops	Δt_{total}	Bubble Number		α		Void fraction	v_{g1}	v_{g2}	$v_{g,avg}$	$\alpha_1 v_1 + \alpha_2 v_2$
r [mm]	r/R	N_{total}	[sec]	N_1	N_2	α_1	α_2	α total	[m/s]	[m/s]	[m/s]	[m/s]
0.00	0.00	75	10.909	1821	450	0.033	0.868	0.901	9.8	8.800	9.5	7.959
										8.690		
1.27	0.20	75	10.909	1684	415	0.020	0.911	0.931	8.59		8.55	8.087
2.54	0.40	75	10.909	1522	387	0.040	0.869	0.908	8.69	8.320	8.51	7.573
3.18	0.50	75	10.909	1516	358	0.031	0.889	0.920	8.05	7.920	7.96	7.291
3.81	0.60	75	10.909	1425	320	0.026	0.829	0.855	8	6.980	7.52	5.993
4.45	0.70	75	10.909	1102	319	0.034	0.720	0.754	8.2	6.820	7.63	5.192
5.09	0.80	75	10.909	850	211	0.106	0.469	0.575	7.88	7.320	7.61	4.269
5.72	0.90	75	10.909	690	180	0.069	0.254	0.323	7.680	7.800	7.660	2.511
Area Averaged Values		=				0.03	0.75	0.77	7.58	7.27	7.42	6.45

Exerimental Condition for Churn flow: Run 2 at Port3 (L/D=217)

Experimental Conditions:		$j_{g,inlet}[m/s] =$	7.95	loc. press. [psi]=	13.041	Probe Configuration [mm]	
$Q_g[ml/min]=$	100.00	$j_{g,local}[m/s] =$	8.96	$N_{sample;}$	8000	$S_{01} =$	0.84
$P_{back}[psi]=$	4.50	$j_{f,inlet}[m/s] =$	0.06	$f_{sample;}$	40000		

$<<v_g>>=$	8.881	m/s	$<\alpha><<v_g>>=$	7.348	m/s	Percent difference between $<j_g>_z$ and $<\alpha>_z<<v_g>>_z =$	17.99 %

Probe Position		No. Loops	Δt_{total}	Bubble Number		α		Void fraction	v_{g1}	v_{g2}	$v_{g.avg}$	$\alpha_1 v_1 + \alpha_2 v_2$
r [mm]	r/R	N_{total}	[sec]	N_1	N_2	α_1	α_2	α total	[m/s]	[m/s]	[m/s]	[m/s]
0.00	0.00	62	12.400	2561	382	0.048	0.950	0.998	10.2	9.800	9.88	9.800
										9.200		
1.27	0.20	62	12.400	2450	370	0.042	0.980	1.022	9.5		9.35	9.416
2.54	0.40	62	12.400	2150	321	0.033	0.899	0.932	8.62	8.260	8.41	7.709
3.18	0.50	62	12.400	1845	305	0.032	0.911	0.942	8.39	7.980	8.2	7.533
3.81	0.60	62	12.400	1652	284	0.043	0.808	0.850	8.2	7.680	7.92	6.553
4.45	0.70	62	12.400	1111	111	0.107	0.678	0.785	7.8	7.050	7.52	5.615
5.09	0.80	62	12.400	1210	81	0.120	0.411	0.531	7.9	7.680	7.76	4.105
5.72	0.90	62	12.400	942	41	0.100	0.210	0.310	7.300	7.500	7.400	2.305
Area Averaged Values			=			0.04	0.78	0.83	8.04	7.72	7.86	7.35

Exerimental Condition for Churn flow: Run 1 at Port3 (L/D=217)

Experimental Conditions:		$j_{g,inlet}[m/s]=$	6.99	loc. press. [psi]= 13.146		Probe Configuration [mm]	
$Q_g[ml/min]=$	88.00	$j_{g,local}\ [m/s]=$	7.82	N_{sample};	8000	$S_{01}=$	0.84
$P_{back}[psi]=$	4.50	$j_{f,inlet}\ [m/s]=$	0.06	f_{sample};	40000		

$<<v_g>>=$	7.746	m/s	$<\alpha><<v_g>>=$	5.996	m/s	Percent difference between $<j_g>_z$ and $<\alpha>_z<<v_g>>_z=$	23.34 %

Probe Position		No. Loops	Δt_{total}	Bubble Number		α		Void fraction	v_{g1}	v_{g2}	$v_{g.avg}$	$\alpha_1 v_1 + \alpha_2 v_2$
r [mm]	r/R	N_{total}	[sec]	N_1	N_2	α_1	α_2	α total	[m/s]	[m/s]	[m/s]	[m/s]
0.00	0.00	40	8.000	1121	211	0.003	0.900	0.903	8.6	8.200	8.4	7.406
										8.100		
1.27	0.20	40	8.000	1100	215	0.001	0.910	0.911	8.5		8.4	7.380
2.54	0.40	40	8.000	1101	203	0.005	0.900	0.905	8.5	7.600	8.05	6.883
3.18	0.50	40	8.000	1002	191	0.010	0.920	0.930	7.8	7.400	7.61	6.886
3.81	0.60	40	8.000	995	188	0.040	0.890	0.930	7.3	6.720	7.01	6.273
4.45	0.70	40	8.000	870	111	0.042	0.780	0.822	6.5	6.700	6.6	5.499
5.09	0.80	40	8.000	687	81	0.085	0.444	0.529	6.8	6.400	6.61	3.420
5.72	0.90	40	8.000	599	45	0.070	0.150	0.220	6.780	6.600	6.658	1.465
Area Averaged Values			=			0.01	0.76	0.77	7.16	6.77	7.01	6.00

Experimental Conditions:		$j_{g,inlet}$ [m/s] =	0.19	loc. press. [psi]=	4.27	Probe Configuration [mm]					
Q_g [ml/min]=	31.00	$j_{g,local}$ [m/s] =	0.15	N_{sample};	8000	S_{01} =	2.04	S_{02} =	1.94	S_{03} =	1.96
P_{back} [psi]=	7.50	$j_{f,inlet}$ [m/s] =	0.40	f_{sample};	8000	S_{12} =	0.48	S_{13} =	0.19	S_{23} =	0.43

$<<v_g>>=$	0.755	m/s	$<\alpha><<v_g>>=$		0.172	m/s	Percent difference between $<j_g>_z$ and $<\alpha>_z<<v_g>>_z=$		14.22	%

Probe Position		No. Loops	Δt_{total}	Bubble Number		α		a_i [1/m]		Total		v_{g1}	v_{g2}	$v_{g.avg}$	D_{sm1}	$\alpha_1 v_1 + \alpha_2 v_2$
r [mm]	r/R	N_{total}	[sec]	N_1	N_2	α_1	α_2	a_{i1}	$a_{i\,2}$	α_{Tot}	a_{iTot}	[m/s]	[m/s]	[m/s]	[cm]	[m/s]
0.00	0.00	30	30.000	2749	92	0.290	0.032	550.000	18.570	0.322	568.57	0.784	0.73	0.784	0.316	0.251
											543.24				0.289	
1.27	0.20	30	30.000	2870	103	0.250	0.036	519.860	23.380	0.286		0.767	0.74	0.767		0.218
2.54	0.40	30	30.000	2757	88	0.240	0.031	510.290	22.700	0.271	532.99	0.749	0.74	0.749	0.282	0.203
3.18	0.50	30	30.000	2577	83	0.210	0.028	485.770	19.260	0.238	505.03	0.735	0.72	0.735	0.259	0.175
3.81	0.60	30	30.000	2297	29	0.180	0.011	460.000	10.700	0.191	470.70	0.691	0.68	0.691	0.235	0.132
4.45	0.70	30	30.000	2001	16	0.160	0.005	387.050	4.770	0.165	391.82	0.721	0.72	0.721	0.248	0.119
5.09	0.80	30	30.000	1579	64	0.100	0.016	214.300	66.900	0.116	281.20	0.72	0.69	0.72	0.280	0.083
5.72	0.90	30	30.000	1300	21	0.090	0.020	200.00	21.00	0.110	221.00	0.680	0.590	0.680	0.270	0.073
Area Averaged Values			=													
						0.20	0.03	429.37	19.92	0.23	449.29	0.66	0.64	0.66	0.25	0.17

Experimental Conditions:		$j_{g,inlet}[m/s] =$	3.17	loc. press. [psi]=	8.53	Probe Configuration [mm]					
$Q_g[ml/min]=$	31.00	$j_{g,local}[m/s] =$	2.00	N_{sample};	8000	$S_{01} =$	2.04	$S_{02} =$	1.94	$S_{03} =$	1.96
$P_{back}[psi]=$	17.00	$j_{f,inlet}[m/s] =$	3.00	f_{sample};	15000	$S_{12} =$	0.48	$S_{13} =$	0.19	$S_{23} =$	0.43

$<<v_g>>=$	5.368	m/s	$<\alpha><<v_g>>=$	2.172	m/s	Percent difference between $<j_g>_z$ and $<\alpha>_z<<v_g>>_z =$	8.42	%

Probe Position		No. Loops	Δt_{total}	Bubble Number		α		a_i [1/m]		Total		v_{g1}	v_{g2}	$v_{g.avg}$	D_{sm1}	$\alpha_1v_1+\alpha_2v_2$
R [mm]	r/R	N_{total}	[sec]	N_1	N_2	α_1	α_2	a_{i1}	$a_{i\,2}$	α_{Tot}	a_{iTot}	[m/s]	[m/s]	[m/s]	[cm]	[m/s]
	0.00	12	12.000	2182	163	0.110	0.361	213.40	34.50	0.471	247.90	5.600	5.400	5.560	0.309	2.565
											280.70				0.262	
1.27	0.20	12	12.000	2309	148	0.111	0.360	254.10	26.60	0.471		6.230	5.300	6.210		2.600
2.54	0.40	12	12.000	2367	144	0.120	0.350	264.40	29.90	0.470	294.30	6.270	5.010	6.200	0.272	2.506
3.18	0.50	12	12.000	2700	170	0.135	0.326	320.20	37.50	0.461	357.70	5.930	4.410	5.840	0.253	2.238
3.81	0.60	12	12.000	2923	200	0.157	0.294	386.20	56.70	0.451	442.90	5.370	4.600	5.270	0.244	2.195
4.45	0.70	12	12.000	5991	600	0.240	0.160	512.00	60.00	0.400	572.00	5.600	5.300	4.710	0.281	2.192
5.09	0.80	12	12.000	5902	450	0.280	0.140	480.00	56.00	0.420	536.00	5.400	4.900	5.250	0.350	2.198
5.72	0.90	12	12.000	5845	312	0.158	0.084	293.37	32.05	0.242	325.42	5.040	4.600	5.180	0.323	1.183
Area Averaged Values	=					0.12	0.29	257.71	31.21	0.40	288.92	5.22	4.52	5.14	0.24	2.17

66

Exerimental Condition: Run 7 at Port3 (L/D=217)

Experimental Conditions:		$j_{g,inlet}$ [m/s] =	0.71	loc. press. [psi]=	2.73	Probe Configuration [mm]					
Q_g[ml/min]=	8.50	$j_{g,local}$ [m/s] =	0.60	N_{sample}:	8000	S_{01} =	2.04	S_{02} =	1.94	S_{03} =	1.96
P_{back}[psi]=	6.50	$j_{f,inlet}$ [m/s] =	0.40	f_{sample}:	8000	S_{12} =	0.48	S_{13} =	0.19	S_{23} =	0.43

$<<v_g>>$= 0.734	m/s	$<\alpha><<v_g>>$=	0.471	m/s	Percent difference between $<j_g>_z$ and $<\alpha>_z<<v_g>>_z$ =	21.38	%

Probe Position		No. Loops	Δt_{total}	Bubble Number		α		a_i [1/m]		Total		v_{g1}	v_{g2}	$v_{g.avg}$	D_{sm1}	$\alpha_1 v_1 + \alpha_2 v_2$
r [mm]	r/R	N_{total}	[sec]	N_1	N_2	α_1	α_2	a_{i1}	a_{i2}	α_{Tot}	a_{iTot}	[m/s]	[m/s]	[m/s]	[cm]	[m/s]
	0.00	20	20.000	3960	546	0.536	0.200	602.120	128.180	0.736	730.30	0.73	0.68	0.73	0.534	0.527
											725.01				0.561	
1.27	0.20	20	20.000	3856	523	0.558	0.230	597.180	127.830	0.788		0.767	0.73	0.75		0.596
2.54	0.40	20	20.000	3679	600	0.548	0.250	593.350	137.690	0.798	731.04	0.76	0.74	0.75	0.554	0.601
3.18	0.50	20	20.000	3459	715	0.491	0.215	528.650	185.970	0.706	714.62	0.79	0.73	0.79	0.557	0.545
3.81	0.60	20	20.000	3209	705	0.446	0.207	496.290	185.830	0.653	682.12	0.632	0.63	0.62	0.539	0.412
4.45	0.70	20	20.000	3080	423	0.392	0.200	468.180	132.490	0.592	600.67	0.721	0.69	0.71	0.502	0.421
5.09	0.80	20	20.000	2773	174	0.298	0.150	357.000	81.310	0.448	438.31	0.74	0.71	0.73	0.501	0.327
5.72	0.90	20	20.000	1300	211	0.250	0.130	220.00	65.00	0.380	285.00	0.770	0.640	0.780	0.682	0.276
Area Averaged Values		=				0.45	0.19	492.18	118.70	0.64	610.88	0.65	0.62	0.64	0.48	0.47

Exerimental Condition: Run 2 at Port3 (L/D=217)

Experimental Conditions:		$j_{g,inlet}[m/s] =$	0.20	loc. Press. [psi]=	2.85	Probe Configuration [mm]					
$Q_g[ml/min]=$	31.00	$j_{g,local} [m/s] =$	0.16	N_{sample}:	8000	$S_{01} =$	2.37	$S_{02} =$	2.38	$S_{03} =$	2.48
$P_{back}[psi]=$	7.80	$j_{f,inlet} [m/s] =$	1.00	f_{sample}:	10000	$S_{12} =$	0.50	$S_{13} =$	0.61	$S_{23} =$	0.46

Probe Position		No. Loops	Δt_{total}	Bubble Number		α		a_i [1/m]		Total		v_{g1}	v_{g2}	$v_{g,avg}$	D_{sm1}	$\alpha_1 v_1 + \alpha_2 v_2$
r [mm]	r/R	N_{total}	[sec]	N_1	N_2	α_1	α_2	a_{i1}	$a_{i\,2}$	α_{Tot}	a_{iTot}	[m/s]	[m/s]	[m/s]	[cm]	[m/s]
0.00	0.00	50	40.000	1513	0	0.070	0.000	121.60	0.00	0.070	121.60	1.280	0.000	1.280	0.345	0.090
											146.50				0.332	
1.27	0.20	50	40.000	1805	0	0.081	0.000	146.50	0.00	0.081		1.270	0.000	1.270		0.103
2.54	0.40	50	40.000	3083	0	0.137	0.000	261.70	0.00	0.137	261.70	1.220	0.000	1.220	0.314	0.167
3.18	0.50	50	40.000	3901	0	0.181	0.000	341.50	0.00	0.181	341.50	1.180	0.000	1.180	0.318	0.214
3.81	0.60	50	40.000	4300	0	0.210	0.000	381.10	0.00	0.210	381.10	1.170	0.000	1.170	0.331	0.246
4.45	0.70	50	40.000	4106	0	0.199	0.000	367.04	0.00	0.199	367.04	1.150	0.000	1.150	0.325	0.229
5.09	0.80	50	40.000	3145	0	0.150	0.000	298.00	0.00	0.150	298.00	1.160	0.000	1.160	0.302	0.174
5.72	0.90	50	40.000	3160	0	0.130	0.000	270.40	0.00	0.130	270.40	1.167	0.000	1.167	0.288	0.152
Area Averaged Values		=				0.10	0.00	183.93	0.00	0.10	183.93	1.09	0.00	1.09	0.29	0.12

Exerimental Condition: Run 4 at Port3 (L/D=217)

Experimental Conditions:		$j_{g,inlet}[m/s]$ =	1.26	loc. press. [psi]=	7.64	Probe Configuration [mm]					
$Q_v[ml/min]$=	13.00	$j_{g,local}[m/s]$ =	0.83	N_{sample}:	8000	S_{01} =	2.04	S_{02} =	1.94	S_{03} =	1.96
$P_{back}[psi]$=	14.00	$j_{f,inlet}[m/s]$ =	3.00	f_{sample}:	15000	S_{12} =	0.48	S_{13} =	0.19	S_{23} =	0.43

$<<v_g>>$=	4.381	m/s	$<\alpha><<v_g>>$=	0.922	m/s	Percent difference between $<j_g>_z$ and $<\alpha>_z<<v_g>>_z$ =	10.95	%

Probe Position		No. Loops	Δt_{total}	Bubble Number		α		a_i [1/m]		Total		v_{g1}	v_{g2}	$v_{g,avg}$	D_{sm1}	$\alpha_1 v_1 + \alpha_2 v_2$
r [mm]	r/R	N_{total}	[sec]	N_1	N_2	α_1	α_2	a_{i1}	a_{i2}	α_{tot}	$a_{i,tot}$	[m/s]	[m/s]	[m/s]	[cm]	[m/s]
	0.00	12	12.000	2176	297	0.090	0.182	318.70	71.40	0.272	390.10	4.550	4.300	4.520	0.169	1.192
											446.80				0.150	
1.27	0.20	12	12.000	2578	325	0.095	0.178	380.00	66.80	0.273		4.620	4.230	4.580		1.192
2.54	0.40	12	12.000	2346	190	0.189	0.097	376.20	39.60	0.286	415.80	4.260	4.500	4.220	0.301	1.242
3.18	0.50	12	12.000	2009	134	0.140	0.057	281.40	37.60	0.197	319.00	5.000	4.580	4.970	0.299	0.962
3.81	0.60	12	12.000	1540	84	0.093	0.046	242.20	27.70	0.139	269.90	4.480	3.990	4.460	0.230	0.598
4.45	0.70	12	12.000	1265	82	0.074	0.055	226.50	99.10	0.128	325.60	4.300	3.800	3.890	0.195	0.524
5.09	0.80	12	12.000	750	128	0.041	0.110	88.30	79.40	0.151	167.70	4.700	4.530	5.890	0.279	0.691
5.72	0.90	12	12.000	460	30	0.019	0.052	57.90	35.00	0.070	92.90	4.870	4.590	5.870	0.194	0.328
Area Averaged Values	=					0.09	0.12	284.05	53.79	0.21	337.85	4.02	3.74	4.04	0.17	0.92

Exerimental Condition: Run 3 at Port3 (L/D=217)

Experimental Conditions:		$j_{g.inlet}[m/s] =$	0.22	Loc. Press. [psi]=	7.43	Probe Configuration [mm]					
$Q_g[ml/min]=$	31.00	$j_{g.local}[m/s] =$	0.15	N_{sample}:	8000	$S_{01} =$	2.04	$S_{02} =$	1.94	$S_{03} =$	1.96
$P_{back}[psi]=$	14.50	$j_{f.inlet}[m/s] =$	3.00	f_{sample}:	15000	$S_{12} =$	0.48	$S_{13} =$	0.19	$S_{23} =$	0.43

$<<v_g>> =$	3.014	m/s	$<\alpha><<v_g>> =$	0.202	m/s	Percent difference between $<j_g>_i$ and $<\alpha>_i<<v_g>>_i =$	36.02	%

Probe Position		No. Loops	Δt_{total}	Bubble Number		α		a_i [1/m]		Total		v_{g1}	v_{g2}	$v_{g.avg}$	D_{sm1}	$\alpha_1v_1+\alpha_2v_2$
r [mm]	r/R	N_{total}	[sec]	N_1	N_2	α_1	α_2	a_{i1}	a_{i2}	α_{Tot}	a_{iTot}	[m/s]	[m/s]	[m/s]	[cm]	[m/s]
0.00	0.00	12	12.000	1406	0	0.090	0.000	126.70	0.00	0.090	126.70	2.750	0.000	2.750	0.426	0.248
											185.00				0.324	
1.27	0.20	12	12.000	1500	0	0.100	0.000	185.00	0.00	0.100		3.100	0.000	3.100		0.310
2.54	0.40	12	12.000	960	0	0.068	0.000	98.00	0.00	0.068	98.00	2.800	0.000	2.800	0.417	0.191
3.18	0.50	12	12.000	955	0	0.040	0.000	72.00	0.00	0.040	72.00	3.200	0.000	3.200	0.333	0.128
3.81	0.60	12	12.000	712	0	0.034	0.000	50.40	0.00	0.034	50.40	3.100	0.000	3.100	0.405	0.105
4.45	0.70	12	12.000	762	0	0.025	0.000	32.90	0.00	0.025	32.90	3.200	0.000	3.200	0.456	0.080
5.09	0.80	12	12.000	669	0	0.015	0.000	27.00	0.00	0.015	27.00	2.900	0.000	2.900	0.333	0.044
5.72	0.90	12	12.000	693	0	0.010	0.000	26.00	0.00	0.010	26.00	3.600	0.000	3.600	0.231	0.036
Area Averaged Values =						0.07	0.00	114.36	0.00	0.07	114.36	2.66	0.00	2.66	0.32	0.20

Exerimental Condition: Run 5 at Port3 (L/D=217)

Experimental Conditions:		$j_{g,inlet}[m/s] =$	0.75	loc. press. [psi]=	5.32	Probe Configuration [mm]					
$Q_g[ml/min]=$	8.50	$j_{g,local}[m/s] =$	0.55	N_{sample}:	8000	$S_{01} =$	2.04	$S_{02} =$	1.94	$S_{03} =$	1.96
$P_{back}[psi]=$	9.00	$j_{f,inlet}[m/s] =$	1.00	f_{sample}:	10000	$S_{12} =$	0.48	$S_{13} =$	0.19	$S_{23} =$	0.43

$<<v_r>>=$	1.469	m/s	$<\alpha><<v_r>>=$	0.588	m/s	Percent difference between $<j_g>$ and $<\alpha>\cdot<<v_r>>_i =$	6.66	%

Probe Position		No. Loops	Δt_{total}	Bubble Number		α		a_i [1/m]		Total		v_{g1}	v_{g2}	$v_{g.avg}$	D_{sm1}	$\alpha_1v_1+\alpha_2v_2$
r [mm]	r/R	N_{total}	[sec]	N_1	N_2	α_1	α_2	a_{i1}	$a_{i\,2}$	α_{Tot}	a_{iTot}	[m/s]	[m/s]	[m/s]	[cm]	[m/s]
	0.00	30	30.000	6229	1060	0.320	0.305	493.500	157.100	0.625	650.60	1.630	1.580	1.630	0.389	1.004
											668.30				0.353	
1.27	0.20	30	30.000	6362	923	0.310	0.194	526.700	141.600	0.504		1.510	1.500	1.510		0.759
2.54	0.40	30	30.000	6038	830	0.280	0.180	513.000	122.600	0.460	635.60	1.370	1.360	1.370	0.327	0.628
3.18	0.50	30	30.000	5556	812	0.200	0.176	476.300	129.400	0.376	605.70	1.250	1.200	1.240	0.252	0.461
3.81	0.60	30	30.000	5332	527	0.180	0.112	420.000	114.100	0.292	534.10	1.200	1.300	1.250	0.257	0.362
4.45	0.70	30	30.000	4304	364	0.190	0.076	350.200	90.260	0.266	440.46	1.250	1.280	1.270	0.326	0.335
5.09	0.80	30	30.000	3394	100	0.164	0.021	305.900	54.500	0.185	360.40	1.190	1.200	1.950	0.322	0.220
5.72	0.90	30	30.000	3320	60	0.100	0.015	200.00	35.00	0.115	235.00	1.200	1.150	1.180	0.300	0.137
Area Averaged Values	=					0.24	0.16	423.76	114.38	0.40	538.14	1.26	1.26	1.31	0.30	0.59

Experimental Conditions:		$j_{g,inlet}[m/s] =$	0.07	loc. press. [psi]=	5.34	Probe Configuration [mm]					
$Q_g[ml/min]=$	75.00	$j_{g,local}[m/s] =$	0.05	N_{sample}:	8000	$S_{01} =$	2.63	$S_{02} =$	2.76	$S_{03} =$	2.69
$P_{back}[psi]=$	8.50	$j_{f,inlet}[m/s] =$	0.40	f_{sample}:	8000	$S_{12} =$	0.24	$S_{13} =$	0.23	$S_{23} =$	0.43

$<<v_g>>= $ 0.665 m/s	$<\alpha><<v_g>>= $ 0.062 m/s	Percent difference between $<j_g>_z$ and $<\alpha>_z<<v_g>>_z =$	16.66	%

Probe Position		No. Loops	Δt_{total}	Bubble Number		α		a_i [1/m]		Total		v_{g1}	v_{g2}	$v_{g,avg}$	D_{sm1}	$\alpha_1 v_1 + \alpha_2 v_2$
r [mm]	r/R	N_{total}	[sec]	N_1	N_2	α_1	α_2	a_{i1}	$a_{i\,2}$	α_{Tot}	a_{iTot}	[m/s]	[m/s]	[m/s]	[cm]	[m/s]
	0.00	40	40.000	1641	0	0.120	0.000	253.280	0.00	0.120	253.28	0.674	0.000	0.674	0.284	0.081
											257.99				0.302	
1.27	0.20	40	40.000	1681	0	0.130	0.000	257.990	0.00	0.130		0.682	0.000	0.682		0.089
2.54	0.40	40	40.000	1654	0	0.110	0.000	257.740	0.00	0.110	257.74	0.6608	0.000	0.6608	0.256	0.073
3.18	0.50	40	40.000	1517	0	0.100	0.000	232.400	0.00	0.100	232.40	0.6798	0.000	0.6798	0.258	0.068
3.81	0.60	40	40.000	1077	0	0.056	0.000	101.900	0.00	0.056	101.90	0.53	0.000	0.53	0.330	0.030
4.45	0.70	40	40.000	1072	0	0.040	0.000	141.730	0.00	0.040	141.73	0.53	0.000	0.53	0.169	0.021
5.09	0.80	40	40.000	793	0	0.032	0.000	86.440	0.00	0.032	86.44	0.65	0.000	0.65	0.222	0.021
5.72	0.90	40	40.000	689	0	0.040	0.000	75.00	0.00	0.040	75.00	0.600	0.000	0.600	0.320	0.024
Area Averaged Values			=													
						0.09	0.00	193.82	0.00	0.09	193.82	0.57	0.00	0.57	0.25	0.06

Exerimental Condition: Run 8 at Port2 (L/D=120)

Experimental Conditions:		$j_{g,inlet}[m/s] =$	3.17	loc. press. [psi]=	14.369	Probe Configuration [mm]					
$Q_g[ml/min]=$	31.00	$j_{g,local}[m/s] =$	1.60	N_{sample}:	8000	$S_{01} =$	2.04	$S_{02} =$	0.94	$S_{03} =$	1.96
$P_{back}[psi]=$	17.00	$j_{f,inlet}[m/s] =$	3.00	f_{sample}:	15000	$S_{12} =$	0.48	$S_{13} =$	0.19	$S_{23} =$	0.43

$<<v_g>>=$	5.084	m/s	$<\alpha><<v_g>>=$	1.914	m/s	Percent difference between $<j_g>_z$ and $<\alpha>_z<<v_g>>_z =$	19.57	%

Probe Position		No. Loops	Δt_{total}	Bubble Number		α		a_i [1/m]		Total		v_{g1}	v_{g2}	$v_{g.avg}$	D_{sm1}	$\alpha_1 v_1 + \alpha_2 v_2$
r [mm]	r/R	N_{total}	[sec]	N_1	N_2	α_1	α_2	a_{i1}	a_{i2}	α_{Tot}	a_{iTot}	[m/s]	[m/s]	[m/s]	[cm]	[m/s]
	0.00	12	12.000	1900	202	0.090	0.393	182.10	65.70	0.483	247.80	5.820	5.580	5.540	0.297	2.717
											291.60				0.205	
1.27	0.20	12	12.000	2088	142	0.090	0.385	263.40	28.20	0.475		5.620	5.220	5.590		2.516
2.54	0.40	12	12.000	1959	122	0.104	0.347	275.20	34.50	0.451	309.70	4.980	4.220	4.920	0.227	1.982
3.18	0.50	12	12.000	1742	166	0.090	0.339	252.10	42.10	0.429	294.20	4.840	4.370	4.920	0.213	1.916
3.81	0.60	12	12.000	1750	196	0.092	0.293	247.70	76.10	0.385	323.80	5.020	4.000	4.790	0.223	1.634
4.45	0.70	12	12.000	1916	202	0.080	0.150	298.00	94.00	0.230	392.00	4.710	4.370	4.900	0.161	1.032
5.09	0.80	12	12.000	1658	151	0.060	0.090	206.00	254.40	0.150	460.40	4.700	4.450	4.600	0.175	0.681
5.72	0.90	12	12.000	1510	161	0.040	0.102	191.00	187.40	0.142	378.40	5.800	5.000	5.990	0.126	0.742
Area Averaged Values	=					0.08	0.30	217.59	51.53	0.38	269.12	4.74	4.32	4.67	0.19	1.91

Experimental Conditions:		$j_{g.inlet}[m/s] =$	0.71	loc. press. [psi]=	3.329	Probe Configuration [mm]					
$Q_g[ml/min]=$	8.50	$j_{g.local}[m/s] =$	0.58	N_{sample}:	8000	$S_{01} =$	2.04	$S_{02} =$	1.94	$S_{03} =$	1.96
$P_{back}[psi]=$	6.50	$j_{f.inlet}[m/s] =$	1.00	f_{sample}:	8000	$S_{12} =$	0.48	$S_{13} =$	0.19	$S_{23} =$	0.43

$<<v_g>>=$	0.889	m/s	$<\alpha><<v_g>>=$	0.471	m/s	Percent difference between $<j_g>_z$ and $<\alpha>_z<<v_g>>_z =$	18.69	%

Probe Position		No. Loops	Δt_{total}	Bubble Number		α		a_i [1/m]		Total		v_{g1}	v_{g2}	$v_{g.avg}$	D_{sm1}	$\alpha_1 v_1 + \alpha_2 v_2$
r [mm]	r/R	N_{total}	[sec]	N_1	N_2	α_1	α_2	a_{i1}	$a_{i\,2}$	α_{Tot}	a_{iTot}	[m/s]	[m/s]	[m/s]	[cm]	[m/s]
	0.00	15	15.000	2277	47	0.560	0.050	592.90	0.00	0.610	592.90	0.800	0.000	0.710	0.567	0.448
0.20										612.10						
	15	15.000	2242	22	0.600	0.040	612.10	0.00	0.640	1.100	0.000	0.711	0.588		0.660
2.54	0.40	15	15.000	2174	21	0.620	0.050	651.80	0.00	0.670	651.80	0.705	0.000	0.705	0.571	0.437
3.18	0.50	15	15.000	1958	19	0.610	0.030	640.00	0.00	0.640	640.00	0.850	0.000	0.690	0.572	0.519
3.81	0.60	15	15.000	1731	23	0.550	0.023	609.40	0.00	0.573	609.40	0.780	0.000	0.620	0.542	0.429
4.45	0.70	15	15.000	1272	32	0.480	0.023	497.20	0.00	0.503	497.20	0.880	0.000	0.624	0.579	0.422
5.09	0.80	15	15.000	695	15	0.320	0.010	289.90	0.00	0.330	289.90	0.780	0.000	0.595	0.662	0.250
5.72	0.90	15	15.000	421	11	0.240	0.010	280.00	0.00	0.250	280.00	0.780	0.000	0.688	0.514	0.187
Area Averaged Values		=														
						0.50	0.03	515.78	0.00	0.53	515.78	0.83	0.00	0.60	0.51	0.47

Experimental Conditions:		$j_{g,inlet}[m/s] =$	1.26	loc. press. [psi]=	9.214	Probe Configuration [mm]					
$Q_g[ml/min]=$	13.00	$j_{g,local}$ [m/s] =	0.78	$N_{sample;}$	8000	$S_{01} =$	2.04	$S_{02} =$	1.94	$S_{03} =$	1.96
$P_{back}[psi]=$	14.00	$j_{f,inlet}$ [m/s] =	3.00	$f_{sample;}$	15000	$S_{12} =$	0.48	$S_{13} =$	0.19	$S_{23} =$	0.43

$<<v_g>>=$	1.842	m/s	$<\alpha><<v_g>>=$	0.619	m/s	Percent difference between $<j_g>_z$ and $<\alpha>_z<<v_g>>_z =$	20.31	%

Probe Position		No. Loops	Δt_{total}	Bubble Number		α		a_i [1/m]		Total		v_{g1}	v_{g2}	$v_{g,avg}$	D_{sm1}	$\alpha_1 v_1 + \alpha_2 v_2$
r [mm]	r/R	N_{total}	[sec]	N_1	N_2	α_1	α_2	a_{i1}	$a_{i\,2}$	α_{Tot}	a_{iTot}	[m/s]	[m/s]	[m/s]	[cm]	[m/s]
0.00	0.00	12	12.000	1912	253	0.200	0.255	281.10	58.40	0.455	339.50	4.660	0.000	4.660	0.427	0.932
											396.70				0.306	
1.27	0.20	12	12.000	2089	273	0.170	0.270	333.50	63.20	0.440		4.230	0.000	4.230		0.719
2.54	0.40	12	12.000	1905	239	0.180	0.224	298.40	71.90	0.404	370.30	4.410	0.000	4.410	0.362	0.794
3.18	0.50	12	12.000	1768	201	0.140	0.170	302.00	72.00	0.310	374.00	4.090	0.000	4.090	0.278	0.573
3.81	0.60	12	12.000	1685	151	0.130	0.115	303.40	59.20	0.245	362.60	4.000	0.000	4.000	0.257	0.520
4.45	0.70	12	12.000	1286	136	0.120	0.086	174.90	93.00	0.206	267.90	4.300	0.000	5.390	0.412	0.516
5.09	0.80	12	12.000	1200	60	0.110	0.070	150.00	45.00	0.180	195.00	4.500	0.000	5.270	0.440	0.495
5.72	0.90	12	12.000	678	67	0.090	0.058	95.60	38.00	0.148	133.60	4.800	0.000	5.750	0.565	0.432
Area Averaged Values		=				0.14	0.19	261.64	55.57	0.34	317.21	3.78	0.00	3.87	0.30	0.62

Experimental Conditions:		$j_{g,inlet}[m/s] =$	0.75	loc. press. [psi]=	5.434	Probe Configuration [mm]					
$Q_g[ml/min]=$	8.50	$j_{g,local}[m/s] =$	0.55	N_{sample}:	8000	$S_{01} =$	2.04	$S_{02} =$	1.94	$S_{03} =$	1.96
$P_{back}[psi]=$	9.00	$j_{l,inlet}[m/s] =$	1.00	f_{sample}:	10000	$S_{12} =$	0.48	$S_{13} =$	0.19	$S_{23} =$	0.43

$<<v_g>>=$	1.416	m/s	$<\alpha><<v_g>>=$	0.410	m/s	Percent difference between $<j_g>$ and $<\alpha>_z<<v_{gz}>>_z =$	25.21	%

Probe Position		No. Loops	Δt_{total}	Bubble Number		α		a_i [1/m]		Total		v_{g1}	v_{g2}	$v_{g.avg}$	D_{sm1}	$\alpha_1 v_1 + \alpha_2 v_2$
r [mm]	r/R	N_{total}	[sec]	N_1	N_2	α_1	α_2	a_{i1}	a_{i2}	α_{tot}	a_{itot}	[m/s]	[m/s]	[m/s]	[cm]	[m/s]
	0.00	11	11.000	1842	62	0.355	0.079	584.60	17.10	0.434	601.70	1.510	1.500	1.510	0.364	0.655
											633.10				0.335	
1.27	0.20	11	11.000	1866	47	0.346	0.048	620.10	13.00	0.394		1.440	1.510	1.440		0.570
2.54	0.40	11	11.000	1388	27	0.228	0.027	523.60	10.20	0.255	533.80	1.270	1.200	1.270	0.261	0.322
3.18	0.50	11	11.000	990	12	0.200	0.015	385.60	10.00	0.215	395.60	1.240	1.020	1.230	0.311	0.263
3.81	0.60	11	11.000	1459	36	0.120	0.020	198.50	13.00	0.140	211.50	1.130	1.100	1.130	0.363	0.158
4.45	0.70	11	11.000	1130	34	0.090	0.036	170.00	18.00	0.126	188.00	1.390	1.250	1.390	0.318	0.170
5.09	0.80	11	11.000	1258	30	0.060	0.232	105.00	64.00	0.292	169.00	1.400	1.300	1.350	0.343	0.386
5.72	0.90	11	11.000	1880	55	0.050	0.030	95.00	45.00	0.080	140.00	1.350	1.500	1.410	0.316	0.113
Area Averaged Values =						0.24	0.05	431.42	14.77	0.29	446.19	1.22	1.22	1.22	0.29	0.41

Experimental Conditions:		$j_{g,inlet}[m/s] =$	0.19	loc. press. [psi]=	4.557	Probe Configuration [mm]					
$Q_g[ml/min]=$	31.00	$j_{g,local}$ [m/s] =	0.15	N_{sample}:	8000	$S_{01} =$	2.04	$S_{02} =$	1.94	$S_{03} =$	1.96
$P_{back}[psi]=$	7.50	$j_{f,inlet}$ [m/s] =	0.40	f_{sample}:	8000	$S_{12} =$	0.48	$S_{13} =$	0.19	$S_{23} =$	0.43

$<<v_g>>= 0.697$	m/s	$<\alpha><<v_g>>=$	0.139	m/s	Percent difference between $<j_g>_z$ and $<\alpha>_z<<v_g>>_z =$	6.73	%

Probe Position		No. Loops	Δt_{total}	Bubble Number		α		a_i [1/m]		Total		v_{g1}	v_{g2}	$v_{g,avg}$	D_{sm1}	$\alpha_1 v_1 + \alpha_2 v_2$
r [mm]	r/R	N_{total}	[sec]	N_1	N_2	α_1	α_2	a_{i1}	a_{i2}	α_{Tot}	a_{iTot}	[m/s]	[m/s]	[m/s]	[cm]	[m/s]
0.00	0.00	20	20.000	1719	0	0.280	0.000	509.10	0.00	0.280	509.10	0.710	0.000	0.710	0.330	0.199
											509.30				0.306	
1.27	0.20	20	20.000	1723	0	0.260	0.000	509.30	0.00	0.260		0.711	0.000	0.711		0.185
2.54	0.40	20	20.000	1764	0	0.220	0.000	526.30	0.00	0.220	526.30	0.705	0.000	0.705	0.251	0.155
3.18	0.50	20	20.000	1766	0	0.190	0.000	536.40	0.00	0.190	536.40	0.690	0.000	0.690	0.213	0.131
3.81	0.60	20	20.000	1582	0	0.130	0.000	506.40	0.00	0.130	506.40	0.620	0.000	0.620	0.154	0.081
4.45	0.70	20	20.000	1445	0	0.160	0.000	489.90	0.00	0.160	489.90	0.624	0.000	0.624	0.196	0.100
5.09	0.80	20	20.000	1194	0	0.110	0.000	405.90	0.00	0.110	405.90	0.595	0.000	0.595	0.163	0.065
5.72	0.90	20	20.000	743	0	0.094	0.000	239.10	0.00	0.094	239.10	0.688	0.000	0.688	0.236	0.065
Area Averaged Values		=														
						0.20	0.00	441.84	0.00	0.20	441.84	0.60	0.00	0.60	0.24	0.14

Experimental Conditions:		$j_{g,inlet}[m/s] =$	0.22	loc. press. [psi]=	8.876	Probe Configuration [mm]					
$Q_g[ml/min]=$	31.00	$j_{g,local}\ [m/s] =$	0.14	N_{sample}:	8000	$S_{01} =$	2.04	$S_{02} =$	1.94	$S_{03} =$	1.96
$P_{back}[psi]=$	14.50	$j_{f,inlet}\ [m/s] =$	3.00	f_{sample}:	15000	$S_{12} =$	0.48	$S_{13} =$	0.19	$S_{23} =$	0.43

$<<v_g>> =$ 3.265	m/s	$<\alpha><<v_g>> =$	0.208	m/s	Percent difference between $<j_g>_z$ and $<\alpha>_z<<v_g>>_z =$	49.12	%

Probe Position		No. Loops	Δt_{total}	Bubble Number		α		$a_i\ [1/m]$		Total		v_{g1}	v_{g2}	$v_{g,avg}$	D_{sm1}	$\alpha_1 v_1 + \alpha_2 v_2$
r [mm]	r/R	N_{total}	[sec]	N_1	N_2	α_1	α_2	a_{i1}	$a_{i\,2}$	α_{Tot}	a_{iTot}	[m/s]	[m/s]	[m/s]	[cm]	[m/s]
0.00	0.00	33	33.000	3263	0	0.100	0.000	203.40	0.00	0.100	203.40	3.500	0.000	3.500	0.295	0.350
											211.60				0.255	
1.27	0.20	33	33.000	3260	0	0.090	0.000	211.60	0.00	0.090		3.300	0.000	3.300		0.297
2.54	0.40	33	33.000	2578	0	0.050	0.000	174.40	0.00	0.050	174.40	3.000	0.000	3.000	0.172	0.150
3.18	0.50	33	33.000	1937	0	0.040	0.000	136.90	0.00	0.040	136.90	3.100	0.000	3.100	0.175	0.124
3.81	0.60	33	33.000	1459	0	0.040	0.000	106.50	0.00	0.040	106.50	2.800	0.000	2.800	0.225	0.112
4.45	0.70	33	33.000	933	0	0.035	0.000	64.60	0.00	0.035	64.60	2.700	0.000	2.700	0.325	0.095
5.09	0.80	33	33.000	579	0	0.015	0.000	40.00	0.00	0.015	40.00	2.780	0.000	2.780	0.221	0.041
5.72	0.90	33	33.000	408	0	0.013	0.000	20.00	0.00	0.013	20.00	2.800	0.000	2.800	0.378	0.035
Area Averaged Values		=														
						0.06	0.00	152.11	0.00	0.06	152.11	2.79	0.00	2.79	0.22	0.21

Exerimental Condition: Run 2 at Port2 (L/D=120)

Experimental Conditions:		$j_{g,inlet}[m/s]$ =	0.20	loc. press. [psi]=	2.992	Probe Configuration [mm]					
$Q_g[ml/min]$=	31.00	$j_{g,local}\,[m/s]$ =	0.17	N_{sample};	8000	S_{01} =	2.04	S_{02} =	1.94	S_{03} =	1.96
$P_{back}[psi]$=	9.00	$j_{f,inlet}\,[m/s]$ =	1.00	f_{sample};	10000	S_{12} =	0.48	S_{13} =	0.19	S_{23} =	0.43

$<<v_g>>$= 1.317	m/s	$<\alpha><<v_g>>$=	0.164	m/s	Percent difference between $<j_g>_z$ and $<\alpha>_z<<v_g>>_z$=	1.65	%

Probe Position		No. Loops	Δt_{total}	Bubble Number		α		$a_i\,[1/m]$		Total		v_{g1}	v_{g2}	$v_{g.avg}$	D_{sm1}	$\alpha_1 v_1 + \alpha_2 v_2$
r [mm]	r/R	N_{total}	[sec]	N_1	N_2	α_1	α_2	a_{i1}	$a_{i\,2}$	α_{Tot}	a_{iTot}	[m/s]	[m/s]	[m/s]	[cm]	[m/s]
0.00	0.00	30	30.000	1785	0	0.131	0.000	227.60	0.00	0.131	227.60	1.380	0.000	1.380	0.345	0.181
											260.90				0.336	
1.27	0.20	30	30.000	2004	0	0.146	0.000	260.90	0.00	0.146		1.330	0.000	1.330		0.194
2.54	0.40	30	30.000	2341	0	0.186	0.000	321.90	0.00	0.186	321.90	1.270	0.000	1.270	0.347	0.236
3.18	0.50	30	30.000	2339	0	0.188	0.000	355.20	0.00	0.188	355.20	1.120	0.000	1.120	0.318	0.211
3.81	0.60	30	30.000	2212	0	0.164	0.000	314.40	0.00	0.164	314.40	1.290	0.000	1.290	0.313	0.212
4.45	0.70	30	30.000	1673	0	0.099	0.000	152.40	0.00	0.099	152.40	1.440	0.000	1.440	0.388	0.142
5.09	0.80	30	30.000	1060	0	0.041	0.000	77.70	0.00	0.041	77.70	1.300	0.000	1.900	0.315	0.053
5.72	0.90	30	30.000	1246	0	0.050	0.000	99.70	0.00	0.050	99.70	1.500	0.000	1.700	0.303	0.075
Area Averaged Values		=														
						0.12	0.00	223.66	0.00	0.12	223.66	1.16	0.00	1.20	0.30	0.16

Experimental Conditions:		$j_{g.inlet}[m/s] =$	0.07	loc. press. [psi]= 5.423		Probe Configuration [mm]					
$Q_g[ml/min]=$	75.00	$j_{g.local}[m/s] =$	0.05	N_{sample}:	8000	$S_{01} =$	2.63	$S_{02} =$	2.76	$S_{03} =$	2.69
$P_{back}[psi]=$	8.50	$j_{f.inlet}[m/s] =$	0.41	f_{sample}:	8000	$S_{12} =$	0.24	$S_{13} =$	0.23	$S_{23} =$	0.43

$<<v_g>>= 0.643$ m/s $<\alpha><<v_g>>=$ 0.061 m/s   Percent difference between $<j_g>_z$ and $<\alpha>_z<<v_g>>_z =$ 14.85 %

Probe Position		No. Loops	Δt_{total}	Bubble Number		α		a_i [1/m]		Total		v_{g1}	v_{g2}	$v_{g.avg}$	D_{sm1}	$\alpha_1 v_1 + \alpha_2 v_2$
r [mm]	r/R	N_{total}	[sec]	N_1	N_2	α_1	α_2	a_{i1}	$a_{i\,2}$	α_{Tot}	a_{iTot}	[m/s]	[m/s]	[m/s]	[cm]	[m/s]
0.00	0.00	50	50.000	1798	0	0.110	0.000	226.60	0.00	0.110	226.60	0.660	0.000	0.660	0.291	0.073
											230.80				0.312	
1.27	0.20	50	50.000	1823	0	0.120	0.000	230.80	0.00	0.120		0.660	0.000	0.666		0.079
2.54	0.40	50	50.000	1848	0	0.100	0.000	236.15	0.00	0.100	236.15	0.660	0.000	0.660	0.254	0.066
3.18	0.50	50	50.000	1773	0	0.120	0.000	234.70	0.00	0.120	234.70	0.633	0.000	0.633	0.307	0.076
3.81	0.60	50	50.000	1608	0	0.090	0.000	183.14	0.00	0.090	183.14	0.548	0.000	0.544	0.295	0.049
4.45	0.70	50	50.000	1343	0	0.100	0.000	128.10	0.00	0.100	128.10	0.560	0.000	0.570	0.468	0.056
5.09	0.80	50	50.000	903	0	0.053	0.000	70.00	0.00	0.053	70.00	0.650	0.000	0.690	0.453	0.034
5.72	0.90	50	50.000	691	0	0.034	0.000	63.60	0.00	0.034	63.60	0.670	0.000	0.650	0.321	0.023
Area Averaged Values		=				0.09	0.00	184.19	0.00	0.09	184.19	0.56	0.00	0.57	0.28	0.06

Experimental Conditions:		$j_{g,inlet}[m/s] =$	3.17	loc. press. [psi]=	12.705	Probe Configuration [mm]					
$Q_g[ml/min]=$	31.00	$j_{g,local} [m/s] =$	1.70	N_{sample}:	8000	$S_{01} =$	2.04	$S_{02} =$	1.94	$S_{03} =$	1.96
$P_{back}[psi]=$	17.00	$j_{f,inlet} [m/s] =$	3.00	f_{sample}:	15000	$S_{12} =$	0.48	$S_{13} =$	0.19	$S_{23} =$	0.43

$<<v_g>> =$	4.035	m/s	$<\alpha><<v_g>> =$	1.438	m/s	Percent difference between $<j_g>_z$ and $<\alpha>_z<<v_g>>_z =$	15.31	%

Probe Position		No. Loops	Δt_{total}	Bubble Number		α		a_i [1/m]		Total		v_{g1}	v_{g2}	$v_{g,avg}$	D_{sm1}	$\alpha_1 v_1 + \alpha_2 v_2$
r [mm]	r/R	N_{total}	[sec]	N_1	N_2	α_1	α_2	a_{i1}	$a_{i\,2}$	α_{Tot}	a_{iTot}	[m/s]	[m/s]	[m/s]	[cm]	[m/s]
	0.00	40	40.000	3769	492	0.075	0.450	163.80	32.30	0.525	196.10	4.710	4.210	4.660	0.275	2.249
											184.70				0.262	
1.27	0.20	40	40.000	3387	464	0.069	0.400	158.00	26.70	0.469		4.340	4.030	4.310		1.911
2.54	0.40	40	40.000	2956	483	0.062	0.320	146.60	43.80	0.382	190.40	4.090	3.230	4.020	0.254	1.287
3.18	0.50	40	40.000	2615	416	0.058	0.240	139.80	52.10	0.298	191.90	3.860	3.400	3.830	0.249	1.040
3.81	0.60	40	40.000	2598	506	0.067	0.154	129.50	79.40	0.221	208.90	4.630	3.880	4.540	0.310	0.908
4.45	0.70	40	40.000	945	627	0.023	0.220	31.10	31.00	0.243	62.10	3.930	4.740	3.800	0.444	1.133
5.09	0.80	40	40.000	1695	663	0.048	0.160	75.10	72.20	0.208	147.30	4.200	3.100	5.450	0.383	0.698
5.72	0.90	40	40.000	2224	531	0.059	0.168	110.00	88.50	0.227	198.50	4.690	4.000	4.650	0.322	0.949
Area Averaged Values			$=$			0.06	0.30	####	35.05	0.36	160.45	3.84	3.45	3.86	0.25	1.44

Exerimental Condition: Run 7 at Port1 (L/D=17)

Experimental Conditions:		$j_{g,inlet}[m/s] =$	0.71	loc. press. [psi]=	3.917	Probe Configuration [mm]					
$Q_g[ml/min]=$	8.50	$j_{g,local}\ [m/s] =$	0.56	$N_{sample};$	8000	$S_{01} =$ 2.04		$S_{02} =$ 1.94		$S_{03} =$ 1.96	
$P_{back}[psi]=$	6.50	$j_{f,inlet}\ [m/s] =$	0.40	$f_{sample};$	8000	$S_{12} =$ 0.48		$S_{13} =$ 0.19		$S_{23} =$ 0.43	

$<<v_g>>=$ 0.779	m/s	$<\alpha><<v_g>>=$	0.374	m/s	Percent difference between $<j_g>_z$ and $<\alpha>_z<<v_g>>_z =$	33.19	%

Probe Position		No. Loops	Δt_{total}	Bubble Number		α		$a_i\ [1/m]$		Total		v_{g1}	v_{g2}	$v_{g.avg}$	D_{sm1}	$\alpha_1 v_1 + \alpha_2 v_2$
r [mm]	r/R	N_{total}	[sec]	N_1	N_2	α_1	α_2	a_{i1}	a_{i2}	α_{Tot}	a_{iTot}	[m/s]	[m/s]	[m/s]	[cm]	[m/s]
	0.00	20	20.000	3507	68	0.600	0.000	877.80	0.00	0.600	877.80	0.870	0.000	0.840	0.410	0.522
											928.70				0.404	
1.27	0.20	20	20.000	3442	32	0.625	0.000	928.70	0.00	0.625		0.800	0.000	0.770		0.500
2.54	0.40	20	20.000	3182	4	0.516	0.000	940.20	0.00	0.516	940.20	0.704	0.000	0.704	0.329	0.363
3.18	0.50	20	20.000	2883	1	0.530	0.000	901.30	0.00	0.530	901.30	0.657	0.000	0.657	0.353	0.348
3.81	0.60	20	20.000	2261	0	0.450	0.000	816.80	0.00	0.450	816.80	0.650	0.000	0.569	0.331	0.293
4.45	0.70	20	20.000	1004	0	0.350	0.000	350.00	0.00	0.350	350.00	0.750	0.000	0.810	0.600	0.263
5.09	0.80	20	20.000	1609	1	0.200	0.001	244.60	0.00	0.201	244.60	0.750	0.000	0.750	0.491	0.150
5.72	0.90	20	20.000	2228	0	0.340	0.000	430.00	0.00	0.340	430.00	0.560	0.000	0.554	0.474	0.190
Area Averaged Values			=			0.48	0.00	####	0.00	0.48	735.46	0.68	0.00	0.66	0.35	0.37

Experimental Conditions:		$j_{g,inlet}[m/s] =$	1.26	loc. press. [psi]=	10.79	Probe Configuration [mm]					
$Q_g[ml/min]=$	13.00	$j_{g,local}[m/s] =$	0.73	$N_{sample;}$	8000	$S_{01} =$	2.04	$S_{02} =$	1.94	$S_{03} =$	1.96
$P_{back}[psi]=$	14.00	$j_{f,inlet}[m/s] =$	3.00	$f_{sample;}$	15000	$S_{12} =$	0.48	$S_{13} =$	0.19	$S_{23} =$	0.43

$<<v_g>>=$	3.228	m/s	$<\alpha><<v_g>>=$	0.639	m/s	Percent difference between $<j_g>_z$ and $<\alpha>_z<<v_g>>_z =$	12.34	%

Probe Position		No. Loops	Δt_{total}	Bubble Number		α		a_i [1/m]		Total		v_{g1}	v_{g2}	$v_{g,avg}$	D_{sm1}	$\alpha_1 v_1 + \alpha_2 v_2$
r [mm]	r/R	N_{total}	[sec]	N_1	N_2	α_1	α_2	a_{i1}	$a_{i\,2}$	α_{Tot}	a_{iTot}	[m/s]	[m/s]	[m/s]	[cm]	[m/s]
	0.00	20	20.000	2222	136	0.250	0.059	255.40	18.00	0.309	273.40	3.420	3.180	3.410	0.587	1.043
											249.80				0.507	
1.27	0.20	20	20.000	2001	98	0.200	0.050	236.50	13.30	0.250		3.320	3.080	3.310		0.818
2.54	0.40	20	20.000	1281	43	0.150	0.018	180.00	9.60	0.168	189.60	3.090	2.660	3.090	0.500	0.511
3.18	0.50	20	20.000	853	23	0.150	0.050	171.00	5.10	0.200	176.10	2.960	2.940	2.950	0.526	0.591
3.81	0.60	20	20.000	1472	46	0.150	0.017	165.00	6.00	0.167	171.00	3.100	3.200	3.150	0.545	0.519
4.45	0.70	20	20.000	1153	84	0.100	0.051	120.50	12.00	0.151	132.50	2.900	2.900	2.900	0.498	0.438
5.09	0.80	20	20.000	1213	30	0.090	0.010	117.50	10.00	0.100	127.50	2.850	2.700	2.750	0.460	0.284
5.72	0.90	20	20.000	1342	50	0.100	0.012	126.20	15.00	0.112	141.20	2.800	2.870	2.840	0.475	0.314
Area Averaged Values		=				0.16	0.04	184.53	10.76	0.20	195.29	2.83	2.67	2.83	0.46	0.64

Experimental Conditions:		$j_{g,inlet}[m/s] =$	0.75	loc. press. [psi]=	5.572	Probe Configuration [mm]					
$Q_g[ml/min]=$	8.50	$j_{g,local}\ [m/s] =$	0.54	N_{sample}:	8000	$S_{01} =$	2.04	$S_{02} =$	1.94	$S_{03} =$	1.96
$P_{back}[psi]=$	9.00	$j_{f,inlet}\ [m/s] =$	1.00	f_{sample}:	10000	$S_{12} =$	0.48	$S_{13} =$	0.19	$S_{23} =$	0.43

$<<v_g>>=$	1.485	m/s	$<\alpha><<v_g>>=$	0.475	m/s	Percent difference between $<j_g>_z$ and $<\alpha>_z<<v_g>>_z =$	12.73	%

Probe Position		No. Loops	Δt_{total}	Bubble Number		α		$a_i\ [1/m]$		Total		v_{g1}	v_{g2}	$v_{g,avg}$	D_{sm1}	$\alpha_1 v_1 + \alpha_2 v_2$
r [mm]	r/R	N_{total}	[sec]	N_1	N_2	α_1	α_2	a_{i1}	a_{i2}	α_{Tot}	a_{iTot}	[m/s]	[m/s]	[m/s]	[cm]	[m/s]
	0.00	15	15.000	2945	12	0.460	0.006	625.80	2.64	0.466	628.44	1.630	1.580	1.630	0.441	0.759
											663.98				0.396	
1.27	0.20	15	15.000	2892	15	0.437	0.008	661.40	2.58	0.445		1.510	1.500	1.510		0.671
2.54	0.40	15	15.000	2672	1	0.379	0.004	673.60	0.21	0.383	673.81	1.370	1.360	1.370	0.338	0.525
3.18	0.50	15	15.000	2193	1	0.293	0.006	605.20	0.60	0.299	605.80	1.250	1.200	1.250	0.290	0.373
3.81	0.60	15	15.000	1695	0	0.200	0.000	519.20	0.00	0.200	519.20	1.200	1.200	1.200	0.231	0.240
4.45	0.70	15	15.000	1026	0	0.084	0.000	366.70	0.00	0.084	366.70	1.200	1.200	1.200	0.137	0.101
5.09	0.80	15	15.000	899	26	0.045	0.005	350.00	16.00	0.050	366.00	1.180	1.160	1.350	0.078	0.059
5.72	0.90	15	15.000	1133	0	0.035	0.000	320.00	0.00	0.035	320.00	1.100	1.130	1.120	0.066	0.039
Area Averaged Values			=			0.32	0.00	530.38	2.34	0.32	532.72	1.26	1.24	1.27	0.30	0.48

Experimental Conditions:			$j_{g,inlet}[m/s] =$	0.19	loc. press. [psi]=	4.829	Probe Configuration [mm]					
$Q_g[ml/min] =$		31.00	$j_{g,local} [m/s] =$	0.15	N_{sample}:	8000	$S_{01} =$	2.04	$S_{02} =$	1.94	$S_{03} =$	1.96
$P_{back}[psi] =$		7.50	$j_{f,inlet} [m/s] =$	0.40	f_{sample}:	8000	$S_{12} =$	0.48	$S_{13} =$	0.19	$S_{23} =$	0.43

$<<v_g>> = $	0.550	m/s	$<\alpha><<v_g>> = $	0.130	m/s	Percent difference between $<j_g>_z$ and $<\alpha>_z<<v_g>>_z = $	11.59	%

Probe Position		No. Loops	Δt_{total}	Bubble Number		α		a_i [1/m]		Total		v_{g1}	v_{g2}	$v_{g.avg}$	D_{sm1}	$\alpha_1 v_1 + \alpha_2 v_2$
r [mm]	r/R	N_{total}	[sec]	N_1	N_2	α_1	α_2	a_{i1}	$a_{i\,2}$	α_{Tot}	a_{iTot}	[m/s]	[m/s]	[m/s]	[cm]	[m/s]
0.00	0.00	20	20.000	1653	0	0.322	0.000	574.50	0.00	0.322	574.50	0.590	0.000	0.590	0.336	0.190
											597.10				0.336	
1.27	0.20	20	20.000	1638	0	0.334	0.000	597.10	0.00	0.334		0.560	0.000	0.560		0.187
2.54	0.40	20	20.000	1447	0	0.275	0.000	583.30	0.00	0.275	583.30	0.511	0.000	0.511	0.283	0.141
3.18	0.50	20	20.000	1297	0	0.220	0.000	555.60	0.00	0.220	555.60	0.480	0.000	0.480	0.238	0.106
3.81	0.60	20	20.000	1052	0	0.140	0.000	477.10	0.00	0.140	477.10	0.448	0.000	0.448	0.176	0.063
4.45	0.70	20	20.000	700	0	0.043	0.000	171.00	0.00	0.043	171.00	0.490	0.000	0.490	0.151	0.021
5.09	0.80	20	20.000	900	0	0.067	0.000	168.00	0.00	0.067	168.00	0.510	0.000	0.510	0.239	0.034
5.72	0.90	20	20.000	1000	0	0.126	0.000	428.00	0.00	0.126	428.00	0.418	0.000	0.418	0.177	0.053
Area Averaged Values		=														
						0.24	0.00	466.00	0.00	0.24	466.00	0.47	0.00	0.47	0.26	0.13

Experimental Conditions:		$j_{g,inlet}[m/s] =$	0.20	loc. press. [psi]=	10.465	Probe Configuration [mm]					
$Q_g[ml/min]=$	31.00	$j_{g,local}[m/s] =$	0.12	$N_{samples}$:	8000	$S_{01} =$	2.04	$S_{02} =$	1.94	$S_{03} =$	1.96
$P_{buck}[psi]=$	9.00	$j_{f,inlet}[m/s] =$	3.00	f_{sample}:	15000	$S_{12} =$	0.48	$S_{13} =$	0.19	$S_{23} =$	0.43

$<<v_g>>=$	3.326	m/s	$<\alpha><<v_g>>=$	0.144	m/s	Percent difference between $<j_g>_z$ and $<\alpha>_z<<v_g>>_z =$	22.49	%

Probe Position		No. Loops	Δt_{total}	Bubble Number		α		$a_i\ [1/m]$		Total		v_{g1}	v_{g2}	$v_{g,avg}$	D_{sm1}	$\alpha_1 v_1 + \alpha_2 v_2$
r [mm]	r/R	N_{total}	[sec]	N_1	N_2	α_1	α_2	a_{i1}	$a_{i\ 2}$	α_{Tot}	a_{iTot}	[m/s]	[m/s]	[m/s]	[cm]	[m/s]
0.00	0.00	60	60.000	3850	0	0.067	0.000	144.70	0.00	0.067	144.70	3.500	0.000	3.500	0.278	0.235
											150.00				0.264	
1.27	0.20	60	60.000	3771	0	0.066	0.000	150.00	0.00	0.066		3.270	0.000	3.270		0.216
2.54	0.40	60	60.000	2177	0	0.034	0.000	98.90	0.00	0.034	98.90	3.100	0.000	3.500	0.209	0.107
3.18	0.50	60	60.000	1545	0	0.021	0.000	73.70	0.00	0.021	73.70	3.500	0.000	3.100	0.174	0.075
3.81	0.60	60	60.000	1667	0	0.010	0.000	50.00	0.00	0.010	50.00	3.530	0.000	3.530	0.120	0.035
4.45	0.70	60	60.000	1588	0	0.010	0.000	45.00	0.00	0.010	45.00	3.500	0.000	3.700	0.133	0.035
5.09	0.80	60	60.000	1271	0	0.020	0.000	36.00	0.00	0.020	36.00	3.470	0.000	3.470	0.333	0.069
5.72	0.90	60	60.000	1444	0	0.030	0.000	46.00	0.00	0.030	46.00	3.720	0.000	3.720	0.391	0.112
Area Averaged Values			=													
						0.04	0.00	103.00	0.00	0.04	103.00	2.95	0.00	2.98	0.21	0.14

Experimental Conditions:		$j_{g.inlet}[m/s]=$	0.20	loc. press. [psi]=	3.122	Probe Configuration [mm]					
$Q_g[ml/min]=$	31.00	$j_{g.local}[m/s]=$	0.17	N_{sample}:	8000	$S_{01}=$	2.04	$S_{02}=$	1.94	$S_{03}=$	1.96
$P_{back}[psi]=$	9.00	$j_{f.inlet}[m/s]=$	1.00	f_{sample}:	10000	$S_{12}=$	0.48	$S_{13}=$	0.19	$S_{23}=$	0.43

$<<v_g>>=$	1.236	m/s	$<\alpha><<v_g>>=$	0.145	m/s	Percent difference between $<j_g>_z$ and $<\alpha>_z<<v_g>>_z=$	12.64	%

Probe Position		No. Loops	Δt_{total}	Bubble Number		α		$a_i\,[1/m]$		Total		v_{g1}	v_{g2}	$v_{g.avg}$	D_{sm1}	$\alpha_1 v_1+\alpha_2 v_2$
r [mm]	r/R	N_{total}	[sec]	N_1	N_2	α_1	α_2	a_{i1}	$a_{i\,2}$	α_{Tot}	a_{iTot}	[m/s]	[m/s]	[m/s]	[cm]	[m/s]
0.00	0.00	40	40.000	800	0	0.090	0.000	120.00	0.00	0.090	120.00	1.370	0.000	1.370	0.450	0.123
											160.00				0.450	
1.27	0.20	40	40.000	850	0	0.120	0.000	160.00	0.00	0.120		1.340	0.000	1.340		0.161
2.54	0.40	40	40.000	1818	0	0.150	0.000	192.40	0.00	0.150	192.40	1.230	0.000	1.230	0.468	0.185
3.18	0.50	40	40.000	2829	0	0.157	0.000	318.20	0.00	0.157	318.20	1.160	0.000	1.160	0.296	0.182
3.81	0.60	40	40.000	3293	0	0.206	0.000	390.70	0.00	0.206	390.70	1.100	0.000	1.100	0.316	0.227
4.45	0.70	40	40.000	2865	0	0.156	0.000	400.00	0.00	0.156	400.00	1.010	0.000	1.010	0.234	0.158
5.09	0.80	40	40.000	2100	0	0.150	0.000	386.10	0.00	0.150	386.10	1.000	0.000	1.340	0.233	0.150
5.72	0.90	40	40.000	2385	0	0.111	0.000	334.40	0.00	0.111	334.40	0.930	0.000	1.230	0.199	0.103
Area Averaged Values		=				0.12	0.00	190.58	0.00	0.12	190.58	1.11	0.00	1.13	0.36	0.14

العنوان:	INTERFACIAL AREA CONCENTRATION AND VOID FRACTION OF TWO PHASE FLOW IN 12.7 mmID PIPE-
المؤلف الرئيسي:	Al Dorwish, Yousef M.
مؤلفين آخرين:	Ishi, Mamoru(Super.)
التاريخ الميلادي:	2000
موقع:	لافاييت
الصفحات:	1 - 120
رقم MD:	614708
نوع المحتوى:	رسائل جامعية
اللغة:	English
الدرجة العلمية:	رسالة ماجستير
الجامعة:	Purdue University
الكلية:	The Graduate School
الدولة:	الولايات المتحدة الأمريكية
قواعد المعلومات:	Dissertations
مواضيع:	الطاقة النووية، الإشعاع النووي، الهندسة النووية
رابط:	https://search.mandumah.com/Record/614708

TABLE OF CONTENTS

LIST OF TABLES..vii

LIST OF FIGURES viii

NOMENCLATURE xi

ABSTRACT xiv

1. INTRODUCTION...1

    1.1 Literature Review...1

    1.2 Importance of Interfacial Area Measurement..2

    1.3 Two-fluid Model...5

    1.4 Two-Phase Flow Regimes 9

        1.4.1 Flow Description 9

        1.4.2 Criteria for Flow Regime Transitions..10

    1.5 Thesis Objectives...12

2. EXPERIMENTAL FACILTY 15

    2.1 The Experimental Facility..15

    2.2 Test Section and Port Locations 20

    2.3 Experimental Loop Instrumentation 21

        2.3.1 Differential Pressure Cell 21

LIST OF TABLES

LIST OF FIGURES

NOMENCLATURE

D	pipe diameter
E	electric field intensity
f	frequency
g	gravity
G	impedance
h	height
I	electric current
j	superficial velocity
j	current flux density
K	number of PDF
n	number of counts
n	direction normal to the wall
N	total number of counts
P	pressure
P	probability
r	radial coordinate
R	radius of pipe
t	time
T	total sampling time
U	electrical potential
v	fluid velocity
V	voltage
w	weight
$\langle \phi \rangle$	area average propert

a_i   local interfacial area concentration

D_{sm} sauter mean diameter

N_f bubble frequency

Re   Reynolds number (Equation 4.4)

Re_D Particle Reynolds number (Equation 4.5)

We   Weber number (Equation 4.6)

r   radial coordinate

u_g gas phase velocity

GREEK SYMBOLS

α void fraction

Δ change in quantity

μ fluid viscosity

σ surface tension

Γ_g rate of interfacial change per unit volume of mixture

ρ_f liquid density

ρ_g gas density

SUBSCRIPTS AND SUPERSCRIPTS

f   liquid phase

g   gas phase

i,j   number

*   dimensionless quantity

m   mixture

العنوان:	INTERFACIAL AREA CONCENTRATION AND VOID FRACTION OF TWO PHASE FLOW IN 12.7 mmID PIPE-
المؤلف الرئيسي:	Al Dorwish, Yousef M.
مؤلفين آخرين:	Ishi, Mamoru(Super.)
التاريخ الميلادي:	2000
موقع:	لافاييت
الصفحات:	1 - 120
رقم MD:	614708
نوع المحتوى:	رسائل جامعية
اللغة:	English
الدرجة العلمية:	رسالة ماجستير
الجامعة:	Purdue University
الكلية:	The Graduate School
الدولة:	الولايات المتحدة الأمريكية
قواعد المعلومات:	Dissertations
مواضيع:	الطاقة النووية، الإشعاع النووي، الهندسة النووية
رابط:	https://search.mandumah.com/Record/614708

INTERFACIAL AREA CONCENTRATION AND VOID FRACTION

OF TWO-PHASE FLOW IN 12.7 mm ID PIPE

A Thesis

Submitted to the Faculty

of

Purdue University

by

Yousef M. Aldorwish

In Partial Fulfillment of the

Requirements for the Degree

of

Master of Science in Nuclear Engineering

May 2000

4315

PURDUE UNIVERSITY
GRADUATE SCHOOL
Thesis Acceptance

This is to certify that the thesis prepared

By Yousef M Aldorwish

Entitled

Interfacial Area Concentration and Void Fraction of Two-Phase
Flow in 12.7 mm ID Pipe

Complies with University regulations and meets the standards of the Graduate School for originality
and quality

For the degree of Master of Science in Nuclear Engineering

Signed by the final examining committee:
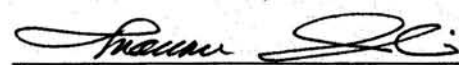
Ishii, Mamoru _____ , chair

Lopez de Bertodano, Martin L. _____

Revankar, Shripad T. _____

Viskanta, Raymond _____

Approved by: _____   4-21-00
                    Department Head   Date

This thesis ☐ is
             ☒ is not to be regarded as confidential. _____
                                                          Major Professor

Format Approved by:

_____   or _____
Chair, Final Examining Committee   Thesis Format Adviser

TO

My Mother

My Father

My Brother Nasser

My Wife

My Family

ACKNOWLEDGEMENTS

TABLE OF CONTENTS

LIST OF TABLES

LIST OF FIGURES

NOMENCLATURE

D	pipe diameter
E	electric field intensity
f	frequency
g	gravity
G	impedance
h	height
I	electric current
j	superficial velocity
j	current flux density
K	number of PDF
n	number of counts
n	direction normal to the wall
N	total number of counts
P	pressure
P	probability
r	radial coordinate
R	radius of pipe
t	time
T	total sampling time
U	electrical potential
v	fluid velocity
V	voltage
w	weight
$\langle \phi \rangle$	area average propert

a_i local interfacial area concentration

D_{sm} sauter mean diameter

N_f bubble frequency

Re   Reynolds number (Equation 4.4)

Re_D Particle Reynolds number (Equation 4.5)

We   Weber number (Equation 4.6)

r   radial coordinate

u_g gas phase velocity

GREEK SYMBOLS

α void fraction

Δ change in quantity

μ fluid viscosity

σ surface tension

Γ_g rate of interfacial change per unit volume of mixture

ρ_f liquid density

ρ_g gas density

SUBSCRIPTS AND SUPERSCRIPTS

f   liquid phase

g   gas phase

i,j   number

*   dimensionless quantity

m   mixture

ABSTRACT

Aldorwish, Yousef M.   M.S.N.E., Purdue University, May, 2000. Interfacial Area Concentration and Void Fraction of Two-Phase Flow in 12.7mm ID Pipe. Major Professor: Mamoru Ishii.

An independent experimental study of the interfacial structure in adiabatic two-phase flow was carried out in a 12.7 mm ID pipe which was constructed at the Thermal-Hydraulic and Reactor Safety Laboratory at Purdue University with specialized instrumentation including impedance meters, magnetic flow meter and local probes. The local void fraction, interfacial area concentration, bubble velocity and Sauter mean diameter parameters were measured by a double-sensor and four-sensor probe. The flow structure development was visualized by measuring the radial distribution of these phasic parameters at axial locations $L/D=17$, 120 and 217. The flow regimes were identified by using the visualization box, the probability density function (PDF) of the void fraction [1]. Different flow regimes such as bubbly, slug and churn turbulent regimes, produce characteristic signal due to their distinct void fraction. The impedance meter signals are used to determine the flow regime through a PDF analysis. The data for the flow regime transitions is compared with the theoretical transition boundaries, which was proposed by Mishima and Ishii [4]. Self-organizing neural network is used to determine the flow regimes based on the output of the impedance meter.

CHAPTER 1

INTRODUCTION

The objective of this thesis was to investigate experimentally the interfacial area concentration and void fraction in a 12.7-mm ID pipe. The multi-sensor resistively probes developed in the Thermal Hydraulics and Reactor Safety Laboratory at Purdue University were used in the experimental study of the local void fraction and the interfacial area concentration. A database was established for flow structure development in a wide range of flow conditions that spanned over the dispersed bubbly flow, slug flow and churn turbulent regimes.

Two-phase flow is characterized by the existence of the interface between phases and discontinuities of properties at the interface. The internal structures of two-phase flow are identified by two-phase regimes. Various transfer mechanisms between the mixture and wall as well as between phases strongly depend on these two-phase flow regimes. This leads to the use of flow regime dependent correlations and closure equations together with appropriate flow regime transition criteria. The basic structure of flow can be characterized by two fundamental geometrical parameters. These are the void fraction and interfacial area concentration. The void fraction expresses the phase distribution whereas the interfacial area describes available area for the interfacial transfer of mass, momentum and energy. Therefore, an accurate knowledge of these parameters is necessary for any two-phases flow analysis. This fact can be further substantiated with respect to two-phase flow formulation.

1.1 Literature Review

Review of related literature gives one a chance to see the history of the topic he/she is researching and to try to continue from where others have stopped.

The problem with interfacial area concentration and void friction is that there has not been work done for the local measurement in a small diameter tube typically 12.7 mm ID for air-water at low pressure. As for the flow regime, Taitel et al [3] have developed an experimental flow regime map for 12.7 mm air/water loop at atmospheric pressure by using flow visualization method. Bennett et al. [4] have also developed a flow regime map for 12.7 mm steam /water loop at high pressure by employing visualization and X-ray photography. Table 1.1 shows a summary of the experimental flow pattern data.

The present study would be an addition to the research done in the field of the interfacial area concentration and void fraction for several reasons. The lack of studies done in the area makes it a proper environment for new findings to create other leads and guides in the research in this field. The outcome of this study's experiments is valuable to the field because of the lack of detailed experimental data on local parameters.

1.2 Importance of Interfacial Area Measurement

In nuclear reactor systems, numerous practical thermal hydraulic phenomena are dominated by interfacial transport. Proper mechanistic models for the interfacial transfer process are the major concern in the current two-phase flow modeling practice. Generally, the interfacial transfer rates can be considered as the product of the interfacial flux and the available interfacial area [5]. Difficulty arises in the treatment of the interfacial area concentration because of the complicated interfacial structure, especially when subject to two-phase flow regime transitions. In system analysis codes such as RELAP5 and TRAC, the interfacial area concentration is given by empirical correlations that are based on two-phase flow regimes and regime transition criteria. This approach has a number of shortcomings such as:

1. The method based on flow regime transition criteria is a two-step method, which requires the regime dependent closure relations to determine the interfacial area concentration effects. The compound errors from the transition criteria and area correlations can be very significant.

2. The flow regime transition criteria are algebraic relations for steady state, fully developed flows. They do not fully reflect the true dynamic nature of changes in the interfacial structure. Hence, the effects of the entrance and developing flow as well as the gradual transition between regimes cannot be accounted correctly.

3. The existing flow regime dependent correlations and criteria are valid in limited parameter ranges for certain specific operational conditions. Most of them are obtained by simple experiments and phenomenological models. Often, the scale effects of geometry and fluid properties are not taken into account properly.

Table 1.1 Experimental flow pattern data

Reference	Gas liquid	Gas density (kg/m3)	Liquid density (kg/m3)	liquid viscosity (Ns/m2*10^2)	Surface tension (N/m)	Tube diameter (m)	Delineation	Number of data points
Taitel et al. (1984)	Air/water	1.29	1000	1	0.072	0.0127	Visual	50
Bennett et al.(1965)	Steam	17.5	810	0.115	0.029	0.0127	Visual +	54
	Water	36.6	740	0.096	0.017	0.012	X-ray	44
Berglies and Suo(1966)	Steam	17.5	810	0.115	0.029	0.01	Conductivity	35
	Water	36.5	740	0.096	0.017	0.01	probe	58
Sorokin et al (1978)	Steam	10	688	0.087	0.011	0.0133	Conductivity	44
	Water	55	850	0.13	0.036		probe	

1.3 Two-fluid Model

The local instant formulation based on the single-phase flow conservation equations with explicit discontinuities due to the interface is mathematically rigorous, but it is difficult to apply. This is because they contain information about the rapidly fluctuating fields and the discontinuities at the interfaces. In order to avoid these microscopic characteristics, the average model is preferred over the local instant formulation. The average model contains no discontinuity and it describes macroscopic properties of the flow fields, it is much easier to manage mathematically. The choice of averaging method depends on the problem to be solved and the necessary constitutive relations should be developed accordingly from the experimental data. Thus, the averaging method and the measurement technique should be consistent with each other. For instance, if a local probe is used to record the flow fluctuation in the time domain, these measurements will be useful to develop constitutive relations for the time average two-fluid model. For most practical applications, a simplified form of the field equations for of the two-phase flow are [6]:

Continuity Equation

$$\frac{\partial}{\partial t}\alpha_k \rho_k + \nabla \cdot \alpha_k \rho_k u_k = \Gamma_k, \tag{1.1}$$

Momentum Equation

$$\frac{\partial}{\partial t}(\alpha_k \rho_k u_k) + \nabla \cdot (\alpha_k \rho_k u_k u_k) = -\alpha_k \nabla p_k + \nabla \cdot \alpha_k (\bar{\bar{\tau}}_k + \tau_k^t) + \alpha_k \rho_k g + u_{ki}\Gamma_k + M_{ki} - \nabla \alpha_k \cdot \tau_i$$

$$\tag{1.2}$$

Enthalpy Energy Equation

$$\frac{\partial}{\partial t}\alpha_k \rho_k H_k + \nabla \cdot \alpha_k \rho_k H_k u_k = -\nabla \cdot \alpha_k (\bar{\bar{q_k}} + q_k^t) + \alpha_k \frac{D_k}{Dt}p_k + H_{ki}\Gamma_k + q_{ki}'' a_i + \Phi_k, \tag{1.3}$$

Here $\Gamma_k, M_{ik}, \tau_i, q_i''$ and Φ_k are the mass generation, generalized interfacial drag, interfacial shear stress, interfacial heat flux, and dissipation, respectively. The subscript k

denotes the kth phase, and i stands for the values at the interface. The variable a_i denotes the interfacial area per unit volume. Since the thickness of the interface is assumed to be infinitesimally small and it has no source or sink, the inflow and outflow of flux must be balanced. The macroscopic interfacial jumps can be obtained in the following forms [6]:

$$\sum \Gamma_k = 0 \tag{1.4}$$

$$\sum M_{ik} = 0 \tag{1.5}$$

$$\sum H_{ki}\Gamma_k + q''_{ki}a_i = 0 \tag{1.6}$$

The set of time average equations yield 4 scalars, 3 vectors and 2 tensors variables for the bulk fluid in each phases. They are similar to the single phase flow formulation. However, the extra interfacial terms add to the variable list by 3 scalars, 2 vectors and 1 tensor. The equations and the associated variables are listed in Table 1.2. There are 2 scalar and 1 vector conservation equations for each phase. In addition, there are jump conditions for mass, momentum and energy transfer at the interfacial discontinuities. Even without the interfacial terms, the number of variables is larger than the number of the equations.

The variables can be divided into two categories. The first type deals with the properties and the flow characteristics in the bulk fluid. The second type deals with the terms derived from the interfacial transfers. It should be noticed that the void fraction does not belong to either types of variables. In fact, it represents the probability or volumetric fraction of the presence of phase k.

The transport characteristics and physical properties in the bulk of each phase can be modeled in a similar way as the single phase. As for the interfacial terms, there is no single phase equivalent. Although they are shown in simple terms, the actual expressions are more complicated. However, the general form of the interfacial transfer terms can be written as a product of the interfacial area concentration, a_i, and the mean driving force:

$$\text{(Interfacial Transfer Term)} = a_i \times \text{(Driving Force)}$$

The area concentration defined as the interfacial area per unit volume of the mixture characterizes the first order geometrical effects; therefore, it must be related to the interfacial structure of the two-phase flow field. The driving forces for the interfacial transport characterize the local transport mechanisms such as the turbulence, molecular transport properties and driving potentials. In two-phase flow systems, the void fraction and interfacial area concentration are two of the most important geometrical parameters. The interfacial area concentration should be specified by a closure relation, or by a transport equation. The above formulation indicates that the knowledge of the interfacial area concentration and the interfacial structure through the flow regimes are indispensable in the two phase flow analysis.

Table 1.2 Balance Equations and associated variables

Conservation Equation	Dependent Variables	Interfacial Transfer Terms
Mass	ρ_k, α_k, u_k	Γ_k
Momentum	$\rho_k, \alpha_k, u_k, p_k, \tau_k, \tau_k^t$	M_{ik}, u_i, τ_i
Energy	$\rho_k, \alpha_k, u_k, H_k, p_k, q_k, q_k^t$	$H_k \Gamma_k, q_{ki}^{\,"} a_i, \Phi_k$

1.4 Two-Phase Flow Regimes

In the analysis of two-phase flow transients, a two-fluid model is very useful due to its detailed description of thermo hydraulic transitions and phase interactions. The main difficulties in modeling arise from the existence of interfaces between phases and discontinuities associated with them. The internal structures of two-phase flow are classified by the flow regimes or flow patterns. Various transfer mechanisms between two-phase mixture and the wall, as well as between two phases, depend on the flow regimes.

1.4.1 Flow Description

When gas-liquid mixtures flow upward in a vertical tube, the two phases may distribute in a number of patterns, each characterizing the radial or / and axial distribution of liquid and gas. The flow is often quite chaotic, and these phase distributions are difficult to describe. The flow regimes are designated into four patterns as follows [7]:

1. Bubbly Flow: the gas phase is dispersed and distribution in the form of discrete bubbles in a continuous liquid phase.

2. Slug Flow: Most of the gas is located in large bullet shaped bubbles, which have a diameter almost equal to the pipe diameter. They move uniformly upward and are sometimes designated as " Taylor bubbles." Taylor bubbles are separated by slugs of continuous liquid which bridge pipe and contain small gas bubbles. Between the Taylor bubbles and the pipe wall, liquid flows downward in the form of a thin falling film.

3. Churn-Turbulent Flow: Churn-Turbulent flow is somewhat similar to slug flow. It is, however, much more chaotic. Churn-Turbulent flow possesses some of the characteristics of slug flow, with the main differences being as follows: (a) The gas slugs become narrower and more irregular. (b) The continuity of the liquid in

the slug is repeatedly destroyed by regions of high gas concentration, and (c) The thin falling film of liquid surrounding the gas slugs can no longer be observed.

4. Annular Flow: Annular flow is characterized by the continuity of the gas phase along the pipe in the core. The liquid flows partially as a film along the walls of the tube, and partially as droplets in the central gas core.

The sketch of typical flow regimes observed in the small tubes is shown in Figure 1.1. The flow regimes of small tubes have the following characteristics. In bubbly flow, bubbles tend to concentrate along the tube axis, small bubbles form a spiral train, while larger bubbles with the diameter closer to the tube inner diameter line up right next to each other to form bubble trains, without coalescing. In slug flows, slug bubbles are relatively long and have a beautiful smooth nose. Bridges of very thin liquid film are observed in a long slug bubble. In liquid slugs, restlessly oscillating small bubbles are observed. In churn-turbulent flow, long slug bubbles are deformed and they do not have a semi-spherical nose any more. A number of tiny bubbles are observed moving rapidly in liquid slugs.

1.4.2 Criteria for Flow Regime Transitions

Traditional two-phase flow regime criteria based on the gas and liquid superficial velocities may not be suitable to the analyses of rapid transient or entrance flows by the two-fluid model. Under these conditions, it is postulated that direct geometrical parameters such as void fraction were simpler and more reliable parameters to be used in flow-regime criteria than the traditional parameters [2].

1. Bubbly flow to slug flow transition:

The transition from bubbly to slug flow occurs due to agglomerations and coalescences of small bubbles into cap bubbles. This transition takes places at the void fraction around 0.3. Mishima and Ishii [2] used a very simple geometrical model of the bubbles distribution. They found that the number of the collisions and coalescences becomes very

العنوان:	INTERFACIAL AREA CONCENTRATION AND VOID FRACTION OF TWO PHASE FLOW IN 12.7 mmID PIPE-
المؤلف الرئيسي:	Al Dorwish, Yousef M.
مؤلفين آخرين:	Ishi, Mamoru(Super.)
التاريخ الميلادي:	2000
موقع:	لافاييت
الصفحات:	1 - 120
رقم MD:	614708
نوع المحتوى:	رسائل جامعية
اللغة:	English
الدرجة العلمية:	رسالة ماجستير
الجامعة:	Purdue University
الكلية:	The Graduate School
الدولة:	الولايات المتحدة الأمريكية
قواعد المعلومات:	Dissertations
مواضيع:	الطاقة النووية، الإشعاع النووي، الهندسة النووية
رابط:	https://search.mandumah.com/Record/614708

ABSTRACT

Aldorwish, Yousef M.   M.S.N.E., Purdue University, May, 2000. Interfacial Area Concentration and Void Fraction of Two-Phase Flow in 12.7mm ID Pipe. Major Professor: Mamoru Ishii.

An independent experimental study of the interfacial structure in adiabatic two-phase flow was carried out in a 12.7 mm ID pipe which was constructed at the Thermal-Hydraulic and Reactor Safety Laboratory at Purdue University with specialized instrumentation including impedance meters, magnetic flow meter and local probes. The local void fraction, interfacial area concentration, bubble velocity and Sauter mean diameter parameters were measured by a double-sensor and four-sensor probe. The flow structure development was visualized by measuring the radial distribution of these phasic parameters at axial locations L/D=17, 120 and 217. The flow regimes were identified by using the visualization box, the probability density function (PDF) of the void fraction [1]. Different flow regimes such as bubbly, slug and churn turbulent regimes, produce characteristic signal due to their distinct void fraction. The impedance meter signals are used to determine the flow regime through a PDF analysis. The data for the flow regime transitions is compared with the theoretical transition boundaries, which was proposed by Mishima and Ishii [4]. Self-organizing neural network is used to determine the flow regimes based on the output of the impedance meter.

CHAPTER 1

INTRODUCTION

The objective of this thesis was to investigate experimentally the interfacial area concentration and void fraction in a 12.7-mm ID pipe. The multi-sensor resistively probes developed in the Thermal Hydraulics and Reactor Safety Laboratory at Purdue University were used in the experimental study of the local void fraction and the interfacial area concentration. A database was established for flow structure development in a wide range of flow conditions that spanned over the dispersed bubbly flow, slug flow and churn turbulent regimes.

Two-phase flow is characterized by the existence of the interface between phases and discontinuities of properties at the interface. The internal structures of two-phase flow are identified by two-phase regimes. Various transfer mechanisms between the mixture and wall as well as between phases strongly depend on these two-phase flow regimes. This leads to the use of flow regime dependent correlations and closure equations together with appropriate flow regime transition criteria. The basic structure of flow can be characterized by two fundamental geometrical parameters. These are the void fraction and interfacial area concentration. The void fraction expresses the phase distribution whereas the interfacial area describes available area for the interfacial transfer of mass, momentum and energy. Therefore, an accurate knowledge of these parameters is necessary for any two-phases flow analysis. This fact can be further substantiated with respect to two-phase flow formulation.

1.1 Literature Review

Review of related literature gives one a chance to see the history of the topic he/she is researching and to try to continue from where others have stopped.

The problem with interfacial area concentration and void friction is that there has not been work done for the local measurement in a small diameter tube typically 12.7 mm ID for air-water at low pressure. As for the flow regime, Taitel et al [3] have developed an experimental flow regime map for 12.7 mm air/water loop at atmospheric pressure by using flow visualization method. Bennett et al. [4] have also developed a flow regime map for 12.7 mm steam /water loop at high pressure by employing visualization and X-ray photography. Table 1.1 shows a summary of the experimental flow pattern data.

The present study would be an addition to the research done in the field of the interfacial area concentration and void fraction for several reasons. The lack of studies done in the area makes it a proper environment for new findings to create other leads and guides in the research in this field. The outcome of this study's experiments is valuable to the field because of the lack of detailed experimental data on local parameters.

1.2 Importance of Interfacial Area Measurement

In nuclear reactor systems, numerous practical thermal hydraulic phenomena are dominated by interfacial transport. Proper mechanistic models for the interfacial transfer process are the major concern in the current two-phase flow modeling practice. Generally, the interfacial transfer rates can be considered as the product of the interfacial flux and the available interfacial area [5]. Difficulty arises in the treatment of the interfacial area concentration because of the complicated interfacial structure, especially when subject to two-phase flow regime transitions. In system analysis codes such as RELAP5 and TRAC, the interfacial area concentration is given by empirical correlations that are based on two-phase flow regimes and regime transition criteria. This approach has a number of shortcomings such as:

1. The method based on flow regime transition criteria is a two-step method, which requires the regime dependent closure relations to determine the interfacial area concentration effects. The compound errors from the transition criteria and area correlations can be very significant.

2. The flow regime transition criteria are algebraic relations for steady state, fully developed flows. They do not fully reflect the true dynamic nature of changes in the interfacial structure. Hence, the effects of the entrance and developing flow as well as the gradual transition between regimes cannot be accounted correctly.

3. The existing flow regime dependent correlations and criteria are valid in limited parameter ranges for certain specific operational conditions. Most of them are obtained by simple experiments and phenomenological models. Often, the scale effects of geometry and fluid properties are not taken into account properly.

Table 1.1 Experimental flow pattern data

Reference	Gas liquid	Gas density (kg/m3)	Liquid density (kg/m3)	liquid viscosity (Ns/m2*10^2)	Surface tension (N/m)	Tube diameter (m)	Delineation	Number of data points
Taitel et al. (1984)	Air/water	1.29	1000	1	0.072	0.0127	Visual	50
Bennett et al.(1965)	Steam	17.5	810	0.115	0.029	0.0127	Visual +	54
	Water	36.6	740	0.096	0.017	0.012	X-ray	44
Berglies and Suo(1966)	Steam	17.5	810	0.115	0.029	0.01	Conductivity	35
	Water	36.5	740	0.096	0.017	0.01	probe	58
Sorokin et al (1978)	Steam	10	688	0.087	0.011	0.0133	Conductivity	44
	Water	55	850	0.13	0.036		probe	

1.3 Two-fluid Model

The local instant formulation based on the single-phase flow conservation equations with explicit discontinuities due to the interface is mathematically rigorous, but it is difficult to apply. This is because they contain information about the rapidly fluctuating fields and the discontinuities at the interfaces. In order to avoid these microscopic characteristics, the average model is preferred over the local instant formulation. The average model contains no discontinuity and it describes macroscopic properties of the flow fields, it is much easier to manage mathematically. The choice of averaging method depends on the problem to be solved and the necessary constitutive relations should be developed accordingly from the experimental data. Thus, the averaging method and the measurement technique should be consistent with each other. For instance, if a local probe is used to record the flow fluctuation in the time domain, these measurements will be useful to develop constitutive relations for the time average two-fluid model. For most practical applications, a simplified form of the field equations for of the two-phase flow are [6]:

Continuity Equation

$$\frac{\partial}{\partial t}\alpha_k\rho_k + \nabla\cdot\alpha_k\rho_k u_k = \Gamma_k, \tag{1.1}$$

Momentum Equation

$$\frac{\partial}{\partial t}(\alpha_k\rho_k u_k) + \nabla\cdot(\alpha_k\rho_k u_k u_k) = -\alpha_k\nabla p_k + \nabla\cdot\alpha_k\left(\overline{\overline{\tau}}_k + \tau_k^t\right) + \alpha_k\rho_k g + u_{ki}\Gamma_k + M_{ki} - \nabla\alpha_k\cdot\tau_i$$

$$\tag{1.2}$$

Enthalpy Energy Equation

$$\frac{\partial}{\partial t}\alpha_k\rho_k H_k + \nabla\cdot\alpha_k\rho_k H_k u_k = -\nabla\cdot\alpha_k\left(\overline{\overline{q_k}} + q_k^t\right) + \alpha_k\frac{D_k}{Dt}p_k + H_{ki}\Gamma_k + q_{ki}''a_i + \Phi_k, \tag{1.3}$$

Here $\Gamma_k, M_{ik}, \tau_i, q_i''$ and Φ_k are the mass generation, generalized interfacial drag, interfacial shear stress, interfacial heat flux, and dissipation, respectively. The subscript k

denotes the kth phase, and i stands for the values at the interface. The variable a_i denotes the interfacial area per unit volume. Since the thickness of the interface is assumed to be infinitesimally small and it has no source or sink, the inflow and outflow of flux must be balanced. The macroscopic interfacial jumps can be obtained in the following forms [6]:

$$\sum \Gamma_k = 0 \tag{1.4}$$

$$\sum M_{ik} = 0 \tag{1.5}$$

$$\sum H_{ki} \Gamma_k + q''_{ki} a_i = 0 \tag{1.6}$$

The set of time average equations yield 4 scalars, 3 vectors and 2 tensors variables for the bulk fluid in each phases. They are similar to the single phase flow formulation. However, the extra interfacial terms add to the variable list by 3 scalars, 2 vectors and 1 tensor. The equations and the associated variables are listed in Table 1.2. There are 2 scalar and 1 vector conservation equations for each phase. In addition, there are jump conditions for mass, momentum and energy transfer at the interfacial discontinuities. Even without the interfacial terms, the number of variables is larger than the number of the equations.

The variables can be divided into two categories. The first type deals with the properties and the flow characteristics in the bulk fluid. The second type deals with the terms derived from the interfacial transfers. It should be noticed that the void fraction does not belong to either types of variables. In fact, it represents the probability or volumetric fraction of the presence of phase k.

The transport characteristics and physical properties in the bulk of each phase can be modeled in a similar way as the single phase. As for the interfacial terms, there is no single phase equivalent. Although they are shown in simple terms, the actual expressions are more complicated. However, the general form of the interfacial transfer terms can be written as a product of the interfacial area concentration, a_i, and the mean driving force:

$$\text{(Interfacial Transfer Term)} = a_i \text{ x (Driving Force)}$$

The area concentration defined as the interfacial area per unit volume of the mixture characterizes the first order geometrical effects; therefore, it must be related to the interfacial structure of the two-phase flow field. The driving forces for the interfacial transport characterize the local transport mechanisms such as the turbulence, molecular transport properties and driving potentials. In two-phase flow systems, the void fraction and interfacial area concentration are two of the most important geometrical parameters. The interfacial area concentration should be specified by a closure relation, or by a transport equation. The above formulation indicates that the knowledge of the interfacial area concentration and the interfacial structure through the flow regimes are indispensable in the two phase flow analysis.

Table 1.2 Balance Equations and associated variables

Conservation Equation	Dependent Variables	Interfacial Transfer Terms
Mass	ρ_k, α_k, u_k	Γ_k
Momentum	$\rho_k, \alpha_k, u_k, p_k, \tau_k, \tau_k^t$	M_{ik}, u_i, τ_i
Energy	$\rho_k, \alpha_k, u_k, H_k, p_k, q_k, q_k^t$	$H_k \Gamma_k, q_{ki}^{"} a_i, \Phi_k$

1.4 Two-Phase Flow Regimes

In the analysis of two-phase flow transients, a two-fluid model is very useful due to its detailed description of thermo hydraulic transitions and phase interactions. The main difficulties in modeling arise from the existence of interfaces between phases and discontinuities associated with them. The internal structures of two-phase flow are classified by the flow regimes or flow patterns. Various transfer mechanisms between two-phase mixture and the wall, as well as between two phases, depend on the flow regimes.

1.4.1 Flow Description

When gas-liquid mixtures flow upward in a vertical tube, the two phases may distribute in a number of patterns, each characterizing the radial or / and axial distribution of liquid and gas. The flow is often quite chaotic, and these phase distributions are difficult to describe. The flow regimes are designated into four patterns as follows [7]:

1. Bubbly Flow: the gas phase is dispersed and distribution in the form of discrete bubbles in a continuous liquid phase.

2. Slug Flow: Most of the gas is located in large bullet shaped bubbles, which have a diameter almost equal to the pipe diameter. They move uniformly upward and are sometimes designated as " Taylor bubbles." Taylor bubbles are separated by slugs of continuous liquid which bridge pipe and contain small gas bubbles. Between the Taylor bubbles and the pipe wall, liquid flows downward in the form of a thin falling film.

3. Churn-Turbulent Flow: Churn-Turbulent flow is somewhat similar to slug flow. It is, however, much more chaotic. Churn-Turbulent flow possesses some of the characteristics of slug flow, with the main differences being as follows: (a) The gas slugs become narrower and more irregular. (b) The continuity of the liquid in

the slug is repeatedly destroyed by regions of high gas concentration, and (c) The thin falling film of liquid surrounding the gas slugs can no longer be observed.

4.   Annular Flow: Annular flow is characterized by the continuity of the gas phase along the pipe in the core. The liquid flows partially as a film along the walls of the tube, and partially as droplets in the central gas core.

The sketch of typical flow regimes observed in the small tubes is shown in Figure 1.1. The flow regimes of small tubes have the following characteristics. In bubbly flow, bubbles tend to concentrate along the tube axis, small bubbles form a spiral train, while larger bubbles with the diameter closer to the tube inner diameter line up right next to each other to form bubble trains, without coalescing. In slug flows, slug bubbles are relatively long and have a beautiful smooth nose. Bridges of very thin liquid film are observed in a long slug bubble. In liquid slugs, restlessly oscillating small bubbles are observed. In churn-turbulent flow, long slug bubbles are deformed and they do not have a semi-spherical nose any more. A number of tiny bubbles are observed moving rapidly in liquid slugs.

1.4.2 Criteria for Flow Regime Transitions

Traditional two-phase flow regime criteria based on the gas and liquid superficial velocities may not be suitable to the analyses of rapid transient or entrance flows by the two-fluid model. Under these conditions, it is postulated that direct geometrical parameters such as void fraction were simpler and more reliable parameters to be used in flow-regime criteria than the traditional parameters [2].

1.   Bubbly flow to slug flow transition:
The transition from bubbly to slug flow occurs due to agglomerations and coalescences of small bubbles into cap bubbles. This transition takes places at the void fraction around 0.3.   Mishima and Ishii [2] used a very simple geometrical model of the bubbles distribution. They found that the number of the collisions and coalescences becomes very

large when the maximum gap between the bubbles becomes less than a bubble's diameter. The drift flux model is used to convert this into relationship between j_g and j_f as follows:

$$j_f = \left(\frac{3.33}{C_o} - 1\right)j_g - \frac{0.76}{Co}\left(\frac{\sigma\, g\Delta\rho}{\rho_f^2}\right)^{1/4} \tag{1.7}$$

where

$$C_o = 1.2 - 0.2\sqrt{\left(\frac{\rho_g}{\rho_f}\right)}$$

For round tubes.

2. Slug flow to churn flow transitions

The transition will take place as the slug bubbles are lined up right next to each other and the tail of the preceding bubbles starts to touch the nose of the following bubble. This causes the liquid slugs to become unstable and can not sustain its individual identity and leads to chaotic churn-turbulent flow with unstable liquid slugs or liquid bridges. The transition criteria is given as follows:

$$\alpha \geq 1 - 0.813\left\{\frac{(C_o - 1)j + 0.35\sqrt{(\Delta\rho g D/\rho_f)}}{j + 0.75\sqrt{(\Delta\rho g D/\rho_f)}(\Delta\rho g D^3/\rho_f v_f^2)^{1/18}}\right\} \tag{1.8}$$

3. Churn-Turbulent flow to annular flow transition:

This transition occurs by two different mechanisms. The first mechanism is flow reversal in the liquid film section along large bubbles while the other is the distraction of liquid slugs or large waves by entrainment.

The criterion based on the first mechanism can be obtained by assuming that the annular drift-velocity for the film section along large bubbles will be taken under one condition, which is $j_f = 0$. Then the transition criterion can be simplified as [2]

$$j_g = \sqrt{\left(\frac{\Delta \rho g D}{\rho_g}\right)}(\alpha - 0.11) \qquad (1.9)$$

The second mechanism is obtained from a force balance on the liquid wave between the starting force and the vapor drag and surface tension force. The condition for entrainment is then given by

$$j_g \geq \left(\frac{\sigma g \Delta \rho}{\rho_g^2}\right)^{1/4} N_{\mu f}^{-0.2} \qquad (1.10)$$

where $N_{\mu f}$ is the viscosity number given by

$$N_{\mu f} \equiv \mu_f / \left[\rho_f \sigma \sqrt{\frac{\sigma}{g \Delta \rho}}\right]^{1/2}$$

1.5 Thesis Objectives

Development of the closure relation for the interfacial area concentration is essential in order to solve the two-fluid model and also to assess the characteristics of the two-phase flow systems. The objectives of the present study are as follows:

1. To experimentally investigate the interfacial area concentration and void fraction, Sauter mean diameter, and bubble velocity.

2. To analyze the data at three different axial locations L/D=17, 120 and 217 and to evaluate the data by using the drift flux model.

Bubbly flow   Slug flow   Churn –Turbulent flow   Annular flow   Annular-mist flow

Figure 1.1 Flow patterns in vertical flow.

العنوان:	INTERFACIAL AREA CONCENTRATION AND VOID FRACTION OF TWO PHASE FLOW IN 12.7 mmID PIPE-
المؤلف الرئيسي:	Al Dorwish, Yousef M.
مؤلفين آخرين:	Ishi, Mamoru(Super.)
التاريخ الميلادي:	2000
موقع:	لافاييت
الصفحات:	1 - 120
رقم MD:	614708
نوع المحتوى:	رسائل جامعية
اللغة:	English
الدرجة العلمية:	رسالة ماجستير
الجامعة:	Purdue University
الكلية:	The Graduate School
الدولة:	الولايات المتحدة الأمريكية
قواعد المعلومات:	Dissertations
مواضيع:	الطاقة النووية، الإشعاع النووي، الهندسة النووية
رابط:	https://search.mandumah.com/Record/614708

www.manaraa.com

CHAPTER 2

EXPERIMENTAL FACILTY

Experimental studies are necessary the "first step" to develop the required closure relations for the two-fluid model. The lateral distributions of gas void fraction, the interfacial area concentration, and the bubble Sauter mean diameter at three different axial levels can be measured accurately with local measurement techniques. These parameters are important in terms of defining the structure and the axial development of the two-phase flow fields. The experimental facility, instrumentation, data acquisition system and measurement methods are described in this chapter.

2.1 The Experimental Facility

The two-phase flow experiments were carried out in an air-water system for various different flow regimes. The layout of the experimental loop is shown in Figure 2.1. The deionized water supply is held in a holding tank. A water filter, which can remove particles up to 5 μm, is installed at the by-pass line. Constant filtering is necessary to remove the foreign particles. The water circulation is driven by a centrifugal pump, which can deliver the liquid flow rate up to 10 m/s into a 12.7-mm ID test section. The work performed by the pump may increase the liquid temperature, which can affect bubble size, interfacial area concentration measurements, and general experimental conditions. In order to keep the temperature constant, the heat exchanger is installed in the tank. The water from the pump to the test section is carried through the PVC pipes 1-inch schedule 80. In order to achieve a uniform bubble size at the inlet, the liquid flow shearing the air off from the porous tip (shown in Figure 2.1 as j_{f_1}) is fixed at constant flow rate of 0.04 m/s. The total liquid flow rate at the test section is then controlled by

varying the liquid flow rate through the additional inlets, denoted in Figure 2.1 as j_{f2}. The bubble generator has the capability to control and produce different bubble sizes at different flow rates. This is a key element in order to simulate correctly the two-phase phenomena and to understand their effect in the interfacial area concentration. The porous material utilized is designed in order to allow the maximum air flow rate according to our conditions. So, Air is injected through a porous tube, with averaged porous size of 10 microns, located in the mixing chamber as shown in Figure 2.3. The bubbles generated by this special design injector are in the order of 1 mm. The back pressure of a large storage tank, which is pressurized, to 130 psig, drives the air. This pressurized storage tank can provide air flow rates up to 10 m/s in 12.7 mm ID test section for many hours of steady state flows. The operating pressure in the air line is controlled with a regulator and a throttle valve controls the air flow rate.

The water and air flow rates are measured by on-line meters. For the water flow rate, electromagnetic flowmeters (Honeywell Magnew 300) and rotameter are used for different ranges of velocities. The electromagnetic meter consists of a detector and a converter. The system is powered with a 120VAC line. A 24 VDC is required to read and make the changes to the flow meter via the SFC field communicator. The diameter is 1in and used to cover liquid superficial velocity ranges from 1 m/s to 5 m/s. The magnetic flow meter has an accuracy of ± 1% of the reading when the output is between 90% and 100% of scale. The air flow is measured with a rotameter bank of four tubes (Omega, N113-02, N082-03, N092-04). This rotameter covers superficial velocity measurements in the range of 0-1.5 m/s. The airflow enters the two-phase mixing chamber at the bottom of the test section. The air is injected into a stainless steel sparger element.

The double and four point conductivity probes are used to make the two-phase parameter measurements including void fraction, interfacial area concentration and Sauter mean diameter. The conducting tips of the probes are manufactured using acupuncture needles and the probe casing is stainless steel tubing. The probe leads are connected to shielded co-axial cable. The diameter of the probe tip is less than 0.002 mm.
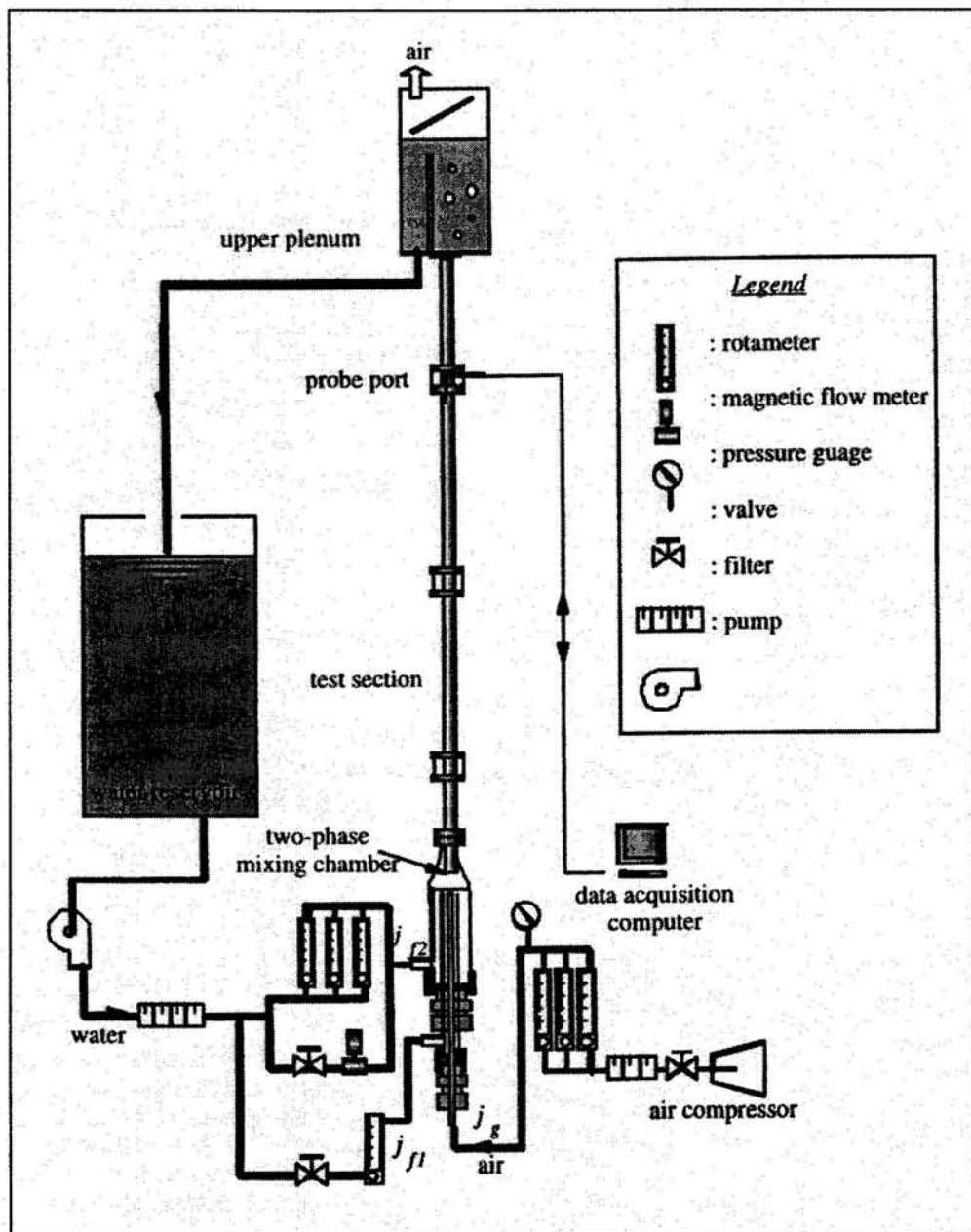
Figure 2.1 General layout of the experimental loop
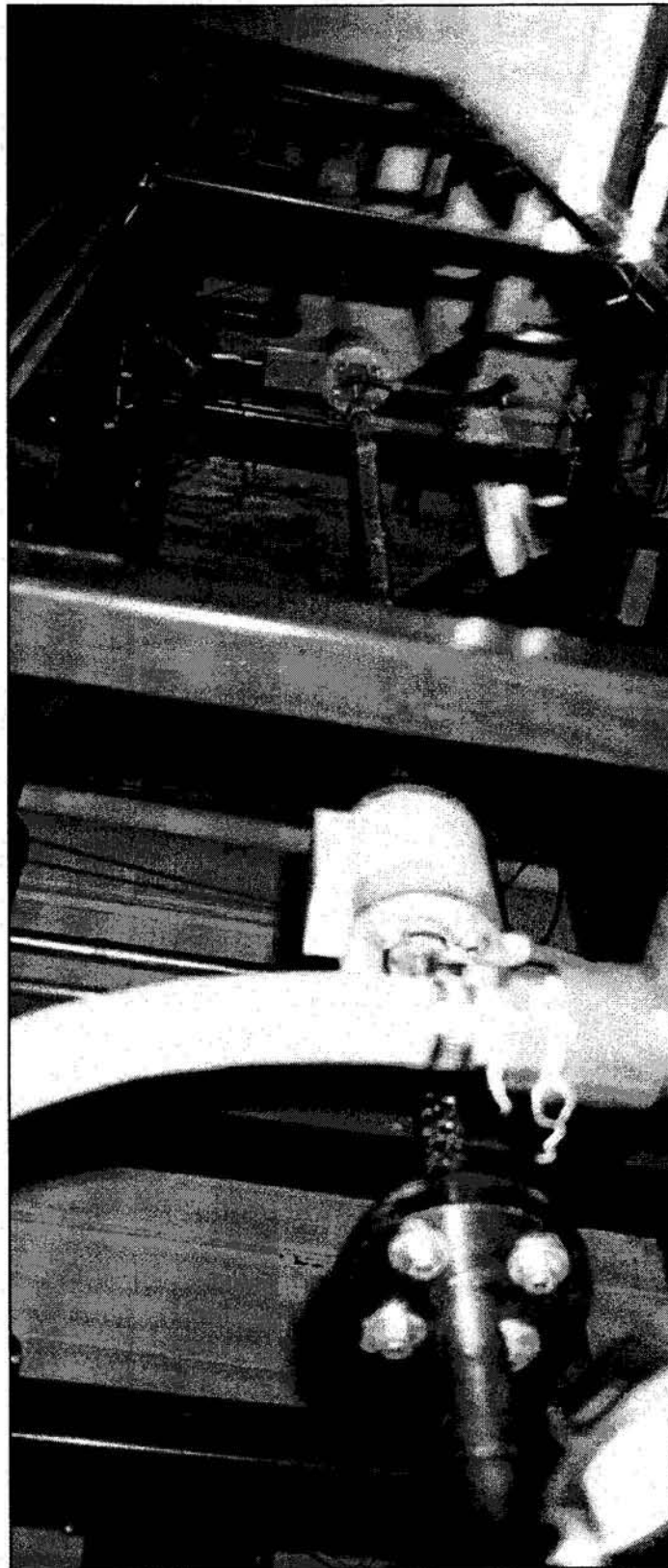
Figure 2.2 Bottom- Top view of the experimental facility
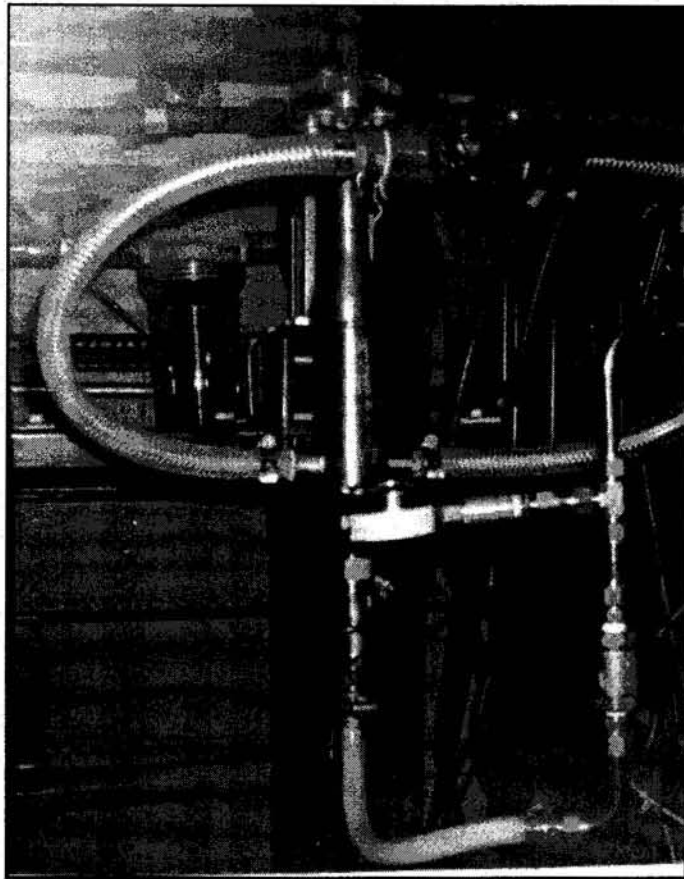
Figure 2.3 the mixture inlet of the two-phase flow

2.2 Test Section and Port Locations

The test section of 12.7 mm ID pipe is shown in Figure 2.4. It has three different port locations and independent four-sensor probe supports. The measurement locations are shown in Table 2.1. The length L is considered from the inlet of the test section after the bubble generator.
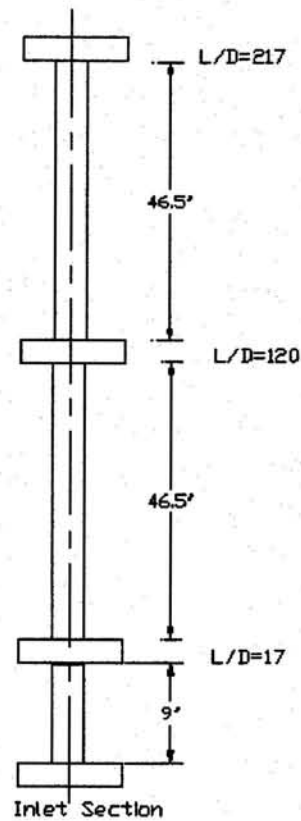
Figure 2.4 Test Section for 12.7 mm diameter

Table 2.1 Port locations for 12.7 mm

Test Section	Port#1 L/D from inlet	Port#2 L/D from the inlet	Port#3 L/D from inlet
12.7 mm	17	120	217

2.3 Experimental Loop Instrumentation

This section describes the instrumentation developed for and used in the experimental loop. The instrumentation consists of conductivity probes to measure the two-phase parameters, a magnetic flow meter to measure the average fluid inlet velocity, a pressure transducer to measure the differential pressure in the test section, and the impedance meters measure the local averaged void fraction which calibration with the conductivity probe and the differential pressure measurement of the volume averaged void fraction.

2.3.1 Differential Pressure Cell

The pressure drop is used to measure by a differential pressure cell, which is Honeywell S900 and mounted in the position to be parallel of port 1(L/D=17). The total pressure drop is the summation of the frictional, acceleration, and gravitational pressure drops. The acceleration component can be neglected due to the constant area of the test section and the frictional component is small in the low flow rate. Accordingly, the total pressure drop along the test section is

$$\Delta P_{grav} = \rho_m gh = \rho_f (1-\alpha)gh$$

where ρ_f and ρ_m are the fluid density and mixture density respectively, h is the height difference between the pressure taps, and g is the acceleration due to the gravity. This equation provides a relationship between the measured pressure drop and the volume averaged void fraction. However, the effect of the frictional pressure drop component will be considered for liquid flow rates around 0.5 m/s.

2.3.2 Local Void Fraction and interfacial Area Concentration Measurements

Two types of multiple-sensor probes have been used: double-and four-senor probes. The end of the probe holder is attached to a mechanical traverse. The probe can be moved back and forth in the radial direction with accuracy to 25.4 micrometer. Hence, the radial distribution of void fraction and interfacial area can be mapped out by successive measurements.

The conductivity probe is based on the difference in conductivity observed between water and air. An exposed sensor coupled with an electrically insulated case can obtain the characteristic rise and fall of the impedance signals between the sensor and common ground as bubble pass through the sensor. The sensors are made of an electrically conductive material, which is insulated except for the tip. The body of the probe is also conductive and is part of the electrical circuit. When a voltage is applied to the sensor tip, contact with the liquid phase completes the circuit between the tip and the probe casing. The presence of a bubble will temporarily disrupt the circuit, and the resulting voltage drop can be measured. The actual probe is a 0.1 mm stainless steel needle, which has been coated with a nonconductive resin except for the very tip. The needle is then connected to a copper wire and inserted into a 3.175 mm diameter stainless steel tube, which serves as the body of the probe.

The void fraction is determined by processing the raw voltage signal, converting it into a square wave. The length of each square is the bubble residence time, Δt. The total residence time divided by the total sampling time, T, is the local time averaged void fraction. To determine a threshold value of 15% above the baseline voltage is set. All points above the threshold value assume a value of 1 and all points below the threshold are 0. The total number of counts in the gas phase, n, divided by the total number of counts, gives a good approximation to the local time averaged void fraction,

$$\alpha = \frac{\sum \Delta t}{T} \cong \frac{n}{N} \qquad (2.1)$$

The capability to measure the local interfacial velocity of bubbles with multiple sensors allows obtaining the local time-averaged interfacial area concentration. The local time-averaged interfacial area concentration is calculated as defined by Ishii [5]:

$$\overline{a}_i^t = \frac{1}{\Delta T} \sum_j \left(\frac{1}{|v_i . n_i|} \right) \qquad (2.2)$$

where j denotes the jth interface that passes a local point during the time interval, ΔT. The variables v_i and n_i are the bubble interfacial velocity and the unit surface normal vector of the jth interface, respectively. Equation (2) implies that the interfacial area concentration can be obtained directly from the bubble interface velocity. A mathematical method to determine the local time-averaged interfacial area concentration was proposed by Kataoka et al. [28] utilizing a double sensor probe for local interfacial measurements. They assumed that there is no correlation between $\frac{1}{|v_i|}$ and $\frac{1}{\cos(\phi_j)}$. Therefore, the interfacial area concentration is calculated by

$$\overline{a}_i^t(x_o, y_o, z_o) = 2N_T \frac{1}{|v_i|\cos(\phi)} \qquad (2.3)$$

where $\overline{a}_i^t(x_o, y_o, z_o)$ is the time averaged interfacial area concentration at (x_o, y_o, z_o), N_T is the number of bubbles which pass the point (x_o, y_o, z_o) per unit of time, and ϕ is the angle between the unit normal of the surface.

When used for double-sensor probe, Equation 2.3 assumes that all bubbles are spherical and that every part of the bubble has an equal probability of being intersected by the probe. It assumes that the angle between the bubble interfacial velocity and the axial direction is random with an equal probability within some maximum angle. However, in many two-phase flow systems bubbles are not always spherical, which makes the applicability of the double-sensor probe limited. One of the advantages the four-sensor conductivity probe is its capability to measure bubbles of different shapes with one common and three independent sensors, where three pairs of double sensor

probes can be formed. Therefore, the three components of interfacial velocities can be obtained locally by measuring the time delay between the signals from these three pairs of double-sensors.

2.3.3 Data Acquisition System

The data acquisition hardware consists of a signal connector block, an acquisition board, and a PC. The acquisition board is a National Instrument Brand (PCI-MIO-16E-4) and has a sampling rate of 250 KS/s with a 12-bit resolution. The board has 16 single ended or 8 differential channels. The signals are sent to the board via the shielded connector block (SCB-68), which acts as an interface between the instrumentation and the acquisition board. The computer is a Compaq Pentium II 233 MHz. The memory of the computer has been upgraded in order to avoid complications during acquisition.

The software used is the National Instruments Brand Labview software. The software uses a graphical programming language and has an extensive library of ready-to-use data acquisition programs. A Signal analysis package is also available which allows for results to be viewed on the screen immediately after acquisition. Thus, the software allows us to check the signal during acquisition, and the results can be viewed and analyzed immediately so that erroneous data can be discarded.

2.3.4 Impedance Meter

2.3.4.1 Theoretical Description

A major part of the hardware of non-intrusive multiphase flow diagnostic system is the impedance void-meter, which is based on the technique of impedance measurements of two-phase flow. Information about void fraction, void distribution, and void propagation velocity can be obtained by measuring the impedance values of a two-phase mixture. Since water is more conductive than air, the electrical potential in the gas phase can be

ignored. The electrodes establish an electrical potential in the flow. In an irrotational electrical field, this potential can be defined as

$$E = -\nabla U \qquad (2.5)$$

The impedance between electrodes, G, is the ratio of the total current passing through each electrode, I, to the imposed potential difference between electrodes, V,

$$G = \frac{I}{V} \qquad (2.6)$$

The current density in the two-phase mixture is the electric current per unit cross-sectional area at any point in space. Since the current density is non-uniform, it is related to the total current by

$$I = \int j.dA \qquad (2.7)$$

where dA is the curve along the interface between an electrode and the two-phase mixture. The current density is also proportional to the electrical field in the mixture, and Ohm's law gives

$$j = \sigma_c E \qquad (2.8)$$

where σ_c is the fluid conductivity. Combining these equations, we can arrive at the result for the impedance in the two-phase mixture

$$G = \frac{\sigma}{V} \int \frac{\partial U}{\partial n} dA \qquad (2.9)$$

The liquid conductivity and the applied voltage are assumed to be constant. Thus, impedance values will change according to the two-phase distribution across the cross-sectional area.

2.3.4.2 Relation between Void Fraction and Impedance

In order to properly calibrate the impedance meter, the relationship between the measured impedance and the void fraction of the flow needs will to be determined. First the impedance values are dimensionalized as follows,

$$G^* = \frac{G_m - G_f}{G_g - G_f} \tag{2.10}$$

where G_m is the measured mixture impedance, G_f is the impedance for the liquid phase only; and G_g is the impedance for the gas phase only. The impedance of the tow-phase mixture depends upon its conductivity and geometrical distribution. For bubbly flow, if the void fraction is assumed uniform, then the dimensionless impedance of the mixture can be predicated by Maxwell's relation [9]

$$G^* = 1 - \frac{3\alpha}{2 + \alpha} \tag{2.11}$$

This relation is based on the assumption that the gas phase consists of non-interacting g equal-sized spheres distributed uniformly across the field, this is what takes place in very dispersed bubbly flows. For separated flows, as annular flow, the void fraction is related to the film thickness of the liquid. In this case the dimensionless impedance can be approximated as

$$G^* = 1 - \alpha \tag{2.12}$$

In either case, a simple relationship exists relating the void fraction to the dimensionless impedance. To determine the applicability of these theoretical relationships, a cross calibration of the impedance meter was performed using the void fraction measurements for the DP cell. It was determined that for bubble and slug flow regimes the relation=$1-\alpha$, is a good approximation. The error in the bubbly flow regime was as low as 0.5% while the error in slug flow regime was 1.0%. The impedance measures 76.2 mm tall and each electrode is 9.525 mm wide by 9.525 mm thick. The body is made of Delrin, which also acts as an electrical insulator. The impedance meter circuit consists of a buffer, a current-voltage amplifier, a demodulator, a low-pass filter, and a voltage amplifier as shown in Figure 2.5. The output of the circuit is designed to be proportional to the measured impedance, i.e. $V_{out} \propto G_m$. Alternating current is supplied at 100 kHz to the electrodes on the impedance probe to avoid double layer effect. The circuit is calibrated by a set of resistors and a very good linearity between input and output has been obtained.

From a fuction
Generator

To electrodes

Buffer

Current- Voltage Amplifier

Demodualtor

To A/D
converter

Low-Pass Filter

Output Amplifier
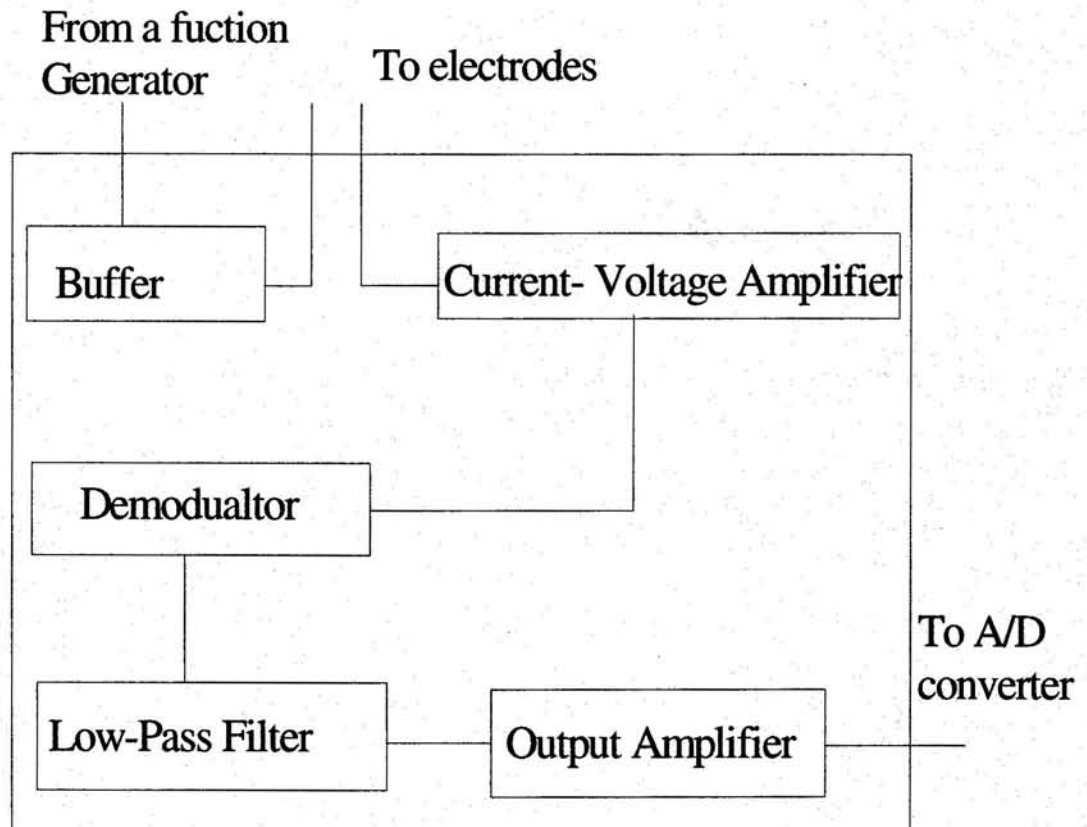
Figure 2.5 Functional block drawing of the circuit for impedance measurements.

2.3.7 Signal Processing

The signal processing scheme is structured in two main parts; namely, the signal conditioning part and the data processing. The signal conditioning part includes filtration, normalization, and generation of step-signal processes, whereas the data processing one consists of categorization, calculation, and correction processes.

The signal conditioning should proceed any other signal processing procedures in order to obtain accurate two-phase parameters. In conditioning the raw signals from the probe, the moving filter is first applied to remove any high frequency noises. Next, the filtered signals are normalized. The remaining noises are removed by setting a certain threshold level after the normalization process. In principle, this level can be determined by the standard deviation of the voltage fluctuations due to noises. In practice, however, the threshold level determined by an experimental observation can be acceptable if the noise fluctuations are small. Therefore, in present experiments, 0.05 Volts threshold level determined by experimental observation is set as an adequate level to remove noises. Moreover, due to the finite rise/fall time in the signal, an ambiguity in identifying the bubble interface can arise. Therefore, the signal is converted into step signal at the initial and final data points of the interfaces.

After the signal conditioning process is completed, the step-signals are then separated into signals of spherical, distorted, cap, and slug bubbles depending on their bubble cord lengths. The separated signals are processed independently and categorized into two groups in light of the building of data basis for two-group interfacial transport equation. Hence, the spherical and distorted bubbles are categorized as group one, and the cap and slug bubbles are categorized as group two. The maximum distorted bubble limit and the spherical bubble limit by Ishii and Zuber [10] are used as criteria in this categorization process. They are given by

$$D_{d\,max} = 4\sqrt{\frac{\sigma}{g\Delta\rho}} \text{ , max distorted bubble limit} \qquad (2.13)$$

and

$$D_{ds} = 4\sqrt{\frac{2\sigma}{g\Delta\rho}}N_{\mu_f}^{1/3} \ , \ \text{spherical bubble limit} \tag{2.14}$$

where

$$N_{\mu_f} = \frac{\mu_f}{\left(\rho_f\sigma\sqrt{\frac{\sigma}{g\Delta\rho}}\right)^{1/2}}$$

For the identification of the slug bubbles, the bubbles, whose diameter is same as the tube diameter, is defined as slug bubbles. In obtaining the two-phase parameters, signals from the common sensor (sensor 0 in Figure 2.6) are used for the bubble cord length and the void fraction. For interfacial area concentration, the signals from the double-sensor probe, sensor 0 and 1, are used to calculate the interfacial area concentration for the spherical bubbles, and signals from three pairs of double-sensor are used to calculate the interfacial area concentration.

When the bubbles pass through all of the four sensors, four consecutive signals from front and rear interfaces of passing bubbles will be registered. Then, the three components of local interfacial velocity of front and rear interfaces can be calculated from the time-delay information. However, due to the finite size of the measurement area of the probe and fluctuation of the bubble interface, there will be some bubble interfaces, which do not penetrate all the four sensors. Since the 'missing bubble' phenomenon would occur, however, small the probe is made, it should be properly accounted for in the calculation of the interfacial area concentration.
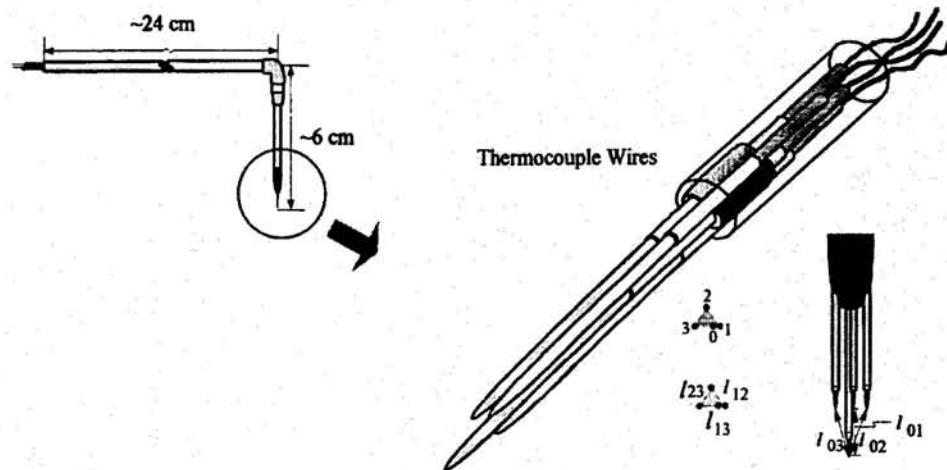
~24 cm

~6 cm

Thermocouple Wires

Specifications
sensor max. O.D.; 0.1 mm
meaurable bubble sizes; ~1 mm to slug bubbles
tip alignment (double-sensor) : < 0.1 mm
measurement cross-sectional area (four-sensor) ; 0.2 mm^2

Configuration (mm)
Double-Sensor; $\Delta s \sim 2.6$
Four-Sensor

l_{01}	: 2.4	l_{12}	: 0.7
l_{02}	: 2.4	l_{13}	: 0.7
l_{03}	: 2.6	l_{23}	: 0.7

Figure 2.6 the four-point conductivity probe configuration

العنوان:	-INTERFACIAL AREA CONCENTRATION AND VOID FRACTION OF TWO PHASE FLOW IN 12.7 mmID PIPE
المؤلف الرئيسي:	Al Dorwish, Yousef M.
مؤلفين آخرين:	Ishi, Mamoru(Super.)
التاريخ الميلادي:	2000
موقع:	لافاييت
الصفحات:	1 - 120
رقم MD:	614708
نوع المحتوى:	رسائل جامعية
اللغة:	English
الدرجة العلمية:	رسالة ماجستير
الجامعة:	Purdue University
الكلية:	The Graduate School
الدولة:	الولايات المتحدة الأمريكية
قواعد المعلومات:	Dissertations
مواضيع:	الطاقة النووية، الإشعاع النووي، الهندسة النووية
رابط:	https://search.mandumah.com/Record/614708

CHAPTER 3

EXPERIMENTAL FLOW REGIME IDENTIFICATION

Due to the lack of data for small pipes, the experiment for flow regime identification was performed to validate the conventional flow regime map given by Mishima and Ishii [2]. The method of flow visualization and that of using impedance meter, and the neural network were employed in flow regime identification. Since the flow visualization method relies on the subjective judgment of the observer, the objective approach employing the self-organized neural network was applied in order to verify and improve the results obtained by the flow visualization method.

3.1 Flow Visualization Method

The simplest method for detecting flow patterns is to visualize the flow through transparent pipe walls. At lower flow rates it is possible to detect the flow patterns with no other method necessary. Unfortunately, at higher rates the human brain cannot process data fast enough to determine the flow, furthermore, the interface configuration become more complicated and it is difficult to see the inside. Thus another process is necessary to capture the flow. At higher rates, photographic methods are useful but they are often limited by the size and depth of the field of view so that only local instantaneous outer behavior may be observed. In the case of slug flow, this strongly hides the viewing of the liquid bridges and could mislead the experimenter into presuming the flow has already changed to another regime when it actually had not. The technology has made it possible to overcome the difficulties of lost resolution with taking high-speed movies. Sony high resolution video camera with a shutter speed of 1/1000 second was used. The result of the flow visualization is shown in Figure 3.1 and 3.2 for different locations at $L/D = 17$ and 217. The comparison with Taitel's flow regime map [11] as shown in Figure 3.3.
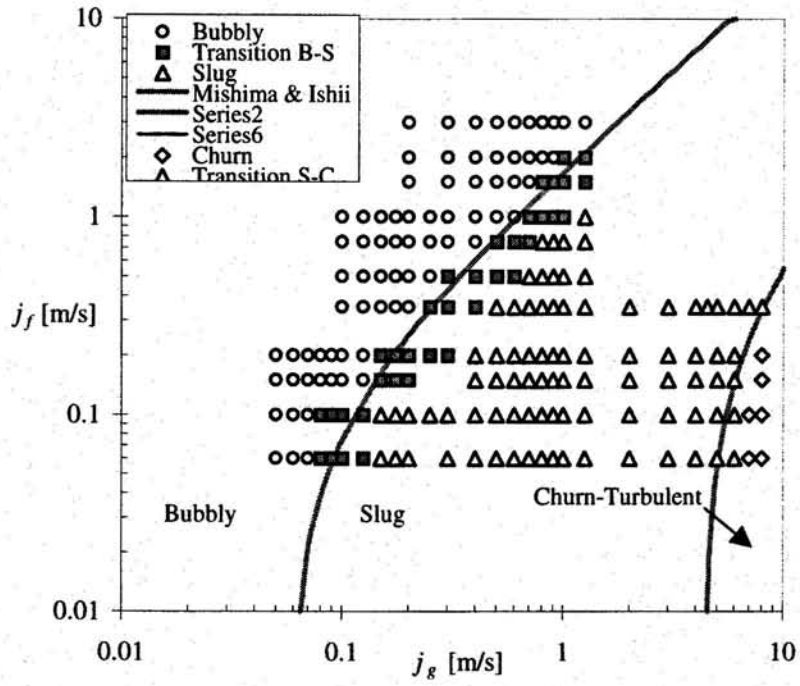
Figure 3.1. The flow regime map by using the visualization method at L/D = 217.
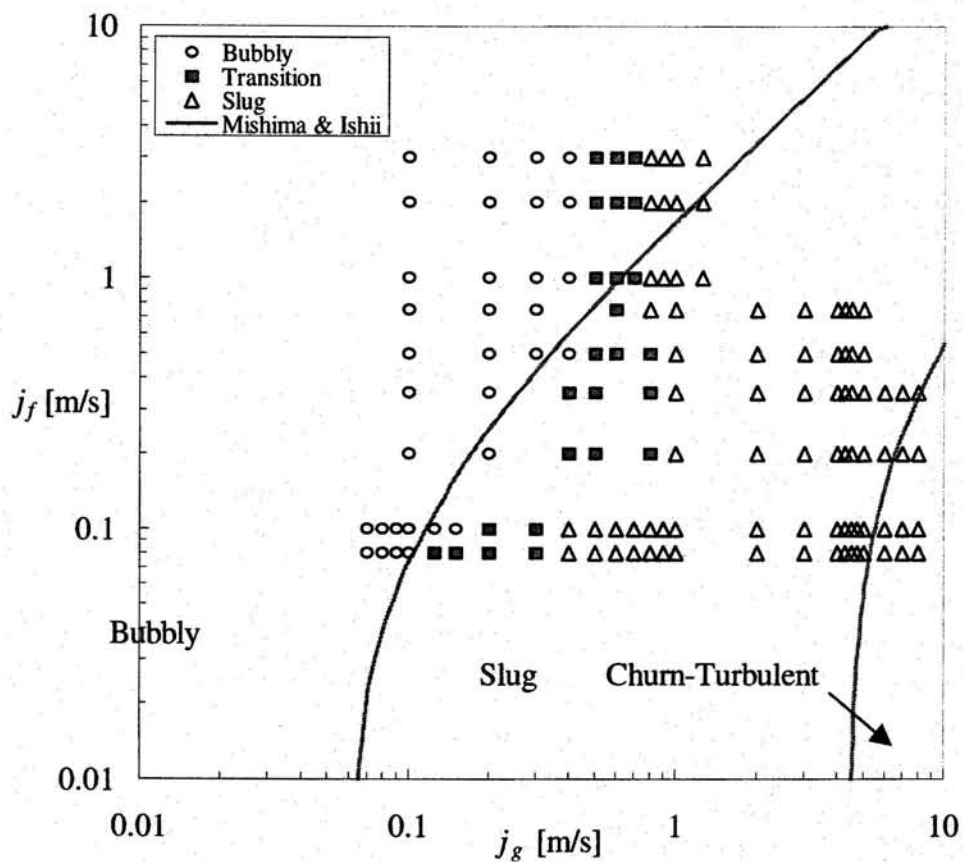
Figure 3.2. The flow regime map by using the visualization method at L/D = 17.
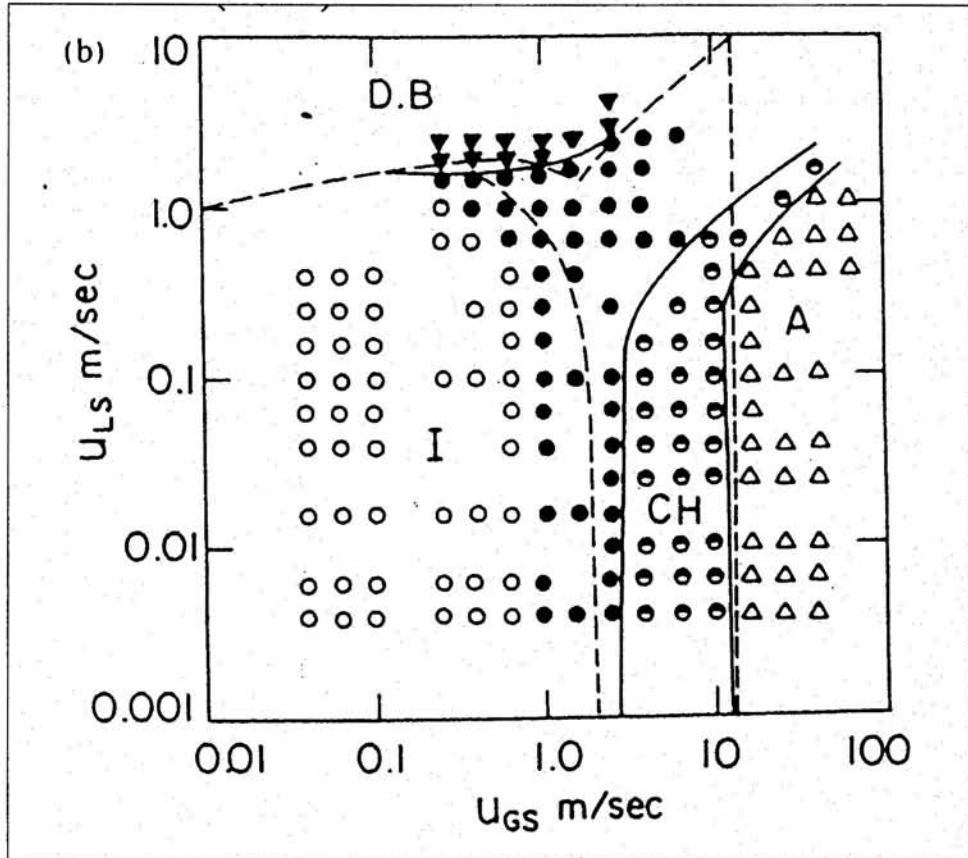
Figure 3.3. Taitel's flow regime map for 12.7 mm vertical air-water loop.

3.2 Impedance Identification Flow Regime Method

The impedance meter is intended for void fraction measurement based on the impedance signals. The output of the impedance is directly related to the void fraction of the flow. Furthermore, each flow regime will create a pattern of impedance fluctuations so that the objective identifier can be used. Any statistical analysis needs to be based on physical understanding of the phenomena. Jones and Zuber [1] show that the probability distribution function (PDF) of the void fraction can be used as an objective parameter to determine the flow regime.

3.2.1 PDF of Impedance Signal

The void fraction is directly proportional to the dimensionless impedance. The mathematical description of the PDF is taken into consideration. The impedance time record is broken up into small increments of ΔG_i^* and the time scale is broken up into increments of Δt_j of the total sampling of T. the ratio $\Sigma t_j / T$ is the probability that the impedance value lies within the given increment ΔG_i^*. The probability density function of a particular interval is given by

$$\lim_{\Delta G^*} \frac{1}{T\Delta G_i^*} \sum_{j=1}^{n_i} \Delta t_j \rightarrow P^i\left(G^*\right) \qquad (3.1)$$

So, if an impedance value is seen to be in a particular ΔG_i^* a total of n_i times within a sampling period T, the time fraction will be related to the count rate by

$$\frac{n_i / N}{\Delta G_i^*} = \frac{1}{T\Delta G_i^*} \sum_{j-1}^{n_i} \Delta t_i \qquad (3.2)$$

where N is the total number of counts over all intervals. By averaging the PDF results over a large number of records, K

$$\overline{P\left(G^*\right)} = \frac{1}{K} \sum_{k=1}^{K} P^k\left(G^*\right) \qquad (3.3)$$

By applying to a statistically stationary process over a time interval significantly larger than the longest period of fluctuation, this averaged result becomes relatively constant.

The PDF plotting for a particular flow regime pattern yields identifiable peaks, which can be related to the physical structure of the flow. The Signals for the impedance for bubbly, slug flow and churn-turbulent are plotted in Figures 3.4, 3.5 and 3.6, as well as their PDF's. It can be seen that the bubbly flow corresponds to a single peak at high dimensionless impedance values. The similarly sized dispersed bubbles in the continuous liquid cause this peak. However, the slug flow is characterized by two peaks. The first peak, which occurs at lower value of the dimensionless impedance value, represents the Taylor bubbles. The second peak is similar to the one in the bubble flow, which is the signal from the liquid slug. The churn flow is characterized by only one peak which is the first peak of the slug flow while the second will be disappeared, which is the signal of the liquid slug.

The flow conditions where these peaks appear or disappear in the PDF have been used to determine the transition points. For instance, Figure 3.7 shows the transition from bubble to slug flow. The three plots show the gradual progression from one regime to anther. The first PDF is a pure bubble flow. The middle one is bubbly flow in which cap bubbles are present. This kind of flow creates a tail on the peak towards the low end. The flow can be considered a slug flow only when the second peak which corresponds to Taylor bubble appears. While the Figure 3.8 shows the transition from slug to churn flow.

3.2.2 Experimental methodology

The flow regimes for 12.7 mm diameter pipe are obtained at different locations L/D = 17, and 217. The procedure of taking the data was as follows. First, a range of different liquid superficial velocity 0.02 –3.0 m/s and also the range of gas superficial velocity 0.2- 8.0 m/s and a large number of data points were taken to determine the transition line between bubble and slug flow. The flow structure was sampled at a rate of 2000 Hz for a period of 30 seconds. By using the Labview software, which can show the PDF signal taken at each data point. Furthermore, after all the data had been acquired, a

Matlab program was used to reconstruct the PDF's of the impedance signals [12]. Finally, the flow regime of each data point determined by the shape of the PDF for $L/D =$ 17 and 217.
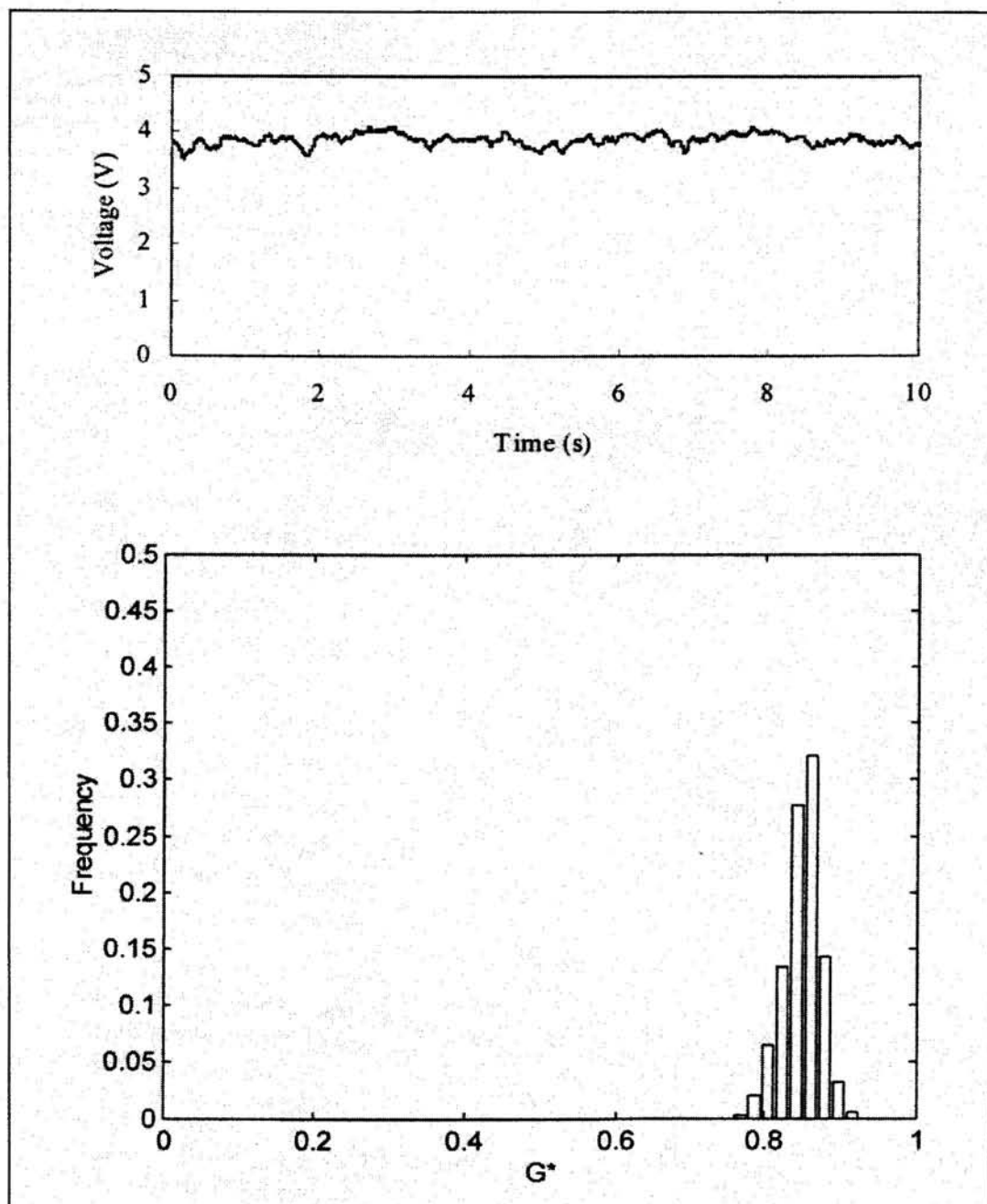
Figure 3.4 Impedance signal and PDF of bubbly flow at L/D = 217.
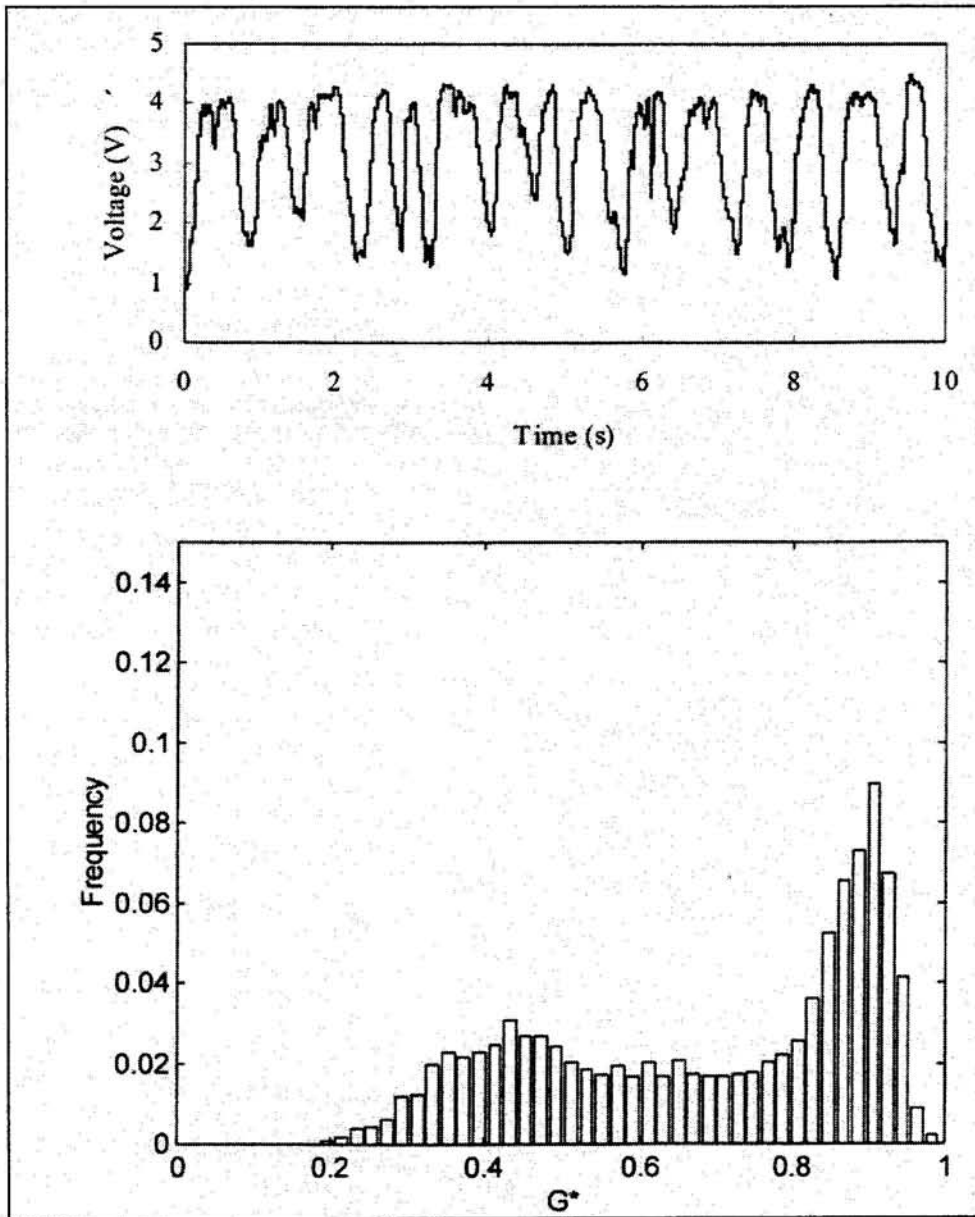
Figure 3.5 Impedance signal and PDF of slug flow at L/D = 217.
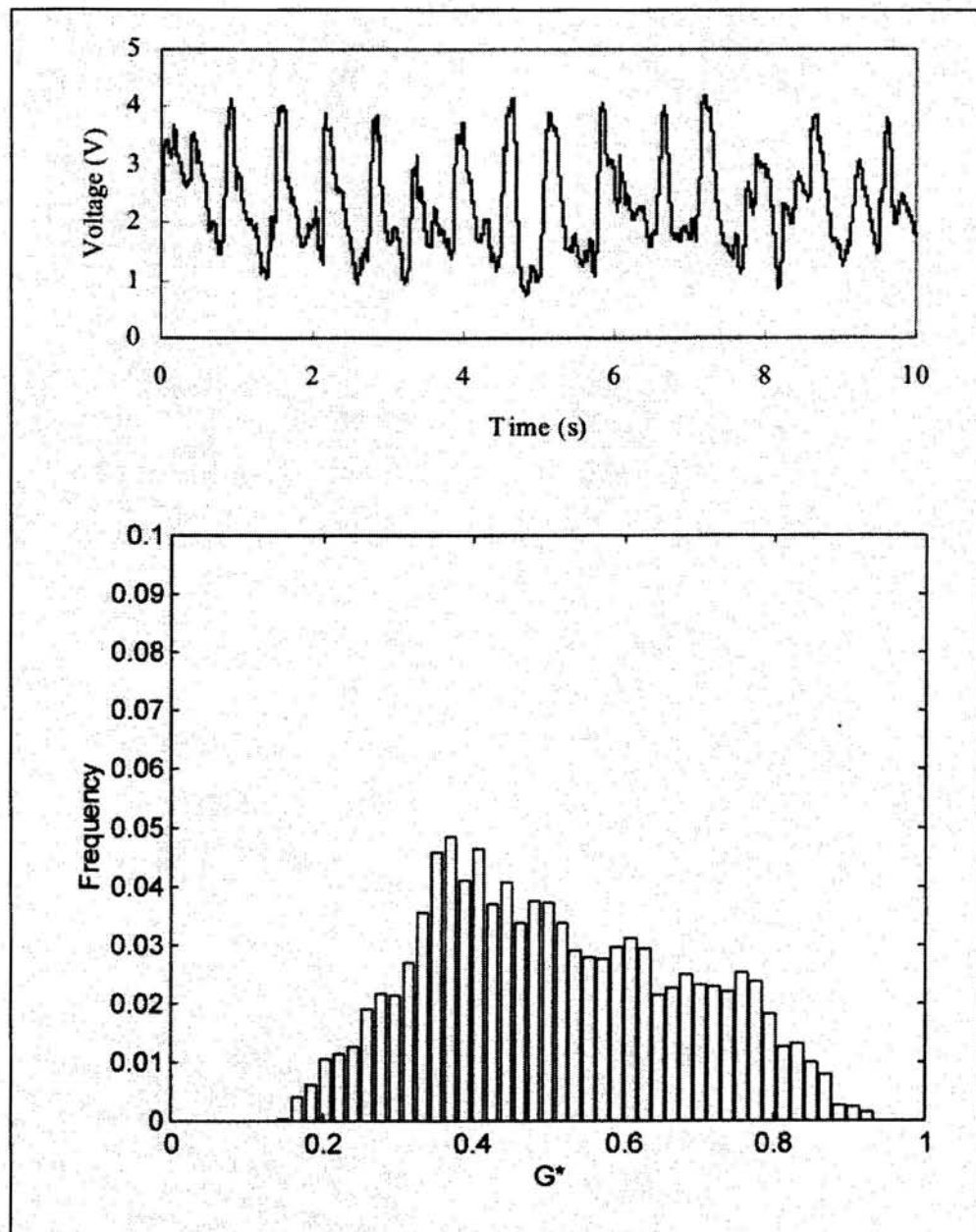
Figure 3.6 Impedance signal and PDF of churn –turbulent flow at L/D = 217.
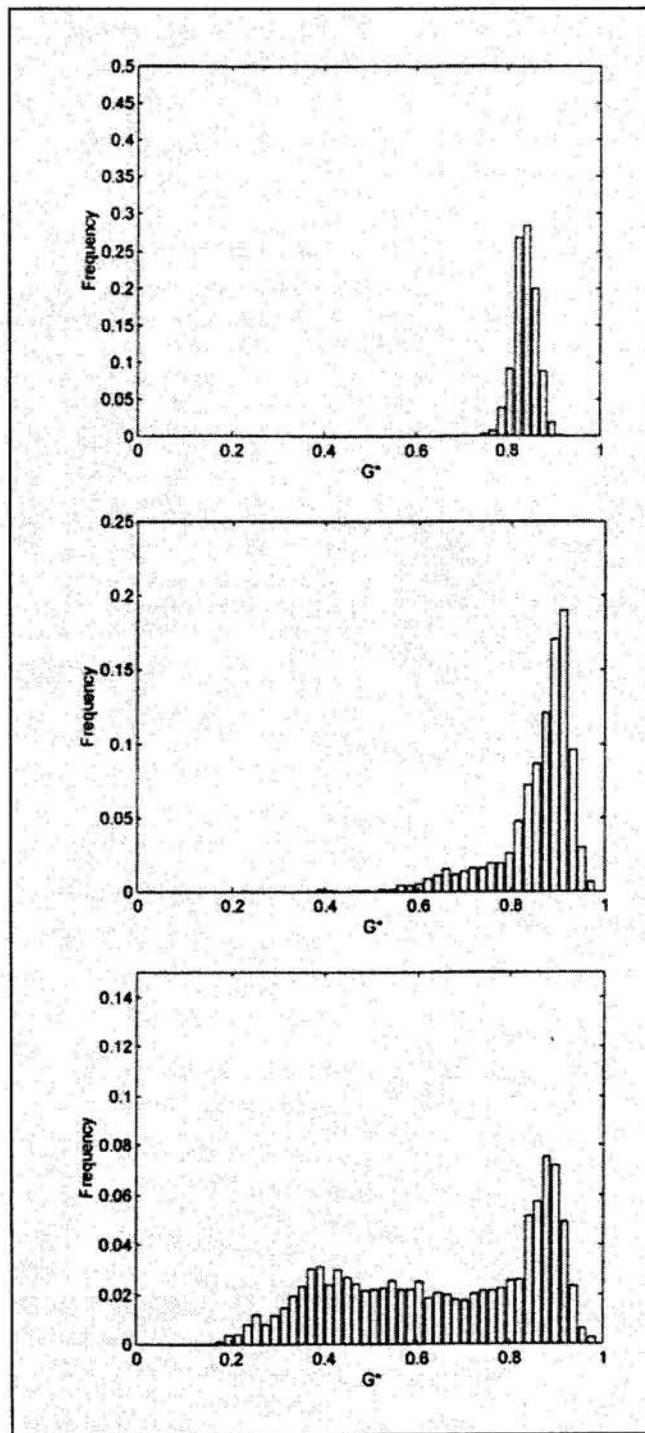
Figure 3.7 Transition from bubbly to slug flow PDF's.
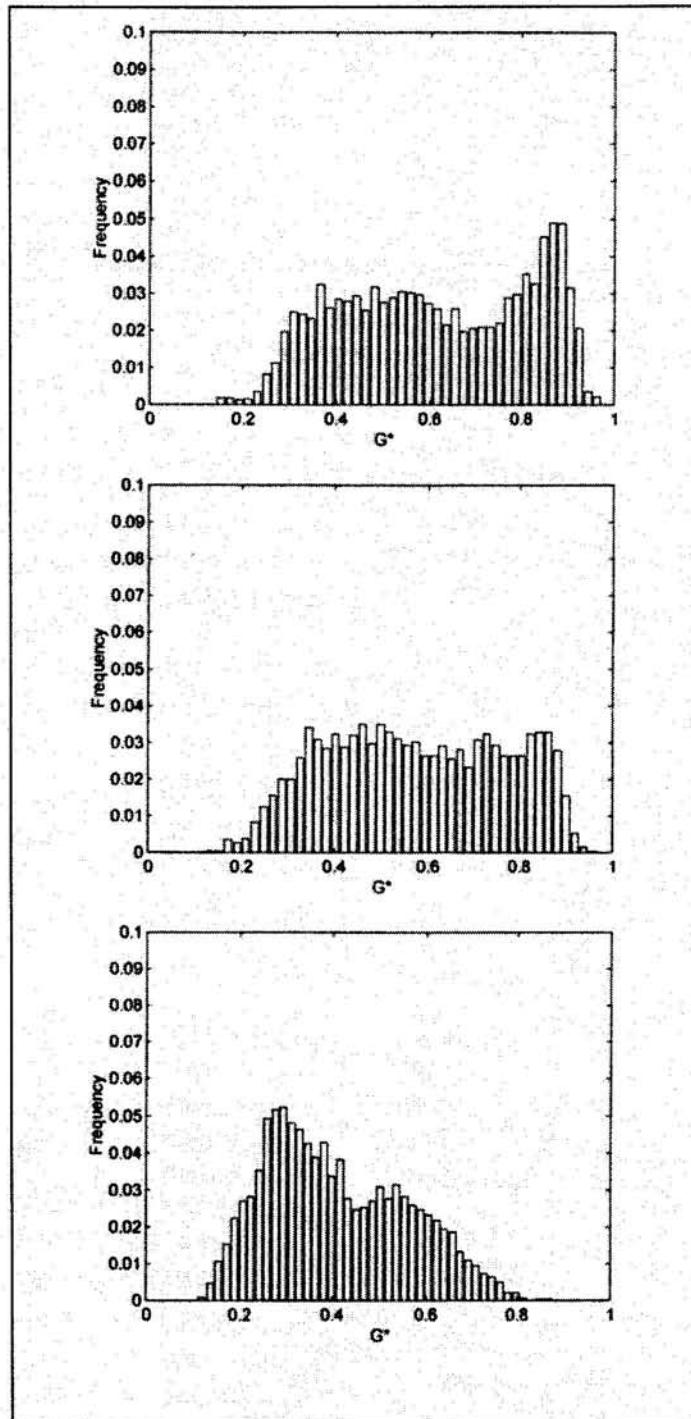
Figure 3.8 Transition from slug to churn-turbulent PDF's.

3.3 Neural Networks Identification Method

The two-phase flow regimes are difficult to be identified by using traditional classifier system. This leads to the use of a non-parametric method, which is capable of non-linear mapping. The supervised and self-organizing neural networks were developed to identify flow regimes through PC-based neural computing [12], [13].

Neural computing (NC) attempts to emulate the workings of the human brain, certainly the most complex computing system in existence, capable of thinking, remembering and problem solving. An essential characteristic of NC is that it uses idealized or artificial neurons and networks to perform arbitrarily nonlinear mappings and discovers hidden relations in various data patterns. In analogy with the biological neuron, which is the fundamental cellular unit of the brain's nervous system, artificial neurons are the elementary processing unit of artificial neural networks. As artificial neural network can be defined as a data processing system consisting of a large number of simple. Highly interconnected artificial neurons. These process elements are usually organized into a sequence of layers with full or random connections between the layers. In this arrangement, where the input layer is a buffer that presents data to the network. The top layer is the output layer, which receives the output response to a given input. The other layer is called the intermediate or hidden layer because it usually has no connections to the outside world [14].

3.3.1 Modeling Approach

A typical; neural network is fully-connected; this means that there is a connection between each of the neurons in any given layer i[th] each of the neurons in the next layer. In all cases, these connections have weighted that must be trained, that is, adjusted through the learning algorithm to best reflect the underlying relation between known inputs and outputs. When known inputs and outputs are presented to the network and the weight modification is supervised by an error minimization algorithm the process is called supervised learning. NC uses supervised learning for approximating complex mappings

and self-organizing neural networks for discovering relations hidden in various data patterns. Both approaches are used for flow regime identification.

A self-organizing neural network [14] is a two-layer network that can cluster input data into several categories that include similar objects detected in the input data. The inputs data to the neural network comes from the impedance signals. The input parameters are the standard deviation and the mean for each flow regimes, which are connected to the first layer through adjustable weights. When an input is presented to the first layer, each neuron receives the weighed input pattern. Then the responses across the layer compete to determine which of the connections to the input signal is the strongest. The neuron with the strongest connection is declared the winner, and the weights of the winning neuron and its immediate neighbors are modified. During this training process, the self-organizing network classifies the input data into similar groups. A very simple neural network, with three output neurons representing the three flow regimes bubbly, slug and churn, is considered.

The normalized average-standard deviation pairs used as inputs to the neural networks as shown in Figures 3.9 and 3.10 for L/D=17 and 217. The neural network toolbox in MATLAB provided all the necessary tools to build a self-organizing network. The process to establish the trained system was to specify the number of nodes or groupings desired and build the output network based on the number of nodes, specifying the initial weights, the learning rate, and training the network using a set of input data. The number of nodes represents the number of flow regimes. First, all the data was presented to the network to be classified into two nodes, which represent the two flow regimes. Then the transition between the two regimes was recalculated using only these two nodes and the corresponding sets of data. Once training is complete, the network can be presented with sets of data for classification.

3.3.2 The Results

In Figures 3.11 and 3.12, the results of the neural network classification at different locations for L/D = 17 and 217 are shown. The agreement between the theoretical transition lines given by Mishima and Ishii [2], and those obtained by the neural network method is plausible. The error percentage is around 5%. The points that are off generally occur near the transition boundaries. The comparison between the visualization and neural network is a clear distinction between the subjective and the objective methods in the transition region. The transition region determined by the neural network is clear and more deterministic, whereas it is wider and vague in the results obtained by the flow visualization method. However, It found that the transient lines between the regimes are moved to the right side at L/D=17. For churn flow, It is shown that at Port 1 (L/D=17) there is no churn flow observed, however at port 3 (L/D=217) the churn flow are observed and this is due to the entrance effect and the flow is not fully developed at port 1. The flow regime inside mixture injector is bubbly flow during all of the flow conditions. As the distance from the injection part increases, more bubble collisions occur to form bigger bubbles such as slug and churn-turbulent flow if the void fraction is sufficiently high. One cannot see the different flow regimes at the inlet of test section, while the different flow regimes can be seen at the outlet because the flow is gradually developed along the test section.
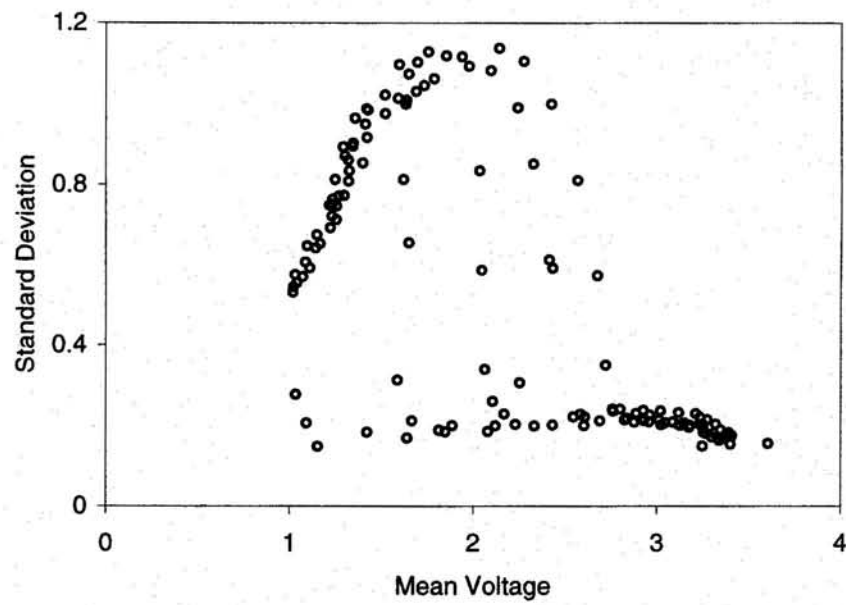
Figure 3.9 Standard deviation of the impedance signals for different conditions at (L/D=17).
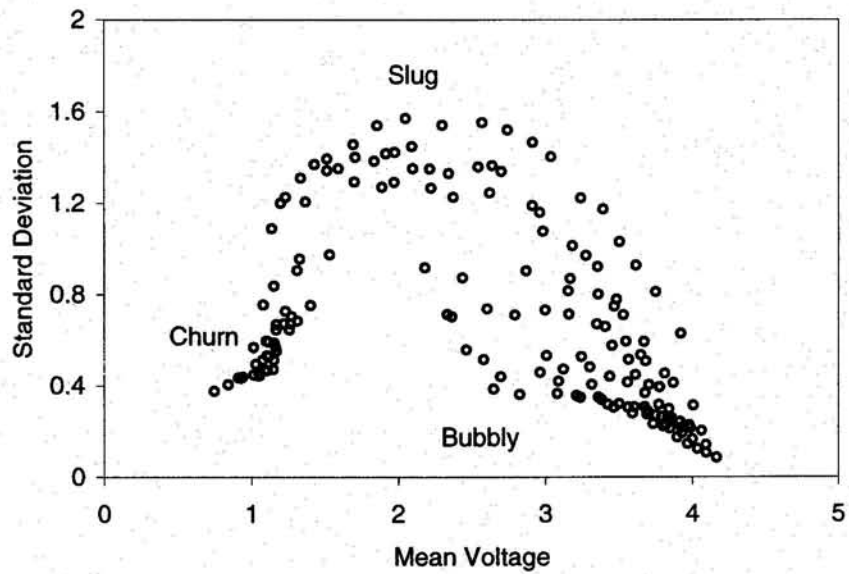
Figure 3.10 Standard deviation of the impedance signals for different conditions at (L/D=217).
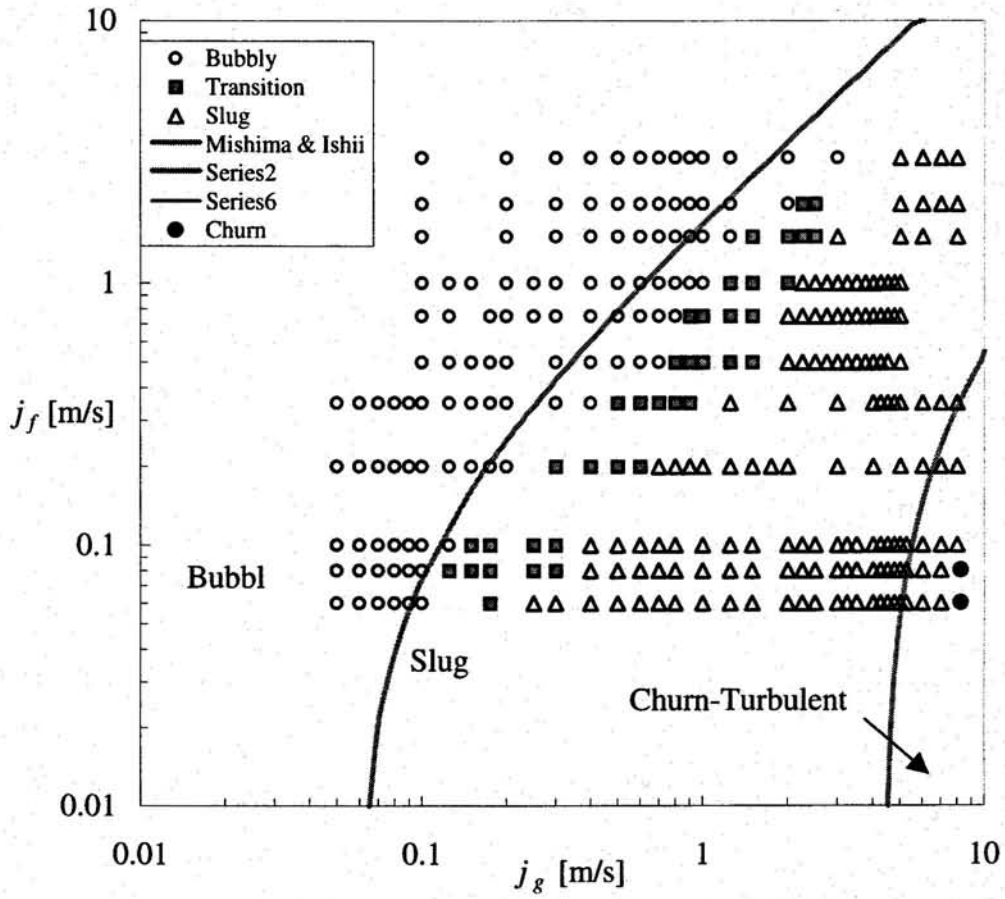
Figure3.10 Flow regime identification in 12.7 mm loop by neural network method at L/D=17.

Figure 3.11 Flow regime identification in loop 12.7 mm by neural network at L/D=217.

العنوان:	INTERFACIAL AREA CONCENTRATION AND VOID FRACTION OF TWO PHASE FLOW IN 12.7 mmID PIPE-
المؤلف الرئيسي:	Al Dorwish, Yousef M.
مؤلفين آخرين:	Ishi, Mamoru(Super.)
التاريخ الميلادي:	2000
موقع:	لافاييت
الصفحات:	1 - 120
رقم MD:	614708
نوع المحتوى:	رسائل جامعية
اللغة:	English
الدرجة العلمية:	رسالة ماجستير
الجامعة:	Purdue University
الكلية:	The Graduate School
الدولة:	الولايات المتحدة الأمريكية
قواعد المعلومات:	Dissertations
مواضيع:	الطاقة النووية، الإشعاع النووي، الهندسة النووية
رابط:	https://search.mandumah.com/Record/614708

CHAPTER 4
THE EXPERIMENTAL RESULTS

This chapter presents the experimental data acquired in the12.7-mm ID vertical co-current air-water loop under adiabatic condition. The local data are acquired by the state-of-the-art four-sensor conductivity probe, which is capable of measuring both small bubbles (group 1) and large bubbles (group 2) for the bubble and slug flows. However, the two-sensor conductivity probe is used for acquiring the void fraction and bubble velocity for the churn flow. The pressure drop measurements are done by both the pressure transducer and the local pressure gauge at each flow conditions.

4.1 Local Flow parameters

In relation to the development of the interfacial area concentration, local measurements of the void fraction, interfacial area concentration, and Sauter mean diameter using the four-sensor probe method were performed extensively for vertical adiabatic co-current air-water flows in a round tube an inner diameter of 12.7 mm at three axial locations of L/D = 17,120 and 217 and from r/R=0 to 0.9. After the flow regime map is determined, the test matrix of interest for the present experimental is determined. Since the objective of the present experimental is to establish the database for the evaluation of the one-group interfacial area transport equation, the focus is made on bubbly flow and bubbly-to-slug transition condition. Hence, the test matrixes for the present experimental are determined as shown in Figure 4.1, which covers the bubbly, transition and slug flows while in Figure 4.2 covers the churn flow. The superficial liquid velocities jf and the superficial gas velocities jg in this experiment are tabulated in Table 4.1 for bubbly and slug and in Table 4.2 for churn flow. The sampling frequency in data acquisition is varied between 8 to 15 KHz depending on the flow conditions. In average,

more than 2000 of group one bubbles and more than 200 group two bubbles are acquired at a local measurement point for the given sampling time at all flow conditions.

By employing the pressure measurements and the inlet superficial gas velocity measured by the rotameters, the local superficial gas velocity at a given axial location is then estimated by

$$\left\langle j_g \right\rangle_{local} = \left\langle j_g \right\rangle_{inlt} \cdot \left(\frac{P_{atm}}{P_{atm} + P_{gage}} \right) \tag{4.1}$$

In order to benchmark the local measurements by the probe, the local superficial gas velocity calculated by equation (4.1) is then compared with the measurements done by the probe by

$$\left\langle j_g \right\rangle_z = \left[\langle \alpha \rangle \langle\langle v_g \rangle\rangle \right]_{probe} \tag{4.2}$$

or

$$\left\langle j_g \right\rangle_z = \left[\langle \alpha_1 + \alpha_2 \rangle \langle\langle \alpha_1 v_{g1} + \alpha_2 v_{g2} \rangle\rangle \right]_{porbe} \qquad \text{For two-group} \tag{4.3}$$

The characteristic results obtained for each flow condition of interest is summarized in Table 4.3. It found out that the error percentage between the probe measurements and rotameter is around 12% however, the rotameter's reading has error within 5 to 7%. So, fairly good agreements were obtained as shown in Figure 4.3 for the bubbly and slug flow and in Figure 4.4 for the churn flow.

4.1.1 Scaling

In order to simulate the prototypic conditions, scaling study is performed to preserve the main physical phenomena for interfacial area transport and mechanistic models for coalescence and break-up term. Air-water is used in the present experiment to model hydrodynamic sources and sinks of interfacial area. The interfacial area transport depends on the following dimensionless groups:

Flow Channel Reynolds Number:

$$Re_f = \frac{\rho_f v_f D}{\mu_f}$$ (4.4)

Particle Reynolds Number:

$$Re_d = \frac{\rho_f v_r D_d}{\mu_f}$$ (4.5)

Particle Weber Number:

$$We = \frac{\rho_f v_f^2 D_d}{\sigma}$$ (4.6)

where Re_f and Re_d are the fluid and particle Reynolds numbers, respectively,

ρ_f, μ_f and σ are liquid density, liquid viscosity and superficial tension,

v_r is the relative velocity, D and D_d are the channel hydraulic and bubble diameter, respectively.

For the design of the simulation experiments, the following prototypic conditions [15] are assumed:

Liquid Velocity	Up to 6 m/s
Hydraulic Diameter	~ 1.2 cm
Weber Number	~ 1.4 to 8
Bubble Reynolds Number	520 ~ 4000
Channel Reynolds Number	up to 5.5×10^5

The bubble size (D_d) for small bubbles is bounded by two limits. These limits are the spherical limit and the maximum distorted bubble size.

The Spherical Limit:

$$D_{d1} = 4\sqrt{\frac{2\sigma}{g\Delta\rho}}N_{\mu_f}^{1/3}$$ (4.7)

where the viscosity number is defined by:

$$N_{\mu_f} = \frac{\mu_f}{\left(\rho_f \sigma \sqrt{\dfrac{\sigma}{g\Delta\rho}}\right)} \tag{4.8}$$

The Maximum Distorted Bubble Size:

$$D_{d2} = 4\sqrt{\frac{\sigma}{g\Delta\rho}} \tag{4.9}$$

The actual lower limit is determined by the particle generating mechanism where the upper limit is mainly determined by the surface stability. Here the lower limit was chosen to be the maximum spherical bubble size, since most of the spherical bubbles do not significantly interact with other bubbles. Thus, the effective lower limit for the bubbles with significant interactions will be D_d. The mean size within the two limits results in an important geometric group, the ratio of the length scales:

$$D_{d^*} = \frac{\overline{D}_d}{D} \tag{4.10}$$

where D is the hydraulic diameter of the flow channel. This length ratio relates to the external length scale to the internal length scale of two-phase flow. The particle size is the most fundamental interfacial length scale to describe the interfacial geometry.

In slug flows, Taylor bubbles and cap bubbles behave differently from spherical/distorted bubbles. The maximum stable transverse dimension of large bubbles (slug or churn-turbulent bubbles) in a large system is determined by the interfacial instability along the leading nose of the bubbles, which is similar to the Kelvin-Helmholz instability. The maximum dimension can be given approximately by:

$$D_{max} = 40\sqrt{\frac{\sigma}{g\Delta\rho}} \tag{4.11}$$

The important internal length scale determines whether or not the slug flow can be developed in terms of the channel dimensions. If D_{max} is small relative to the maximum channel dimension, slug flow regime may not be developed. Instead of having a standard

slug or churn turbulent flow at the intermediate range of void fraction, the flow regime should be cap bubbly or chaotic churn-turbulent flow. The corresponding interfacial area characteristics are also quite different. Thus, it is necessary to introduce another scaling parameter:

$$W^* = \frac{W}{D_{max}}$$
(4.12)

where W is the largest dimension of the cross-sectional area of the flow . Equations 4.10 and 4.12 define the important geometrical dimensional groups that need to be simulated in experimental investigations involving interfacial area transport phenomena.
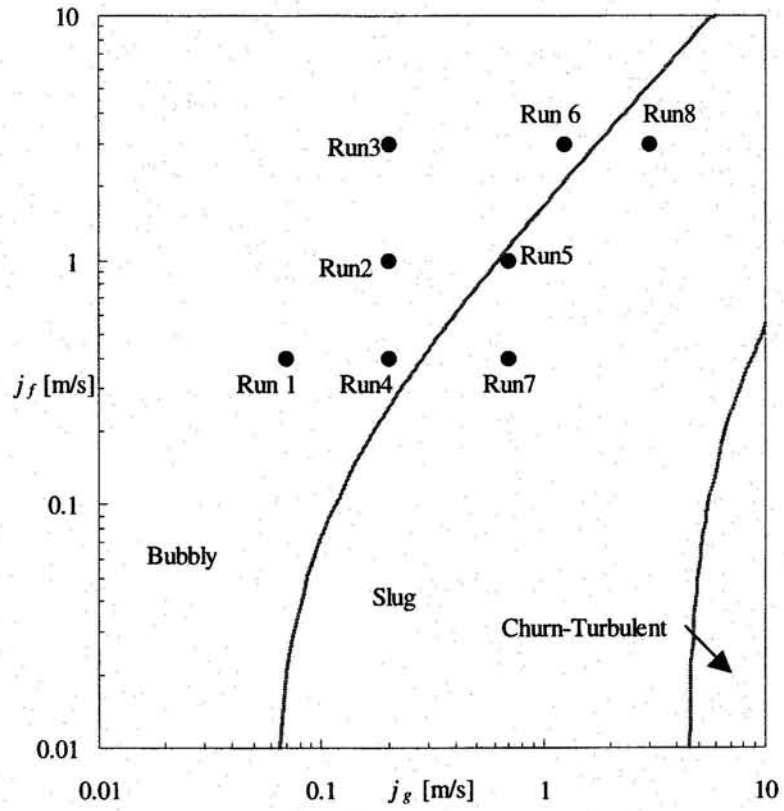
Figure 4.1 Test matrix of the present experimental for the bubbly and slug flow. The solid line is given by Mishima and Ishii [2].

Table 4.1 Flow Conditions for bubbly and slug flow.

Test Matrix		
	j_g [m/s]	j_f [m/s]
Run 1	0.07	0.4
Run 2	0.2	1
Run 3	0.2	3
Run 4	0.2	0.4
Run 5	0.7	1
Run 6	1.25	3
Run 7	0.7	0.4
Run 8	3	3
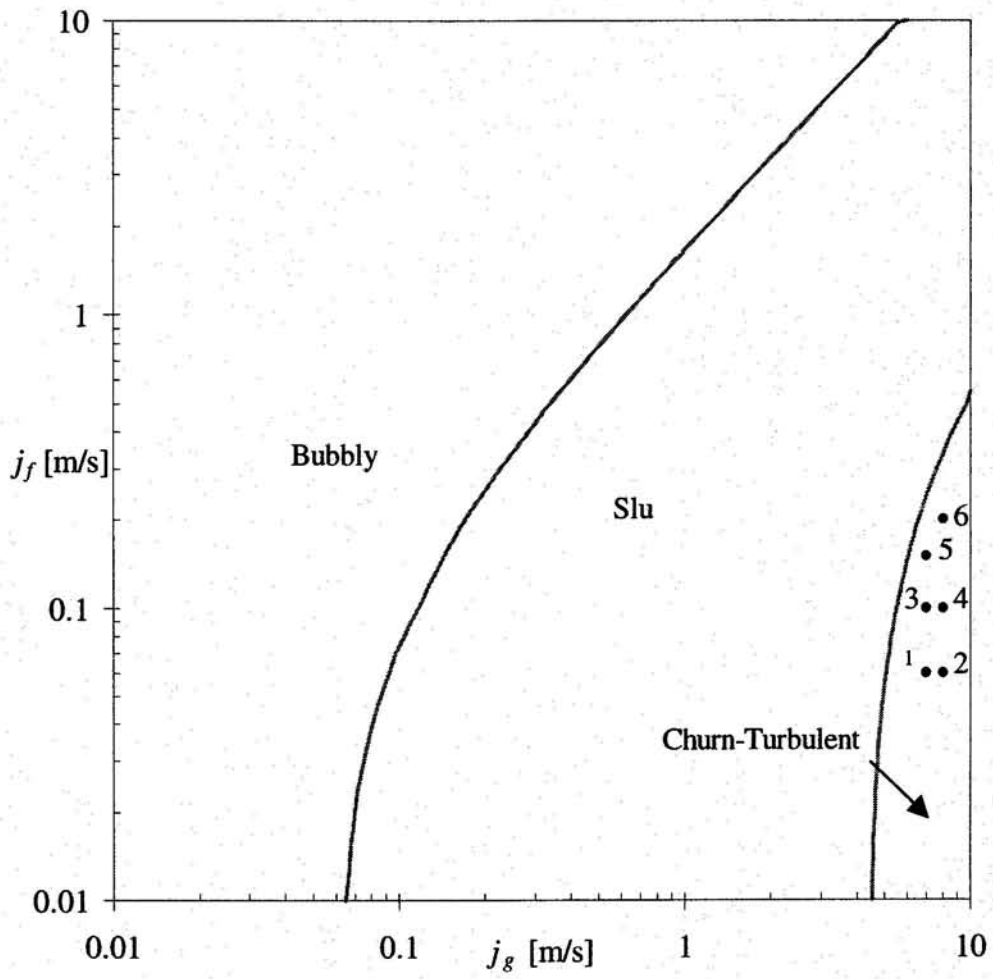
Figure 4.2 Test matrix of the present experimental for the churn flow. The solid line is given by Mishima and Ishii [2].

Table 4.2 Flow Conditions for the churn flow

Test Matrix

	jg [m/s]	jf [m/s]
Run 1	7	0.06
Run 2	8	0.06
Run 3	7	0.1
Run 4	8	0.1
Run 5	7	0.15
Run 6	8	0.2

Table 4.3. Summary of the experimental data for the 12.7 cm ID vertical co-current air-water loop.

Run No.	$j_{g,0}$ [m/s]	j_f [m/s]	j_g [m/s] L/D=17	$<\alpha><<v_g>>$ [m/s]	Gage pressure at L/D=17 [Psig]	[Pa]	Gage pressure at L/D=217 [Psi]	[Pa]	dp/dz [Pa/m]	D_{Sm} [cm] L/D=17	D_{Sm} [cm] L/D=217	DP & Probe at L/D=17
1	0.07000	0.4	0.050	0.0500	5.49	37840.99	5.34	36827.21	399.13	0.220	0.250	0.00
2	0.20000	1	0.170	0.1450	3.12	21530.81	2.85	19654.97	738.52	0.360	0.340	14.71
3	0.20000	3	0.120	0.1440	10.47	72171.68	7.43	51240.86	8240.48	0.210	0.320	20.00
4	0.20000	0.4	0.150	0.1300	4.83	33303.11	4.27	29447.98	1517.77	0.260	0.250	13.33
5	0.70000	1	0.540	0.4710	5.57	38427.19	5.32	36689.28	684.22	0.300	0.290	12.78
6	1.25000	3	0.730	0.6660	10.79	74413.03	7.64	52689.12	8552.72	0.500	0.250	8.77
7	0.70000	0.4	0.561	0.3740	3.92	27013.52	2.73	18827.39	3222.88	0.350	0.480	21.00
8	3.00000	3	1.700	1.4380	12.71	87619.80	8.53	58826.99	11335.75	0.250	0.250	15.41

Run No.	$<\alpha_1>$	$<\alpha_2>$	$<\alpha_{tot}>$	$<a_{i1}>$ [1/m]	$<a_{i2}>$ [1/m]	$<a_{itot}>$ [1/m]	$<a_{i1}>$ [1/m]	$<a_{i2}>$ [1/m]	$<a_{itot}>$ [1/m]	$<a_{i1}>$ [1/m]	$<a_{i2}>$ [1/m]	$<a_{itot}>$ [1/m]
	at L/D=17			at L/D=17			at L/D=120			at L/D=217		
1	0.080	0.000	0.080	191.41	0.0	191.4	184.19	0.0	184.2	193.86	0.0	193.9
2	0.120	0.000	0.120	190.58	0.0	190.6	223.66	0.0	223.7	139.75	0.0	139.8
3	0.040	0.000	0.040	103.00	0.0	103.0	152.11	0.0	152.1	114.36	0.0	114.4
4	0.240	0.000	0.240	466.00	0.0	466.0	441.84	0.0	441.8	429.37	19.9	449.3
5	0.320	0.000	0.320	520.71	2.3	523.1	428.12	14.8	442.9	428.74	114.4	543.1
6	0.160	0.040	0.200	174.33	13.6	187.9	256.98	55.8	312.8	284.05	53.8	337.9
7	0.480	0.000	0.480	735.46	0.0	735.5	515.78	0.0	515.8	492.18	118.7	610.9
8	0.060	0.300	0.360	125.40	35.1	160.5	217.59	51.5	269.1	244.40	35.8	280.2
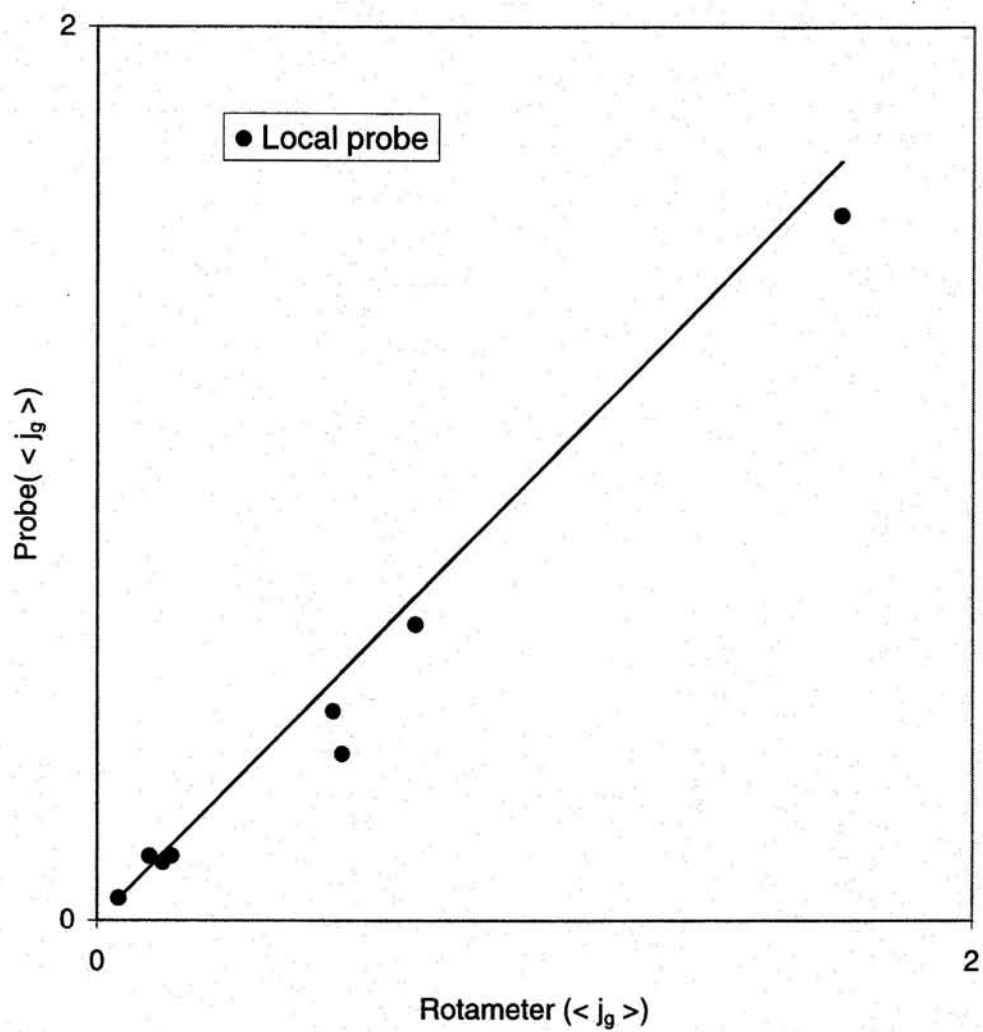
Figure 4.3 The cross-calibration of the superficial velocity between the rotameter and the four-sensor conductivity probe.
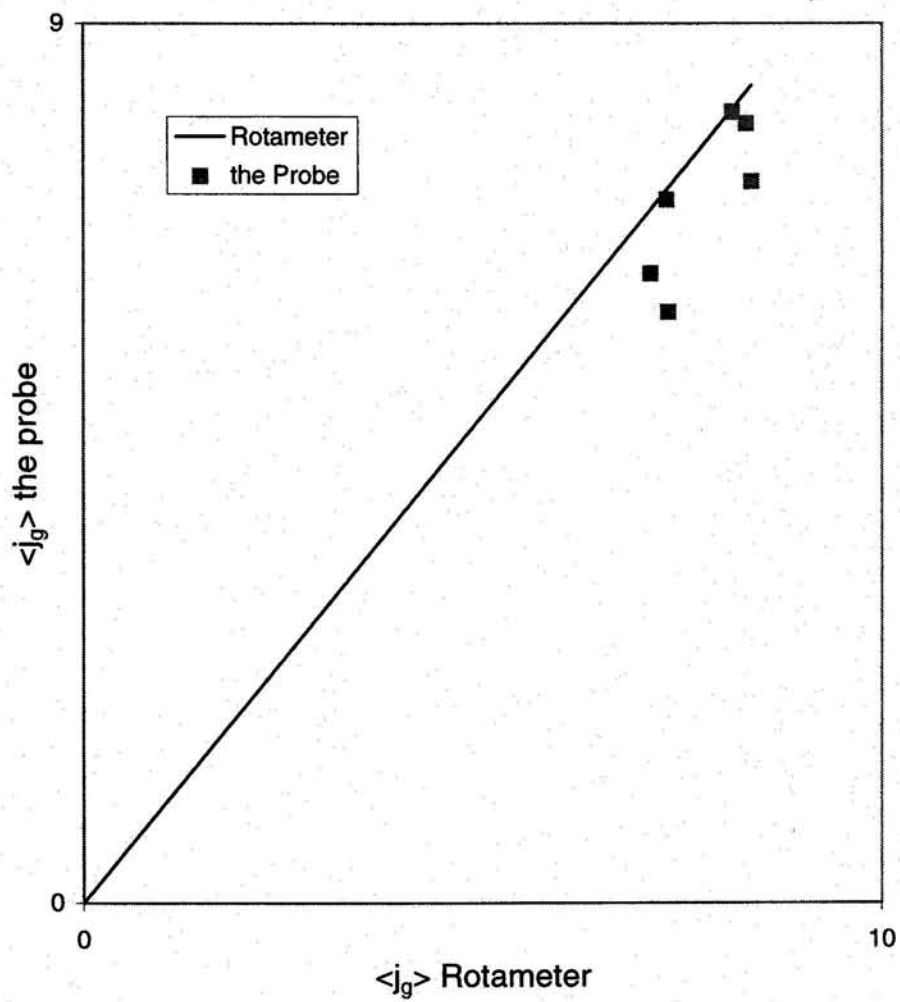
Figure 4.4 The cross-calibration of the superficial velocity between the rotameter and the two-sensor conductivity probe.

4.1.2 Void Fraction

An initial condition (bubble size, generation method and mixing condition), a flow condition (flow rates and physical properties), and a test section condition (geometry and wall surface) generally affect a void distribution [16],[17]. The miniaturized four-sensor probe can be employed successfully for taking the local data in the bubbly flow regime because it is observed that the probe did not miss catching the bubbles with the four sensors. The cross calibration between the DP cell and the miniaturized four-sensor conductivity probe is shown in Figure 4.5. Figure 4.6 shows the cross calibration between the DP cell and the two-sensor. However, good agreements between the DP, the four sensor and two-sensor were obtained.

The profiles of local time-averaged of void fraction in bubbly flow at j_f =0.4 & j_g=0.07 m/s for different locations L/D=17,120 and 217 are shown in Figure 4.7 (a). The center peak and the development of the void fraction profiles along the radial direction of the tube are observed. By increasing the j_g and j_f , the behavior of the void fraction at j_f =1.0 & j_g=0.4 m/s at different locations as shown in Figure 4.7 (b) is a peak near the pipe wall observed. Further increasing the j_f to 3.0 m/s and fixing j_g, the behavior of the void fraction moved to the center peak as shown in Figure 4.8(a). The development of the void fraction can be seen at three different flow conditions, Run 1, Run 2, and Run 3, as shown Figure 4.8(b).

In Figure 4.9 (a) and (b), the local α is categorized into two groups where group one includes the spherical and distorted bubbles and group two includes cap and slug bubbles. The criteria of the divided bubbles in two groups is shown in Figure 4.10. The α of the group one bubbles for Run 5 (j_f= 1.0 m/s and j_g =0.7 m/s) at L/D = 217 peaks at the center of the tube, and α of group two peaks at the center of the tube as well. Under this condition, the contribution to the α from both groups is quite the same. The average cord length of the slug bubbles measured at the center of the flow pipe by the common sensor at this condition is 6.5 cm. In Figure 4.11, the α of the group one bubbles for Run

6 at L/D = 17 peaks at the center of the tube and α of the group two peaks also at the center of the tube. Under this condition, the contribution of the α from group one bubble is about 35% of the total void fraction, and α_{tot} is determined mainly by the group two bubbles. The average cord length of the slug bubble is 14 cm. For the churn flow, at Run 1 (jf=0.06 m/s and j_g= 7.0 m/s), the behavior of the local void fraction profile is shown in Figure 4.12, which is the α of the group two peaks at the center of the test section while the α of group 1 is very small and its peak is at the wall. The contribution of α from group one is very small of the total void fraction and α_{tot} is determined mainly by the group two bubbles.

4.1.3 Interfacial Area Concentration

Figures 4.13, 4.14 and 4.15 show the behavior of interfacial area concentration profiles, corresponding to that of void fraction profiles in Figures 4.7,4.8 and 4.9. As expected for bubbly flow, the interfacial area concentration profiles were similar to the void fraction profiles. Since the interfacial area concentration is directly proportional to the void fraction and the Sauter mean diameter, which was almost uniform in the flow channel, the interfacial area profiles display the same behavior as their respective void fraction profiles. The profiles of interfacial area for Run 5 at L/D = 120 peaks at the center of the tube for the one group bubbles, while for two group a peak near the pipe of the wall is observed. The center peak in the α profile and the sharp peak in the a_i profile clearly demonstrate the characteristic signature of the slug bubbles. It is also shown that both α and a_i increase with increasing gas flow rates for group one and group two bubbles. The increase in the local α and the local peak in the a_i profile indicate that the length of the slug bubble becomes longer, and contribution from the side interface of the slug bubbles in local a_i becomes more significant with increasing gas flow rates. However, the local a_i of group two bubbles remain unchanged between the tube center and r/R=0.45. This would imply that the shapes of the nose of the slug bubbles do not change significantly regardless of the bubble cord length.

4.1.4 Sauter Mean Diameter

In Figure 4.16 (a), Sauter mean diameters were smaller than 3.0 mm and were almost uniform along the radius of the test section with some decrease near to the wall. The reason for the decrease of the Sauter mean diameter near the wall may be explained from the fact that presence of the wall does not allow the arc length at which the bubble is intercepted by the sensor to be a random variable as in the other positions in the test section. In Figure 4.16(b), the core peak in the Sauter mean diameter profile was observed. The main reason would be due to the migration of large bubbles towards the center of the tube. However, the profiles of Suater mean diameter were not changed drastically as the flow developed. The increasing of the bubble sizes along the flow direction for the same flow rate is due to the bubble coalescence and expansion.

4.1.5 Bubble Rise Velocity

The averaged profiles of bubble velocity measured at different axial locations obtained in Run 1 are shown in Figure 4.17. The velocity profiles at all three axial locations are quite flat. Figure 4.18 shows the bubble velocity profiles obtained in Run 5. Under these conditions, a similar trend can be observed in Run 1 at Port 3, except that the two other ports have a peak at center. This peak may be a result of by the high flow rate of the given flow condition and the inlet effect. With the given inlet condition, two-phase mixture may not be fully mixed at the lower axial locations under high liquid flow condition, and it may result in the delay of the fully developed flow condition. Nevertheless, this peak phenomenon disappears at the downstream as shown at Port 3, and the bubble velocity profiles become flat as in Run 1. In all of the rest of the flow conditions, similar trend in the bubble velocity profiles is observed. In Figure 4.19, the behavior of bubble frequency for Run 1 and Run 2 in the bubbly flow is shown. The core peak is observed because most of the bubble is traveling to the center of the test section.
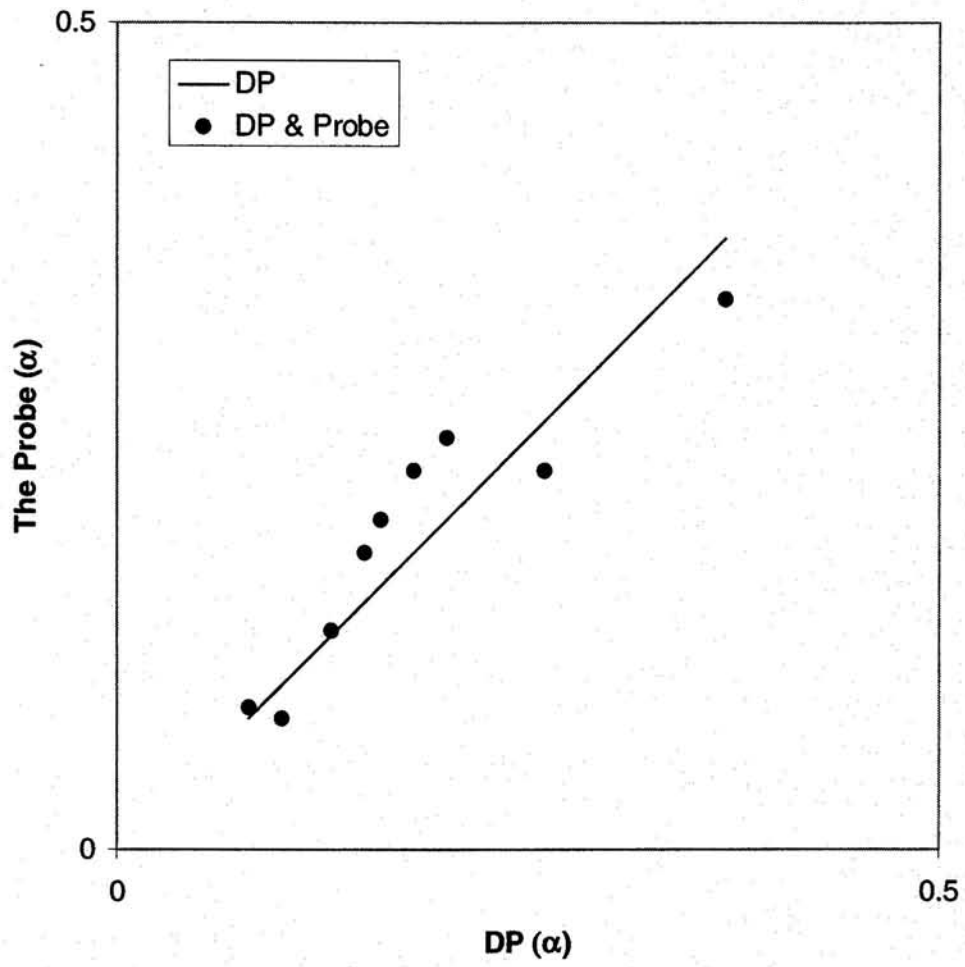
Figure 4.5 Cross-calibration of void fraction between DP cell and four-sensor conductivity probe.
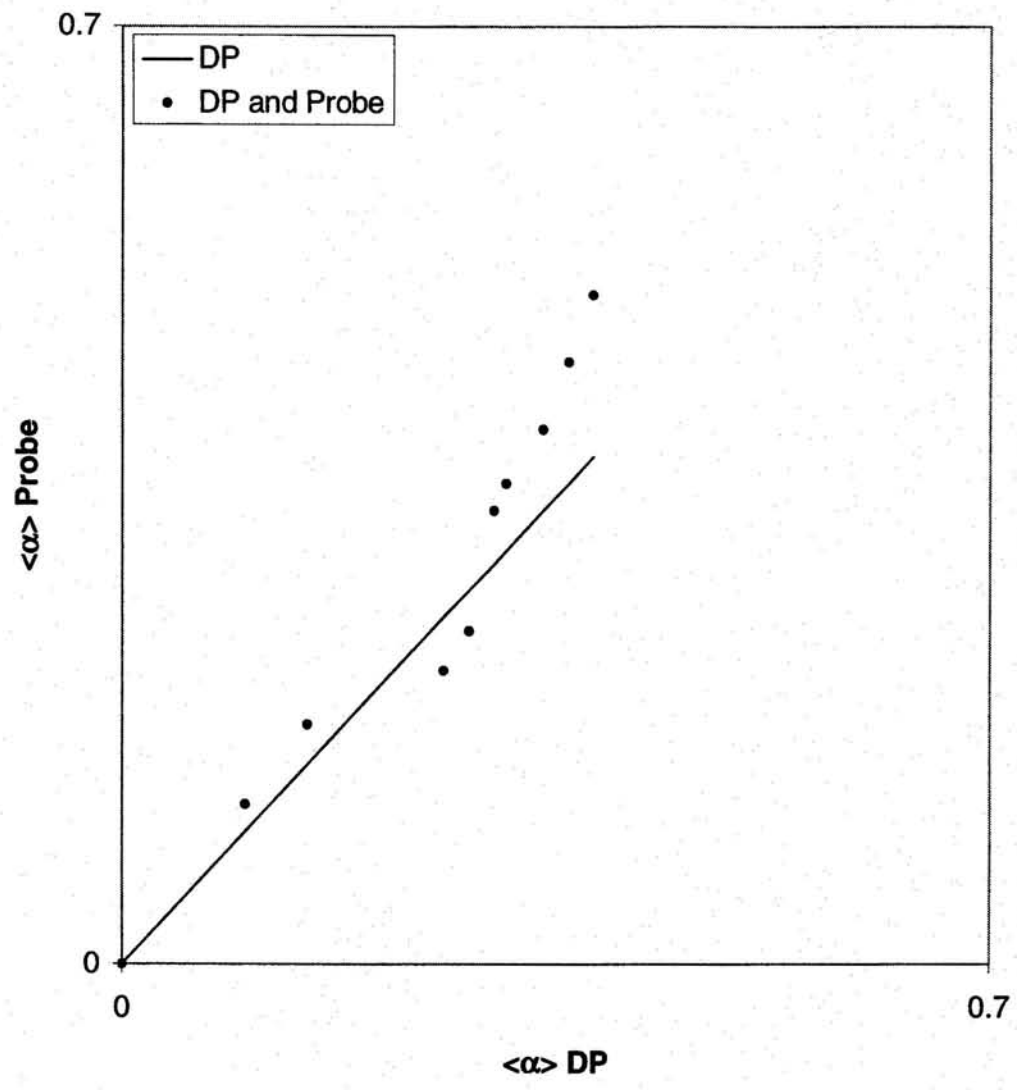
Figure 4.6 Cross-calibration of void fraction between DP cell and two-sensor conductivity probe.
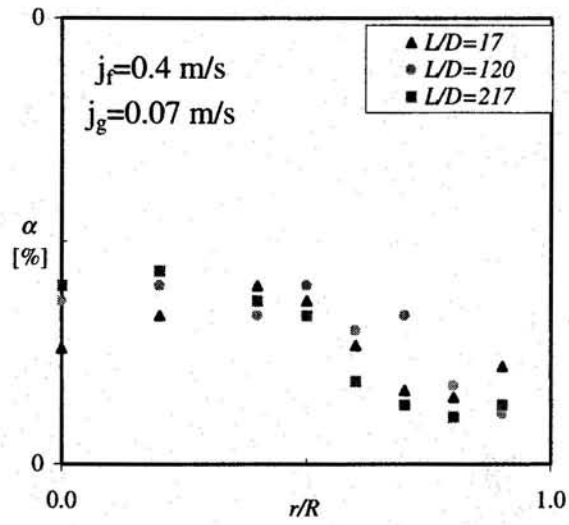
(a)
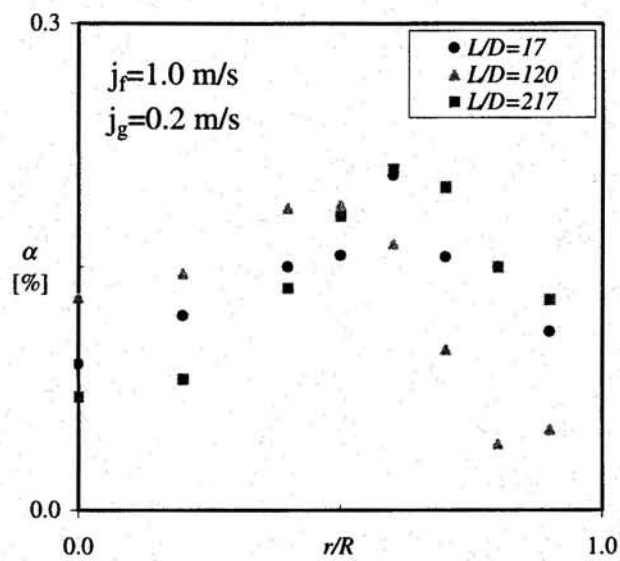
(b)

Figure 4.7 Profiles of local time-averaged void fraction in three different flow conditions: (a) for j_f =0.4 & j_g=0.07 m/s at different locations (b) for j_f =1.0 & j_g=0.4 m/s at different locations.
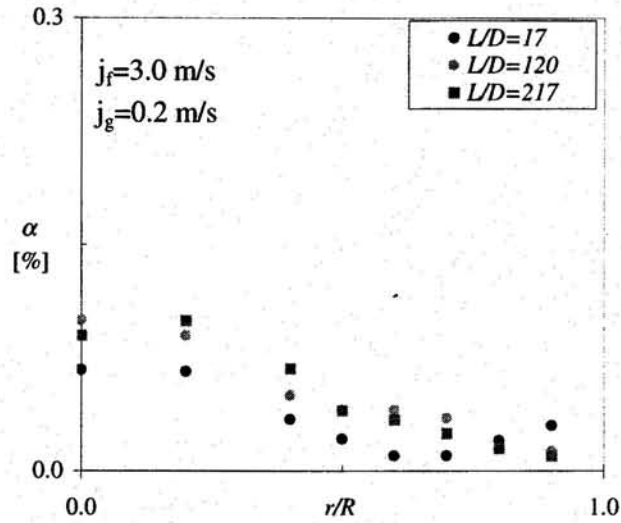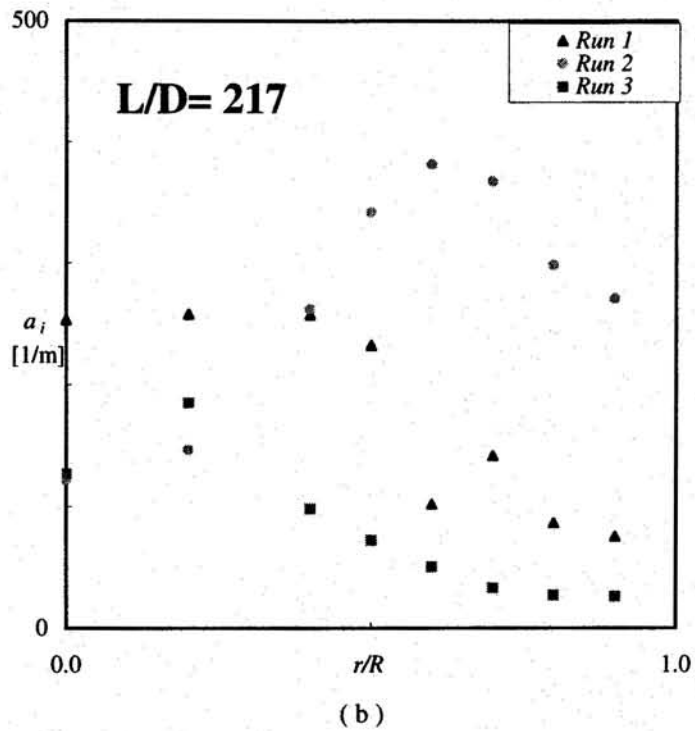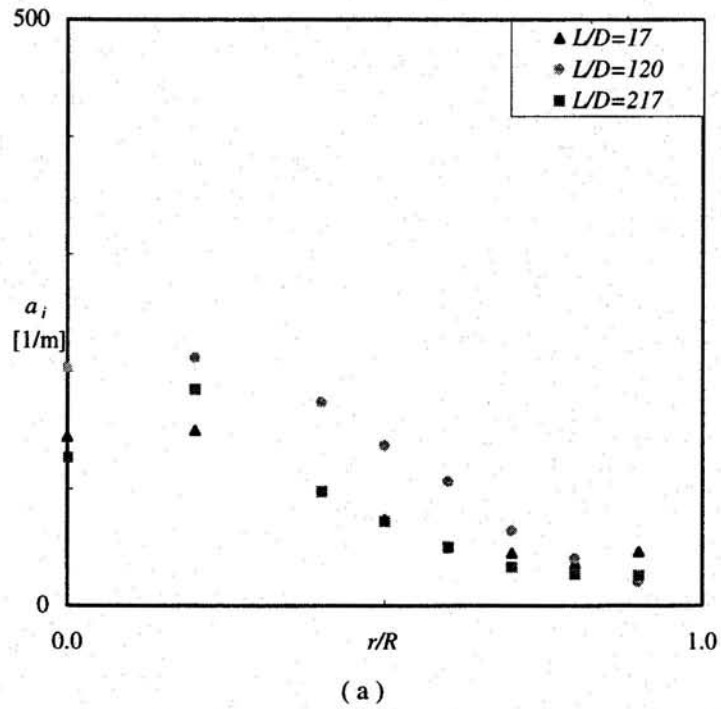
(a)
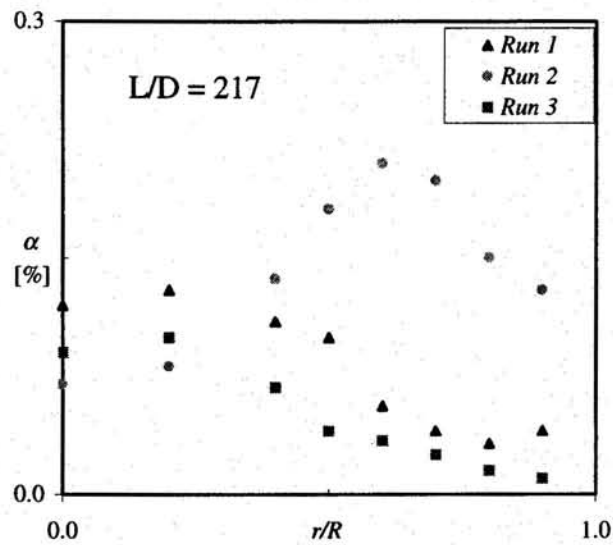
(b)

Figure 4.8 Profiles of local time-averaged void fraction in three different flow conditions: (a) for j_f =3 & j_g=0.2 m/s at different locations (b) for L/D = 217 at different flow conditions.
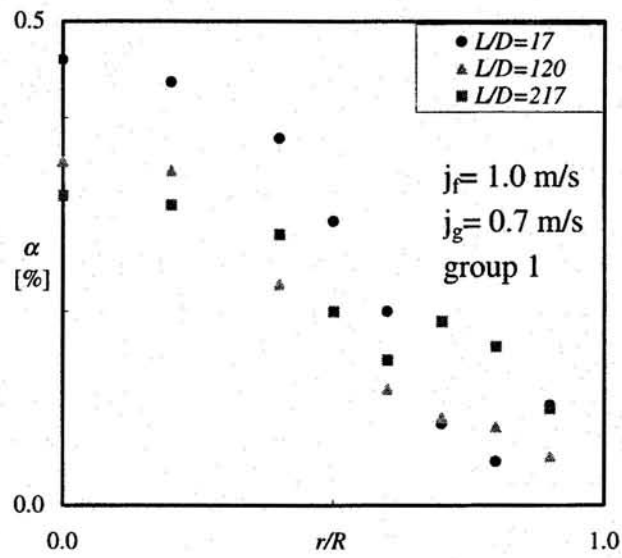
(a)
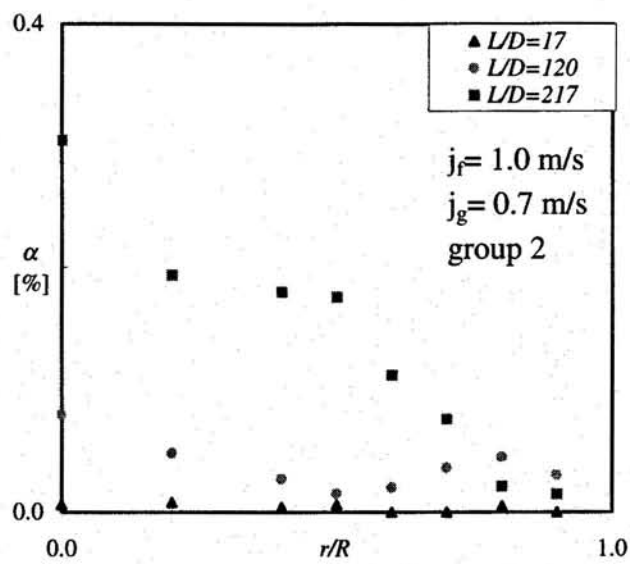
(b)

Figure 4.9 Profiles of local time-averaged void fraction in three different flow conditions: (a) for j_f =1.& j_g=0.7 m/s at different locations for group1 (b) for j_f =1.0 & j_g=0.7 m/s at different locations for group2.
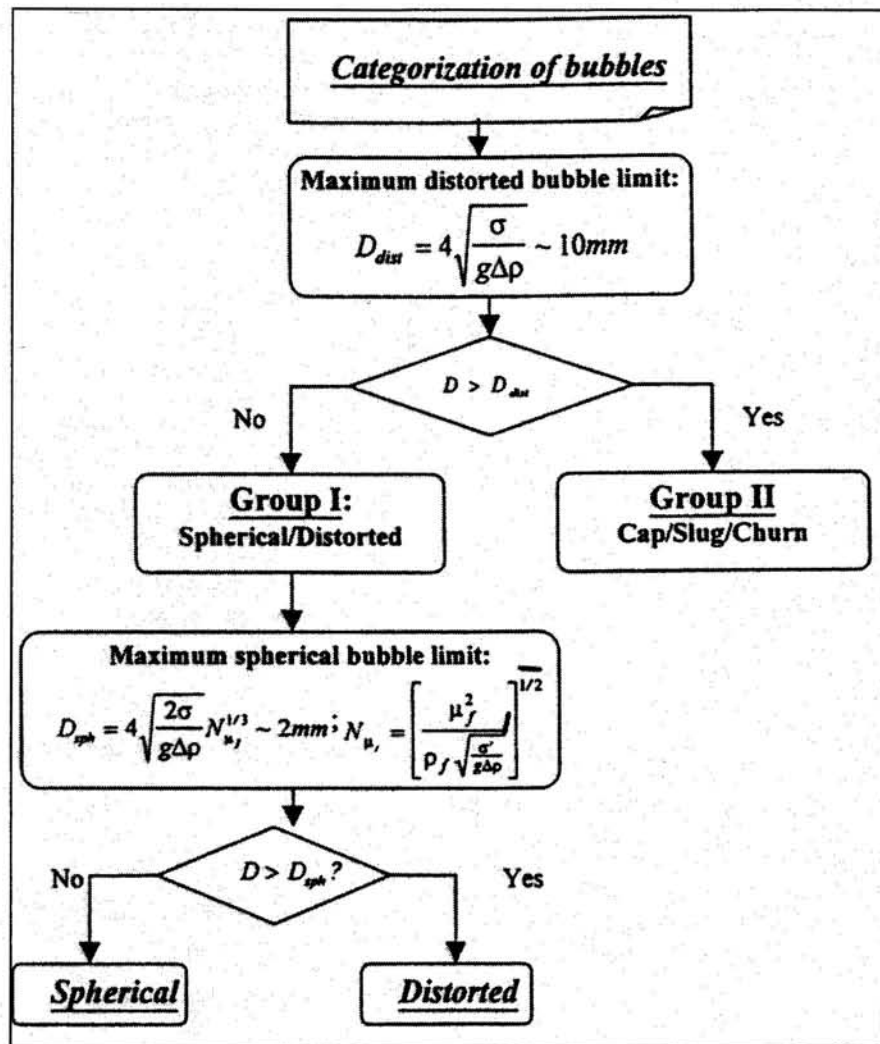
Figure 4.10 Schematic chart of multi-group categorization.
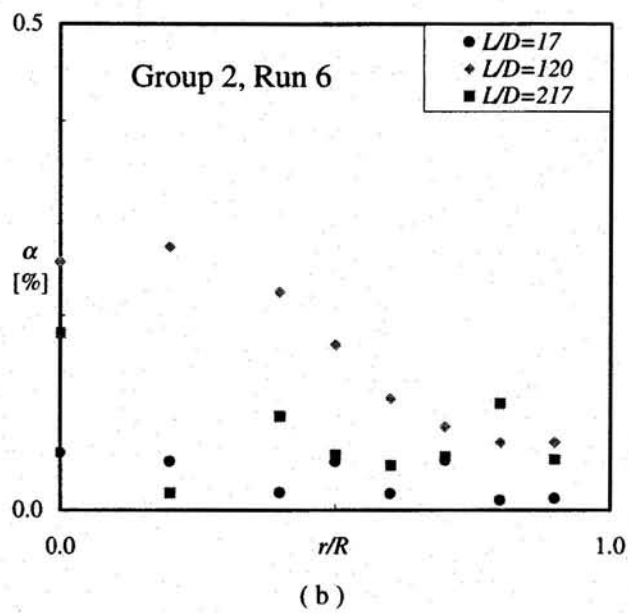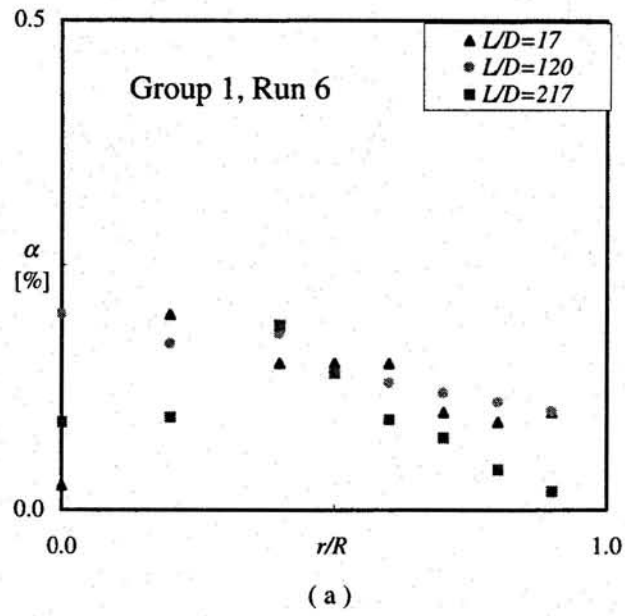
Figure 4.11 Profiles of local time-averaged void fraction in three different flow conditions: (a) for Run 6 (j_f= 3 m/s and j_g= 1.25 m/s)at different locations for group1(b) for Run 6 at different locations for group 2.
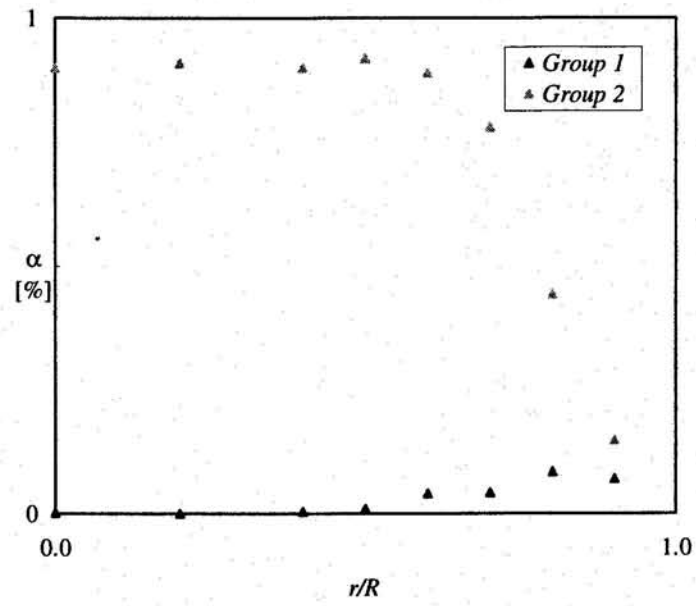
Figure 4.12 Profiles of local time-averaged void fraction at Run 1 for the churn flow (j_f=0.06m/s and j_g= 7.0 m/s).
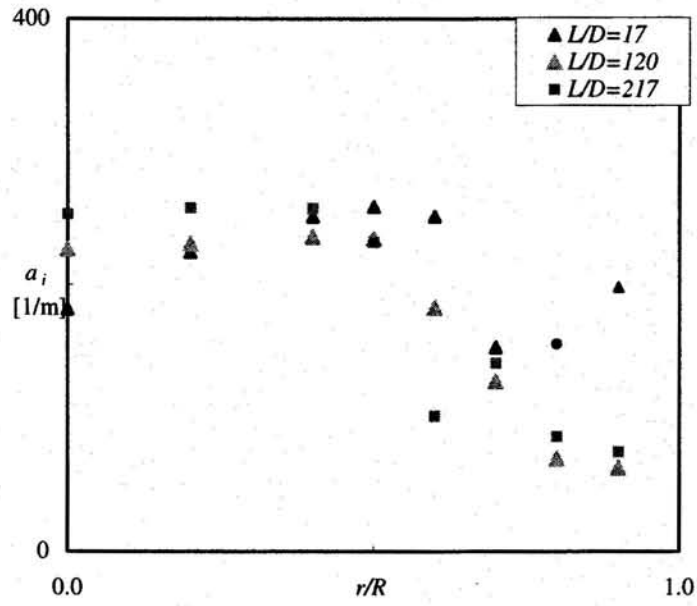
(a)
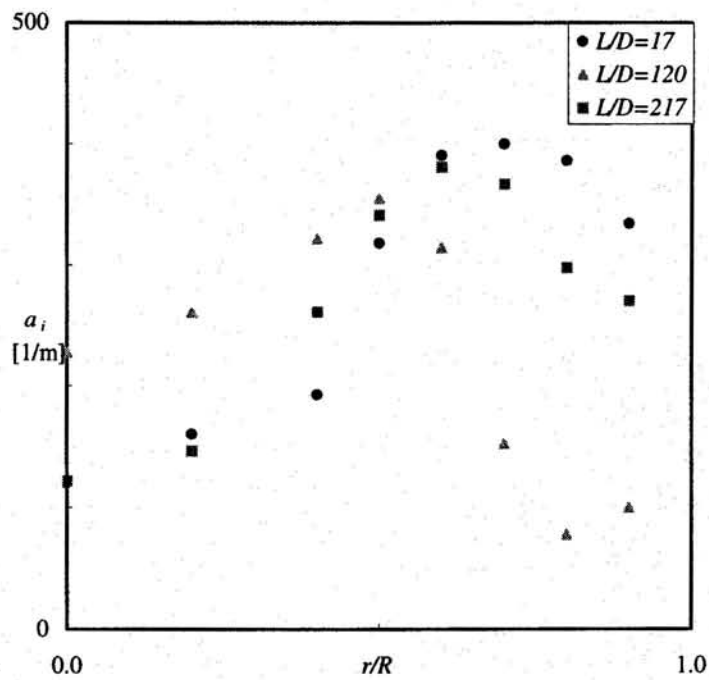
(b)

Figure 4.13 Profiles of local time Interfacial area concentration in three different flow conditions: (a) for j_f =0.4 & j_g=0.07 m/s at different locations (b) for j_f =1.0 & j_g=0.4 m/s at different locations.

Figure 4.14 Profiles of local time Interfacial area concentration in three different flow conditions: (a) for Run 3 (j_f= 3 m/s and j_g=0.2 m/s) at different locations (b) for L/D= 217 for different conditions.
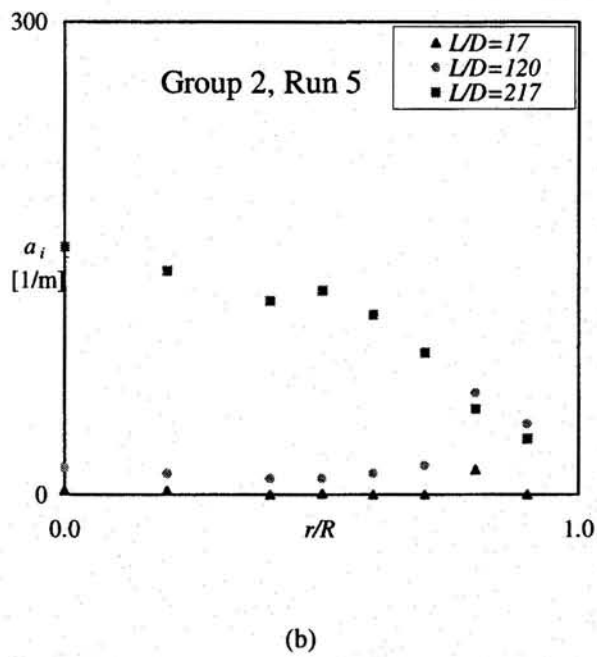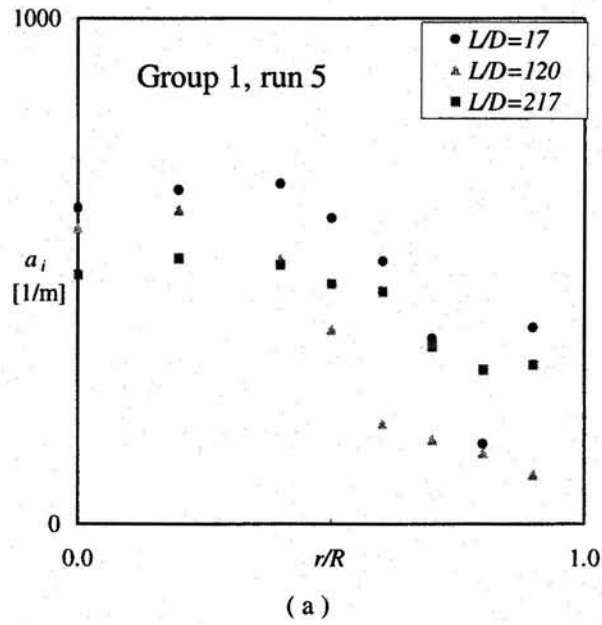
Figure 4.15 Profiles of local time Interfacial area concentration in three different flow conditions: (a) for Run 5 (j_f = 1 m/s and j_g = 0.7 m/s) at different locations for group 1(b) for Run 5 at different locations for group 2.
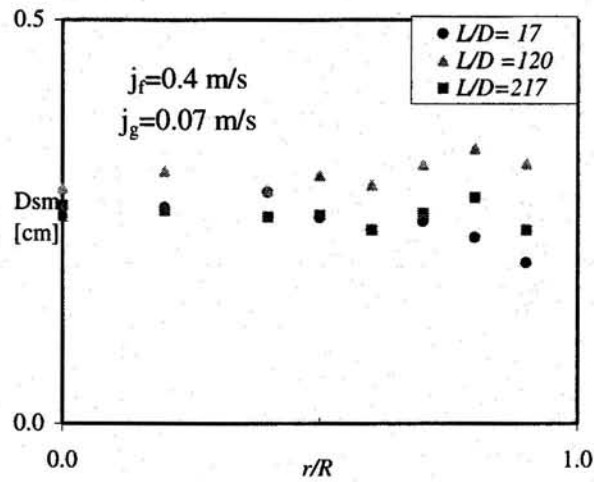
(a)
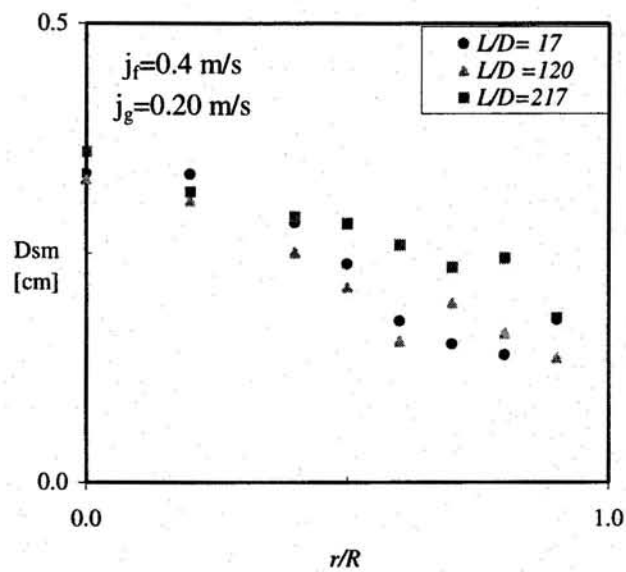
(b)

Figure 4.16 Profiles of Sauter mean diameter in three different flow conditions: (a) for j_f =0.4 & j_g=0.07 m/s at different locations (b) for j_f =0.4 & j_g=0.2 m/s at different locations.
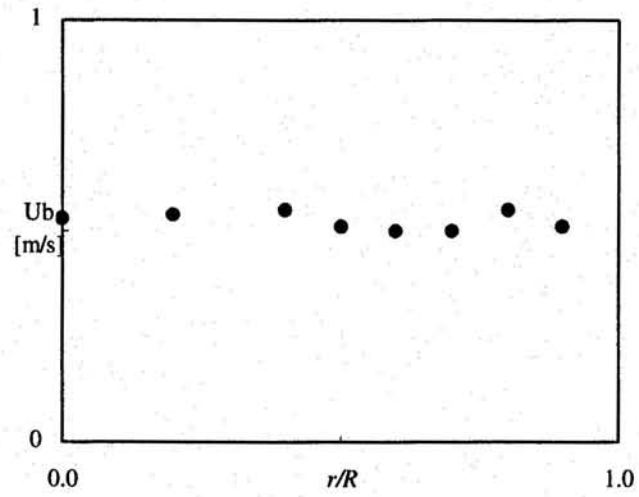
Port 1: L/D= 17
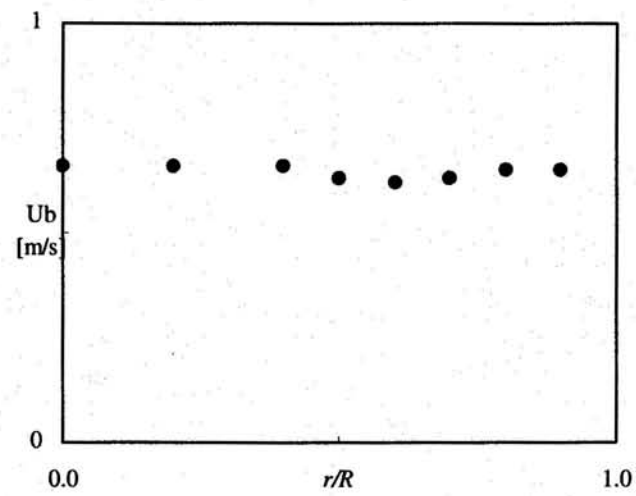
Port 2 : L/D=120
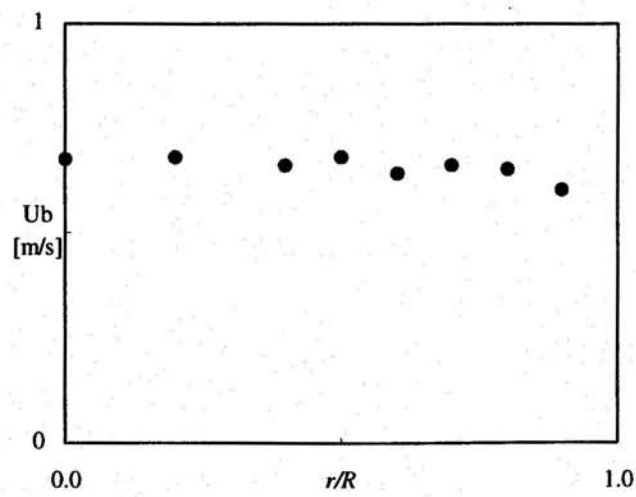
Port 3 : L/D=217

Figure 4.17 Profiles of bubble rise velocity for j_g= 0.07 m/s and j_f=0.4 m/s .
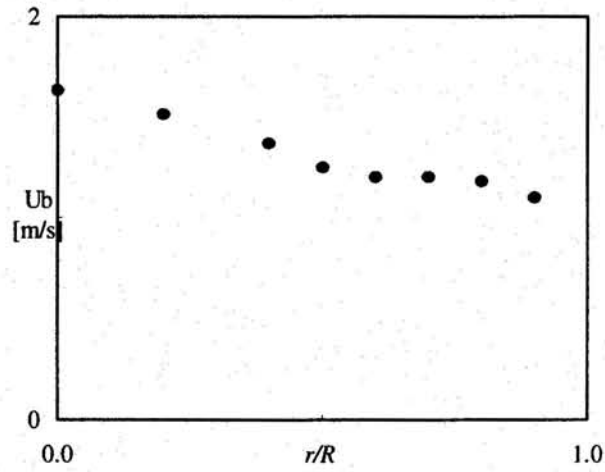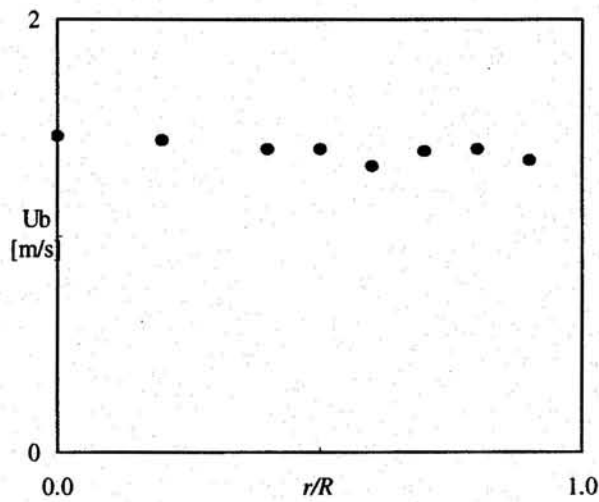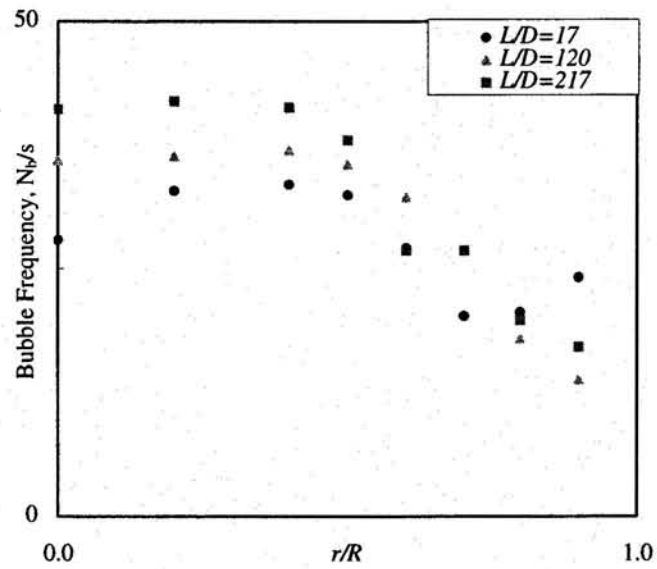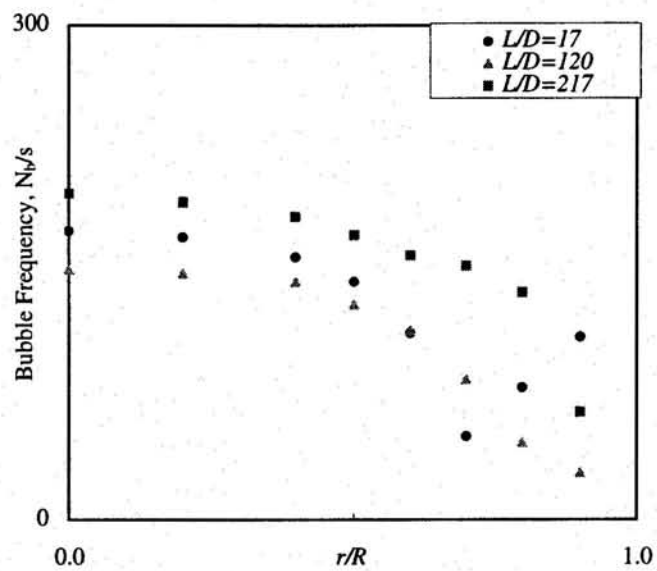
Port 1 : L/D= 17
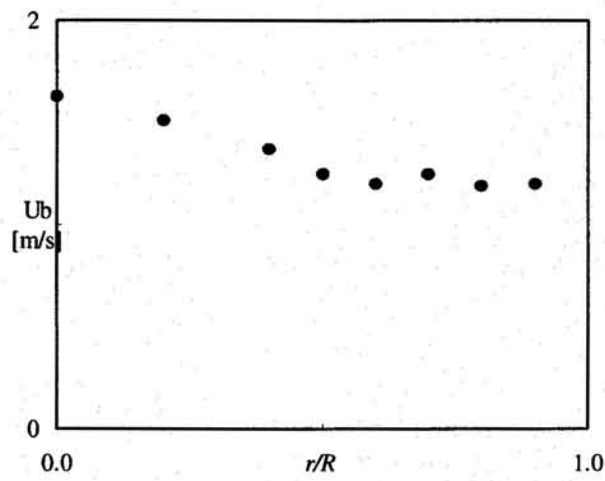
Port 2: L/D=120

Port 3: L/D=217

Figure 4.18 Profiles of bubble rise velocity for Run 5 at different axial locations.
(Flow condition: j_g= 0.75 m/s and j_f=1.0 m/s)

(a)

(b)

Figure 4.19 Profiles of Bubble Frequency in three different flow conditions: (a) for j_f =0.4 & j_g=0.07 m/s at different locations (b) for j_f =1.0 & j_g=0.4 m/s at different locations.

4.2 Evaluation of Drift Flux Model

The drift flux model is proposed by Zuber and Findlay [18],

$$\frac{\langle j_g \rangle}{\langle \alpha \rangle} = C_\circ \langle j \rangle + \langle\langle V_{gj} \rangle\rangle \qquad (4.13)$$

where $C_\circ$ is the distribution parameter defined by

$$C_\circ \equiv \frac{\langle \alpha\, j \rangle}{\langle \alpha \rangle \langle j \rangle} \qquad (4.14)$$

which is described the dispersed phase in the flow pipe at given flow condition. The distribution parameter depends on the density ratio and the liquid Reynolds number. Ishii [19] developed a correlation for $C_\circ$ given by

$$C_\circ \equiv \left[1.2 - 0.2\sqrt{\frac{\rho_g}{\rho_f}} \right], \qquad \text{for round tube} \qquad (4.15)$$

and $\langle\langle V_{gj} \rangle\rangle$ is the drift velocity. It is used to evaluate and interpret the experimental data obtained in a fully developed and steady state flow conditions. The drift velocities for the different flow regimes are given, also by Ishii [19] as follows:

Bubbly flow,

$$\langle\langle V_{gj} \rangle\rangle = \sqrt{2}\left(\frac{\sigma g \Delta \rho}{\rho_f^2} \right)^{0.25} (1-\alpha)^{1.75} \qquad (4.16)$$

Churn turbulent bubbly flow,

$$\langle\langle V_{gj} \rangle\rangle = \sqrt{2}\left(\frac{\sigma g \Delta \rho}{\rho_f^2} \right)^{0.25} \qquad (4.17)$$

and

Slug flow ,

$$\langle\langle V_{gj} \rangle\rangle = 0.35\sqrt{gD} \qquad (4.18)$$

The procedures of evaluating the experimental data with drift flux model are as follows:

Step 1: As a result of the experiment, all the parameters $\langle j_g \rangle$, $\langle \alpha \rangle$ and $\langle j \rangle$ are calculated for different flow conditions at bubbly flow.

Step 2: Plot $\dfrac{\langle j_g \rangle}{\langle \alpha \rangle}$ versus $\langle j \rangle$, equation (4.13).

Step3: $C_\circ$ is the slope from the plot and $\langle\langle V_{gj} \rangle\rangle$ is the juncture with y-axis.

Step4: Repeat steps 1,2, and 3 for slug and churn-turbulent flows.

The results of the evaluation of the experimental data by employing the drift flux model are shown in figures 4.20, 4.21, and 4.22 respectively. The $C_\circ$ and $\langle\langle V_{gj} \rangle\rangle$ values are 1.0004 and 0.090396 m/s, respectively. However, for slug flow the values of $C_\circ$ and $\langle\langle V_{gj} \rangle\rangle$ are 0.9775 and 0.193 m/s, respectively. For the churn flow the values of the $C_\circ$ and $\langle\langle V_{gj} \rangle\rangle$ are 1.0678 and 0.1363 m/s. For bubbly flow, the distribution parameter was found to be $C_\circ = 1$, which indicated that the void profile was flat in the core region. The churn-turbulent regime exhibited the same distribution as the bubble flow regime with $C_\circ = 1.067$.
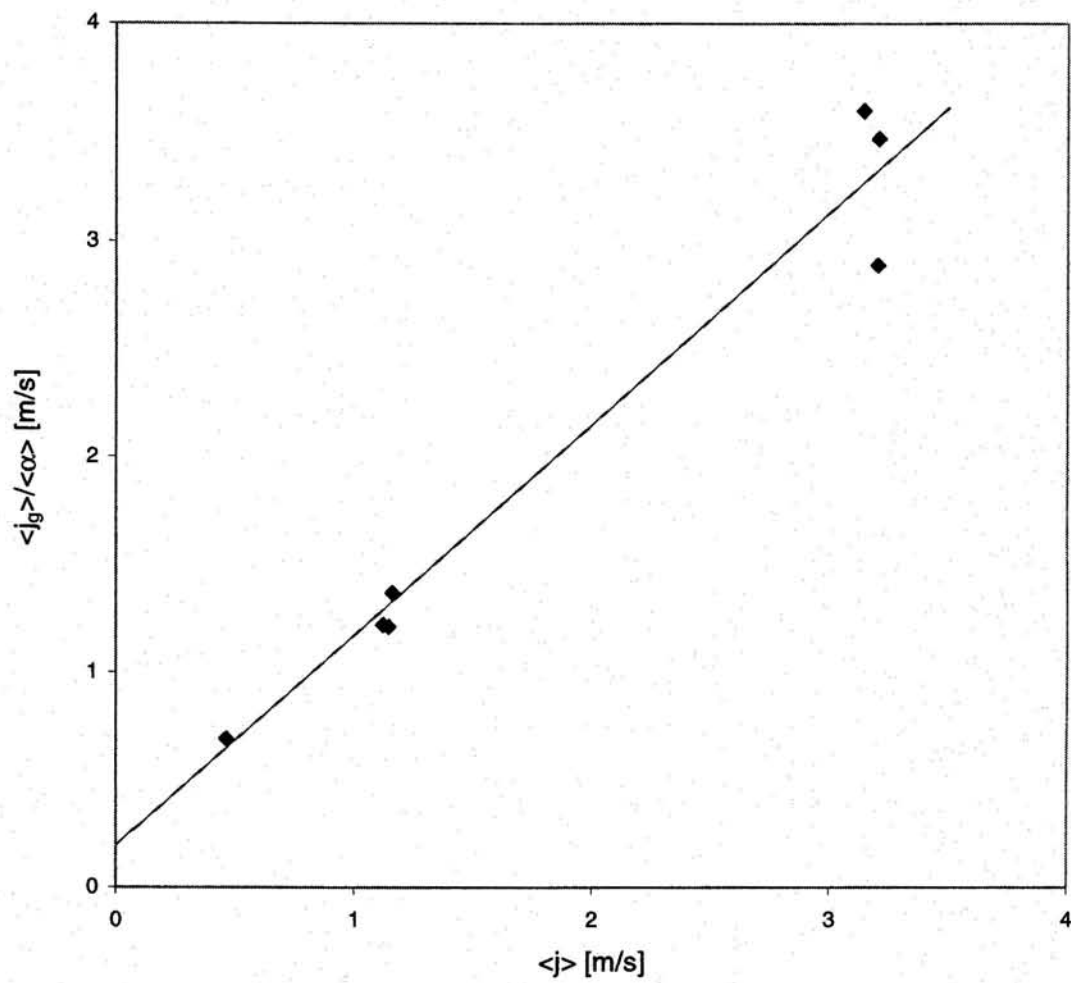
Figure 4.20 Evaluation of the experimental data with drift flux model for bubbly flow.
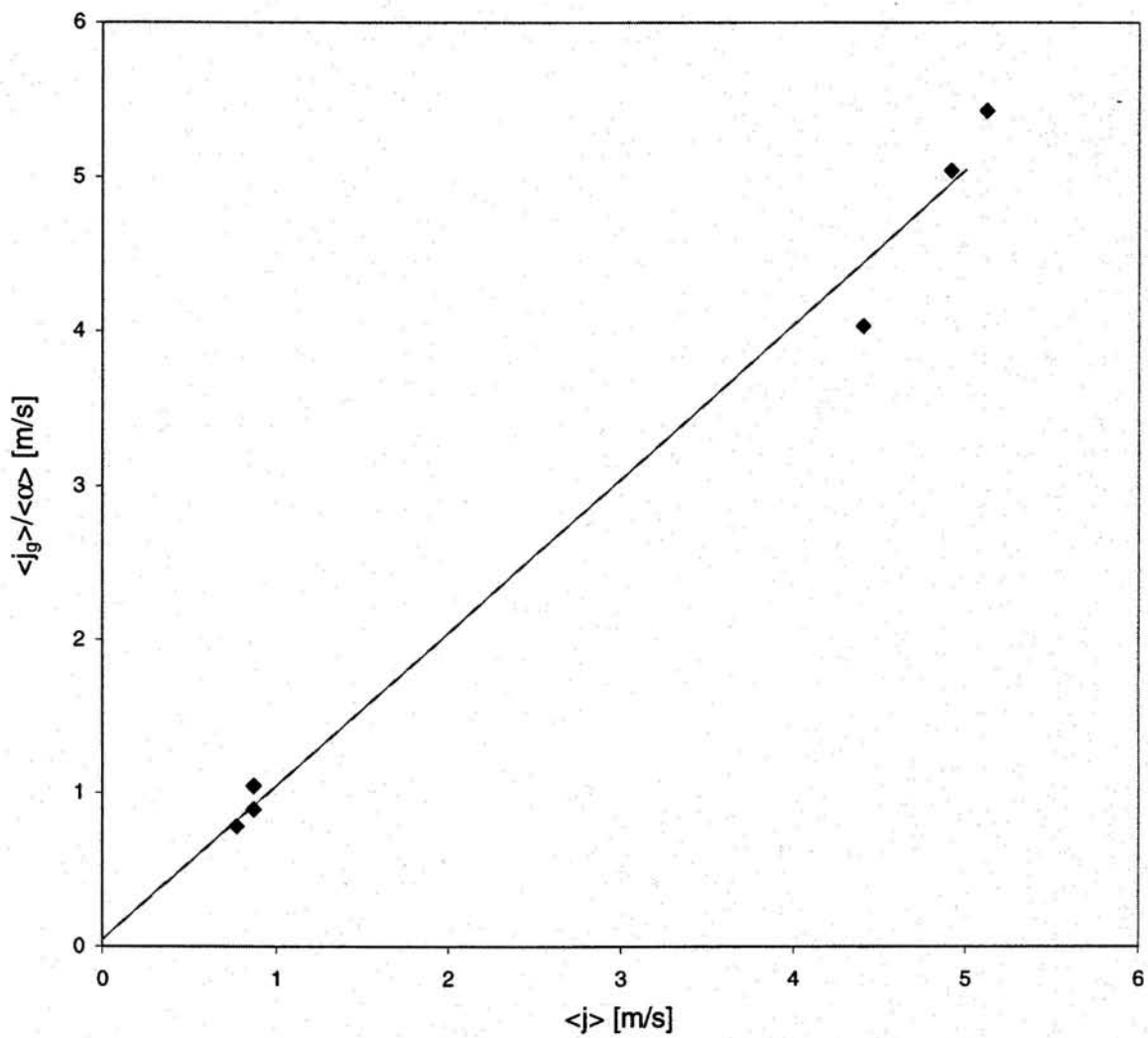
Figure 4.21 Evaluation of the experimental data with drift flux model for Slug flow.
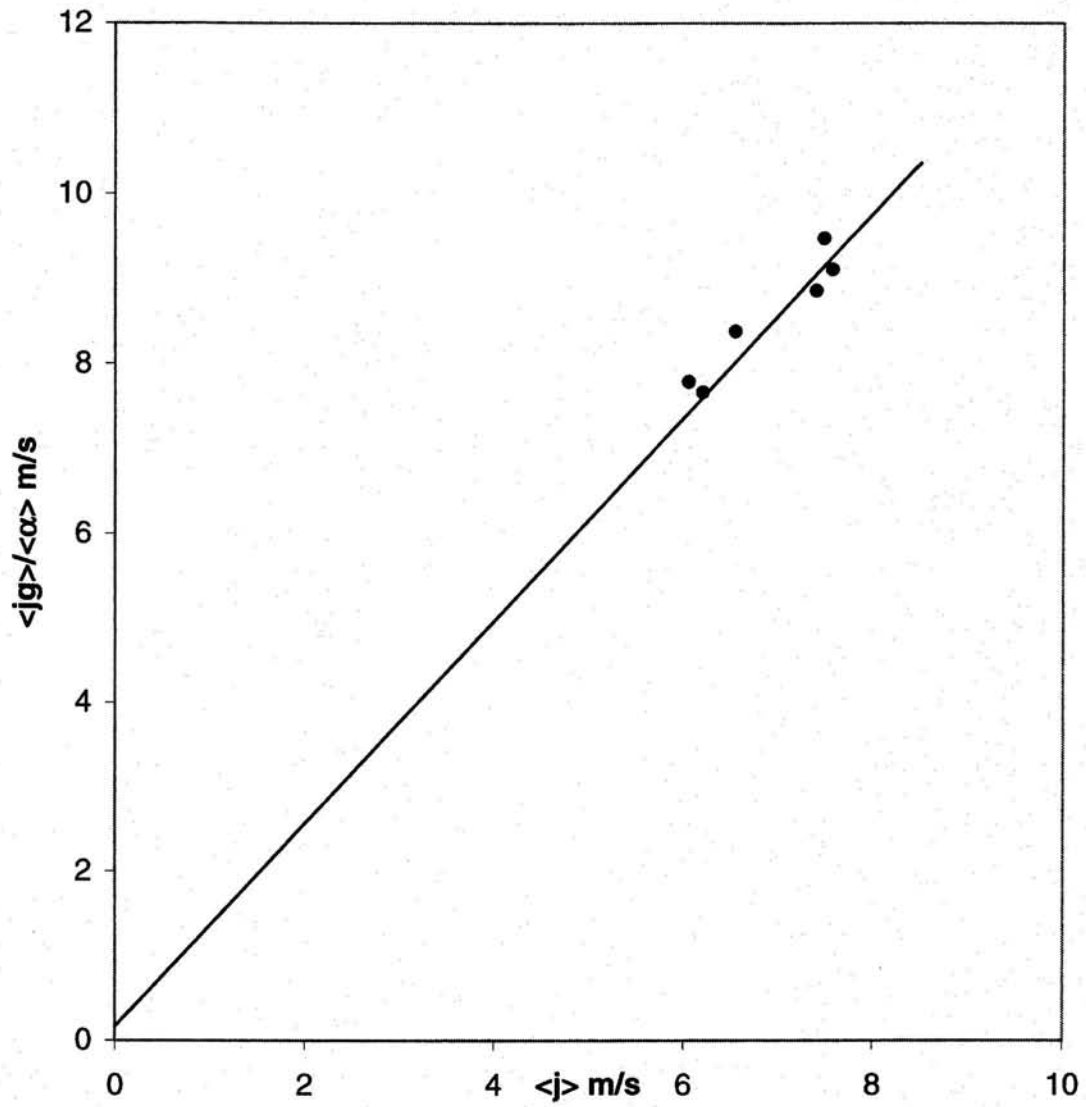
Figure 4.22 Evaluation of the experimental data with drift flux model for Churn flow.

4.3 Uncertainty Analysis

The degree of inaccuracy or the total measurement error is the difference between the measured value and the true value. The total error is the sum of the bias error and the precision error. The bias error is the fixed, systematic, or constant component of the total error and is sometimes referred to simply as the bias. The precision error is the random component of the total error and is sometimes called the repeatability or repeatability error. The bias error is difficult to estimate; however, the calculation of uncertainty is based solely on the precision limits of this experiment.

The calculation of the precision error is based on the method outlined by Coleman and Steele [20]. The precision error for the local average interfacial area concentration and local average void fraction was estimated by using the first-order precision limit, $P_\alpha = \pm tS_\alpha$ and $P_{a_i} = \pm tS_{a_i}$, where t is the t-distribution value corresponding to the number of degree of freedom, M-1, with a 95 percent confidence level. The precision index S_α and S_{a_i} of the sample population of the M individual test results was found using

$$S_\alpha = \left[\frac{1}{M-1} \sum_{k=1}^{M} (\alpha_k - \bar{\alpha}) \right]^{1/2} \text{ for the void fraction}$$

and

$$S_{a_i} = \left[\frac{1}{M-1} \sum_{k=1}^{M} (a_i - \bar{a}_i) \right]^{1/2} \text{ for the interfacial area concentration}$$

The values of P_α and P_{a_i} are the precision limits representing the range around the mean values at which the local average quantities were determined for another measurement would fall within a 95 percent confidence. For this experiment, the precision limit for the local average void fraction was within the range $0.03 \leq P_\alpha \leq 0.43$ and the precision limit for the local average interfacial area concentration was found to be $0.1 \leq P_{a_i} \leq 7.4 (m^{-1})$ with a 95 percent confidence level.

العنوان:	INTERFACIAL AREA CONCENTRATION AND VOID FRACTION OF TWO-PHASE FLOW IN 12.7 mmID PIPE
المؤلف الرئيسي:	Al Dorwish, Yousef M.
مؤلفين آخرين:	Ishi, Mamoru(Super.)
التاريخ الميلادي:	2000
موقع:	لافاييت
الصفحات:	1 - 120
رقم MD:	614708
نوع المحتوى:	رسائل جامعية
اللغة:	English
الدرجة العلمية:	رسالة ماجستير
الجامعة:	Purdue University
الكلية:	The Graduate School
الدولة:	الولايات المتحدة الأمريكية
قواعد المعلومات:	Dissertations
مواضيع:	الطاقة النووية، الإشعاع النووي، الهندسة النووية
رابط:	https://search.mandumah.com/Record/614708

www.manaraa.com

CHAPTER 5

CONCLUSIONS

The primary objective of this study was to develop an experimental investigation of interfacial area concentration and void fraction in 12.7 mm adiabatic test section. This experimental study of interfacial structure was an important first step for developing the model of interfacial area concentration. The multi-sensor conductivity probe methods were employed to measure the local interfacial area concentration. In addition, these probes also measured the local time average void fraction, bubble velocity, Sauter mean diameter and the cord length.

Due to the lack of data for small pipes, the experiment for flow regime identification was performed to evaluate the conventional flow regime map given by Mishima and Ishii [2]. The method of flow visualization and that of using impedance meter, and the neural network were employed in flow regime identification. Since the flow visualization method relies on the subjective judgment of the observer, the objective approach employing the self-organized neural network was applied in order to verify and improve the results obtained by the flow visualization method. The remarkable agreement between the theoretical transition lines given by Mishima and Ishii [2] and those obtained by the neural network method. However, the study found that the transient lines between the regimes are moved to the right side at port $L/D=17$.However, for churn flow, it is shown that at Port 1 ($L/D=17$) there is no churn flow observed, at port 3 ($L/D=217$), the churn flow is observed. This is due to the entrance effect and interfacial structure development the flow was not fully developed at port 1.

The interfacial structure developments were visualized by conducting the measurements at three axial locations: L/D=17,120 and 217. There are two steps of experiments. The first employs the four sensor conductivity probe for the bubbly-slug flow and measures the interfacial area concentration, void fraction, Sauter mean diameter, bubble velocity and bubble frequency. These local interfacial area concentration measurements provided the knowledge about the axial changes of the interfacial structure in steady developing two-phase flow. However, in the second test, which is employing the two-sensor conductivity probe for the churn flow and to measure the void fraction and the bubble velocity. The sets of data are obtained for the 12.7 mm test section at different locations in the appendix. Finally, the drift flux model is employed to evaluate the data at different flow regimes. It was found that the data have a good agreement.

العنوان:	INTERFACIAL AREA CONCENTRATION AND VOID FRACTION OF TWO PHASE FLOW IN 12.7 mmID PIPE-
المؤلف الرئيسي:	Al Dorwish, Yousef M.
مؤلفين آخرين:	Ishi, Mamoru(Super.)
التاريخ الميلادي:	2000
موقع:	لافاييت
الصفحات:	1 - 120
رقم MD:	614708
نوع المحتوى:	رسائل جامعية
اللغة:	English
الدرجة العلمية:	رسالة ماجستير
الجامعة:	Purdue University
الكلية:	The Graduate School
الدولة:	الولايات المتحدة الأمريكية
قواعد المعلومات:	Dissertations
مواضيع:	الطاقة النووية، الإشعاع النووي، الهندسة النووية
رابط:	https://search.mandumah.com/Record/614708

LIST OF REFERENCES

1.	Jones, O.C., and Zuber, N. " The Interrelation Between Void Fraction Fluctuations and Flow Patterns in Two-Phase Flow." Int .J. Multiphase Flow, Vol.2, pp. 273-306, 1975.

2.	Mishima, K., and Ishii, M. " Flow Regime Transition Criteria For Upward Two-Phase Flow in Vertical Tubes." Int. J. Heat Mass Transfer, Vol.27, pp723-737, 1984.

3.	Taitel, Y., and Luninski, Y. " Flow Pattern in Horizontal and Vertical Two Phase Flow in small diameter pipes." Can. J. Chem. Eng, Vol. 61, pp. 617-620, 193.

4.	Bennett, A., Hewitt, G., Kearsey, H., Keeys, R. and Lacey, P. " Flow Visualization Studies of Boiling at High Pressure." AERE-R 4874, 1965.

5.	Ishii, M. Thermo-Fluid Dynamic Theory of Two-Phase Flow, Eyrolles, Paris, Scientific and Medical Publication of France, 1975.

6.	Ishii,M. and Mishima, K. " Two-Fluid Model and Hydrodynamic Constitutive Relations." Nuclear Engineering and Design, Vol. 82,pp. 107-126, 1984.

7.	Hewitt, G.F. and Hall-Taylor, N.S. " Annular Two-Phase Flow." Pergamon Press, New York, 1969.

8.	Kataoka, I., and Serizawa, A. " Modeling and Prediction of Turbulence in Bubbly Two-Phase Flow." Proc. 2nd Int'l Conf. On Multiphase Flow, Kyoto, Japan, April 3-7, 1995.

9.	Maxwell, J.C. " A Treatise on Electricity and Magnetism." Clarendon Press, Oxford, 1881.

10.	Ishii, M. and Zuber, N. " Drug Coefficient and Relative Velocity in Bubbly, Droplet or Particulate Flows." AIChE Journal, Vol. 25, No. 5, pp. 843-855, 1979.

11. Taitel, Y., Bornea, and D., Duckler, A., " Modeling Flow Pattern Transition for Steady Upward Gas-Liquid Flow in Vertical Tubes." AIChE Journal, Vol. 26,pp.345-354,1980.

12. Smith, T., and Pollock, D." Neural Identification of Two-Phase Flow Regimes." Term Project, NUCL597T, Fall 1998.

13. Mi, Ye. "Two-Phase Flow Characterization Based on Advanced Instrumentation, Neural Networks, and Mathematical Modeling." Ph.D. Purdue University, May 1998.

14. Tsoukalas, L., and Uhrig, R., Fuzzy and Neural Approaches in Engineering, Chapters 7-9, John Wiley and Sons, New York, 1997.

15. Ishii, M., Assad, A., Sun, X, Fu, X. and Smith, T." Design of Experimental Loop For Interfacial Area Measurements." PU NE-98-28, 1998.

16. Hibiki, T., Hogsett , S., and Ishii, M. " Local Measurement of interfacial area, interfacial velocity and liquid turbulence in two-Phase Flow." Proceedings of OECD/CSNI Specialist Meeting on Advanced Instrumentation and Measurement Techniques, Santa Barbara, USA, 1997.

17. Wu, Q., Zheng, D., Ishii, M. and Beus, S.G. "Measurements of interfacial area concentration in two-phase flow with two-point conductivity probe." Int. J. of Multiphase Flow, Vol.15, 1984.

18. Zuber, N., and Findlay, J.A., "Average Volumetric Concentration in Two-Phase Flow Systems." Journal of Heat Transfer, pp.43-467, Nov. 1965.

19. Ishii, M. " One-Dimensional Drift-Flux Model and Constitutive Equations for Relative Motion Between Phases in Various Two-Phase Flow Regimes." ANL-77-47, October 1977.

20. Coleman, H. W., and Glenn Steele, W. " Experimentation and Uncertainty Analysis For Engineers." JHON WILEY & SONS, New York, 1989.

21. Kataoka, I., Ishii, M., and Serizawa, A. " Local formulation and measurements of interfacial area concentration in two-phase flow." Int. J. of Multiphase Flow, Vol. 12, pp.505-529, 1984.

22. Revankar, S. and Ishii, M. " Local Interfacial Area Measurement in bubbly flow." Int. J. of Heat and Mass Transfer, Vol. 35, pp. 913-925, 1992.

23. Kataoka, I., and Serizawa, A. "Interfacial Area Concentration in bubbly flow." Nuclear Engineering and Design, Vol. 20, pp. 163-180, 1990.

24. Revankar, S. T., and Ishii, M. " Theory and Measurement of Local Interfacial Area Using a Four Sensor Probe in Two-Phase flow." Int. J. of Heat and Mass Transfer, Vol. 36,pp. 2997-3007, 1993.

25. Kocamustafaogullari, G. and Ishii, M. " Foundation of Interfacial Area Transport Equation and Closure Relations." Int. J. Heat and Mass Transfer, Vol. 38, No. 3, 1995.

26. Kalkach-Navarro, S., Lahey Jr, R.L., Drew, D.A., and Meyder, R. " Interfacial area density, mean radius and number density measurements in bubbly flow two-phase flow." Nuclear Engineering and Design, Vol. 142, pp. 341-3511, 1993.

27. Abernethy, R. B., Bendict, R. P., and Dowdell, R.B. " ASME Measurement Uncertainty." Journal of Fluids Engineering, Vol. 107, pp. 161-164, June 1985.

28. Leung Wai-Hung, " Modeling of Interfacial Area Concentration and Interfacial Momentum Transfer: Theoretical and Experimental Study." Ph.D. Thesis, Purdue University, May 1997.

29. Kataoka, I., Ishii, M. and Serizawa, A. " Local Formulation of Interfacial Area Concentration in Two-Phase Flow." Int. J. Multiphase Flow, Vol. 12, pp. 505-529, 1989.